

A Coupled SQMOM-CFD Population Balance Framework for Modelling and Simulation of Liquid-liquid Extraction Equipment

Vom Fachbereich für Maschinenbau und Verfahrenstechnik
Der Technische Universität Kaiserslautern
zur Erlangung des akademischen Grades

Doktor – Ingenieur (Dr.-Ing.)

Genehmigte Dissertation

Vorgelegt von

M. Sc. Chem. Eng. Samer Alzyod

aus Amman - Jordanien

Eingericht am: 13.08.2018
Mündliche Prüfung am: 27.09.2018

Promotionskommission:

Vorsitzender: Prof. Dr.-Ing. Sergiy Antonyuk

Referenten: Prof. Dipl.-Ing. Dr. techn. Hans-Jörg Bart
Prof. Dr.-Ing. Menwer Attarakih

Dekan: Prof. Dr.-Ing. Jörg Seewig

D 386
2018

ACKNOWLEDGMENT

This research work is carried out during my stay as a Ph.D. student at the Technische Universität Kaiserslautern/ Germany at the Chair of Separation Science and Technology chaired by Prof. Dipl.-Ing. Dr. techn. Hans-Jörg Bart, during the years 2015-2018.

I am deeply indebted to my professors: Prof. Hans-Jörg Bart and Prof. Menwer Attarakih from the University of Jordan. I highly appreciate their permanent support and guidance during my Ph.D. study and their contributions to all of my publications. In this regard, I wish to thank my professors for giving me the opportunity for studying and investigating the field of population balances and liquid-liquid extraction columns, where they supervised and supported my research work during my stay as a Ph.D. student.

This work is partially supported by the Process Engineering and Technology Network of Competence (Verfahrenstechnik-Pro3.de) and the DFG-GrK 1932 “Stochastic Models for Innovations in the Engineering Sciences”, as well as the financial support granted by Prof. Hans-Jörg Bart, to all those I gratefully acknowledge this support.

I am deeply indebted to all my colleagues at the Chair of Separation Science and Technology and especially my colleague M.Sc. Christian Korb from the liquid-liquid extraction group and Dipl.-Ing.(FH) Christian Kirsch for the experimental support, whose continuous help greatly facilitated my research. I would like also to thank my colleague Dipl.-Ing. Dirk Otter for his help in checking the language of some parts of this thesis.

Finally, I would like to thank my family for their endless love and the continuous support.

Kaiserslautern, in August 2018

Samer Alzyod

To my parents and brothers for their love and support

ABSTRACT

A Coupled SQMOM-CFD Population Balance Framework for Modelling and Simulation of Liquid-liquid Extraction Equipment

The growing computational power enables the establishment of the Population Balance Equation (PBE) to model the steady state and dynamic behavior of multiphase flow unit operations. Accordingly, the two-phase flow behavior inside liquid-liquid extraction equipment is characterized by different factors. These factors include: interactions among droplets (breakage and coalescence), different time scales due to the size distribution of the dispersed phase, and micro time scales of the interphase diffusional mass transfer process. As a result of this, the general PBE has no well known analytical solution and therefore robust numerical solution methods with low computational cost are highly admired.

In this work, the Sectional Quadrature Method of Moments (SQMOM) (Attarakih, M. M., Drumm, C., Bart, H.-J. (2009). *Solution of the population balance equation using the Sectional Quadrature Method of Moments (SQMOM)*. *Chem. Eng. Sci.* 64, 742-752) is extended to take into account the continuous flow systems in spatial domain. In this regard, the SQMOM is extended to solve the spatially distributed nonhomogeneous bivariate PBE to model the hydrodynamics and physical/reactive mass transfer behavior of liquid-liquid extraction equipment. Based on the extended SQMOM, two different steady state and dynamic simulation algorithms for hydrodynamics and mass transfer behavior of liquid-liquid extraction equipment are developed and efficiently implemented. At the steady state modeling level, a Spatially-Mixed SQMOM (SM-SQMOM) algorithm is developed and successfully implemented in a one-dimensional physical spatial domain. The integral spatial numerical flux is closed using the mean mass droplet diameter based on the One Primary and One Secondary Particle Method (OPOSPM which is the simplest case of the SQMOM). On the other hand the hydrodynamics integral source terms are closed using the analytical Two-Equal Weight Quadrature (TEQWQ). To avoid the numerical solution of the droplet rise velocity, an analytical solution based on the algebraic velocity model is derived for the particular case of unit velocity exponent appearing in the droplet swarm model. In addition to this, the source term due to mass transport is closed using OPOSPM. The resulting system of ordinary differential equations with respect to space is solved using the MATLAB adaptive Runge–Kutta method (ODE45). At the dynamic modeling level, the SQMOM is extended to a one-dimensional physical spatial domain and resolved using the finite volume method. To close the mathematical model, the required quadrature nodes and weights are calculated using the analytical solution based on the Two Unequal Weights Quadrature (TUEWQ) formula. By applying the finite volume method to the spatial domain, a semi-discrete ordinary differential equation system is obtained and solved. Both steady state and dynamic algorithms are extensively validated at analytical, numerical, and experimental levels. At the numerical level, the predictions of both algorithms are validated using the extended fixed pivot technique as implemented in PPBLab software (Attarakih, M., Alzyod, S., Abu-Khader, M., Bart, H.-J. (2012). *PPBLAB: A new multivariate population balance environment for particulate system modeling and simulation*. *Procedia Eng.* 42, pp. 144-562). At the experimental validation level, the extended SQMOM is successfully used to model the steady state hydrodynamics and physical and reactive mass transfer behavior of agitated liquid-liquid extraction columns under different operating conditions. In this regard, both models are found efficient and able to follow liquid extraction column behavior during column scale-up, where three column diameters were investigated (DN32, DN80, and DN150). To shed more light on the local interactions among the contacted phases, a reduced coupled PBE and CFD framework is used to model the hydrodynamic behavior of pulsed sieve plate columns. In this regard, OPOSPM is utilized and implemented in FLUENT 18.2 commercial software as a special case of the SQMOM. The droplet-droplet interactions (breakage and coalescence) are taken into account using OPOSPM, while the required information about the velocity field and energy dissipation is calculated by the CFD model. In addition to this, the proposed coupled OPOSPM-CFD framework is extended to include the mass transfer. The proposed framework is numerically tested and the results are compared with the published experimental data. The required breakage and coalescence parameters to perform the 2D-CFD simulation are estimated using PPBLab software, where a 1D-CFD simulation using a multi-sectional grid is performed. A very good agreement is obtained at the experimental and the numerical validation levels.

Keywords: Liquid-liquid extraction, steady state, transient state, population balances, SQMOM, SM-SQMOM, hydrodynamics, mass transfer, reactive extraction, 1D-CFD, 2D-CFD, pulsed and stirred columns

ZUSAMMENFASSUNG

Ein hybrider SQMOM-CFD Populationsbilanz-Ansatz für die Modellierung und Simulation von Flüssig-Flüssig-Extraktionsprozessen

Zunehmend wachsende Rechenleistungen ermöglichen die Aufstellung und Lösung komplexer Populationsbilanzgleichungen, um das stationäre sowie dynamische Verhalten von Mehrphasen-Strömungen zu modellieren. Dementsprechend wird die zweiphasige Strömung, wie sie bei der Flüssig-Flüssig-Extraktion vorzufinden ist, durch verschiedene Faktoren gekennzeichnet. Diese Faktoren umfassen Interaktionen zwischen den Tröpfchen (Koaleszenz und Zerfall) sowie Makrozeitskalen aufgrund der Tropfengrößenverteilung der dispersen Phase als auch Mikrozeitskalen des diffusen Stoffübergangprozesses an der Phasengrenzfläche. Infolge dessen ermöglicht die allgemeine Populationsbilanzgleichung (PBE) keine bekannte analytische Lösung, weshalb robuste numerische Methoden mit niedrigem Rechenaufwand in hohem Maße angestrebt werden.

In dieser Arbeit wird die Sektional Quadratur-Methode von Momenten (SQMOM) (Attarakih, M.M., Drumm, C., Bart, H. - J. (2009). *Solution of the population balance equation using the Sectional Quadrature Method of Moments (SQMOM)*. *Chem. Eng. Sci.* 64, 742-752) erweitert, um den kontinuierlichen Betriebszustand in der räumlichen Domäne zu berücksichtigen. Daher wird das SQMOM erweitert, um räumlich verteilte nicht homogene zweidimensionale PBE zu lösen, um das hydrodynamische Verhalten und das Stoffübergangsverhalten (auch bei reaktiven Systemen) entsprechend zu modellieren. Basierend auf der erweiterten SQMOM werden zwei unterschiedliche stationäre und dynamische Simulationsalgorithmen zur Beschreibung der Hydrodynamik und des Stoffübergangs in Flüssig-Flüssig-Extraktionsprozessen entwickelt und implementiert.

Hinsichtlich der stationären Modellierung wird ein Algorithmus, der die eindimensionale räumliche Durchmischung berücksichtigt (SM-SQMOM), entwickelt und implementiert. Der integrale spatiale numerische Zustand wird durch den Tropfendurchmesser basierend auf der One Primary and One Secondary Particle Method (OPOSPM welches die einfachste Methode darstellt) berücksichtigt. Weiter werden die integralen hydrodynamischen Quellterme unter Verwendung der analytischen Two_Equal Weight Quadrature (TEqWQ) erschlossen. Um die numerische Lösung der Tropfenaufstiegsgeschwindigkeit zu umgehen, wird eine analytische Lösung, die auf dem algebraischen Geschwindigkeitsmodell basiert, für den besonderen Fall des Einheitsgeschwindigkeitsexponenten abgeleitet, der in das Tropfenschwarmmodell einfließt. Darüber hinaus wird der durch den Stofftransport bedingte Quellterm mithilfe von OPOSPM erfasst. Das so resultierende räumliche System aus gewöhnlichen Differentialgleichungen wird unter Verwendung der anpassungsfähigen Runge-Kutta MATLAB-Methoden (ODE45) gelöst. Hinsichtlich des dynamischen Modells wird das SQMOM auf ein eindimensionales räumliches Gebiet erweitert und mithilfe der finiten Volumenmethode gelöst. Um das mathematische Modell abzuschließen, werden die erforderlichen Quadraturknoten und die Gewichte unter Verwendung der analytischen Lösung berechnet, die auf der Formel, der Two Unequal Weights Quadrature (TUEWQ) basiert. Indem man die finite Volumenmethode auf den Raum anwendet, wird ein semi-diskretes gewöhnliches Differentialgleichungssystem erhalten und gelöst. Sowohl die stationären als auch dynamischen Algorithmen werden auf dem analytischen, numerischen und experimentellen Wege umfangreich validiert. Auf dem numerischen Niveau werden die Vorhersagen beider Algorithmen mithilfe der erweiterten Fixed Pivot Technik, wie sie in PPBLab-Software implementiert ist, validiert (Attarakih, M., Alzyod, S., Abu-Khader, M., Bart, H.-J. (2012). *PPBLAB: A new multivariate population balance environment for particulate system modeling and simulation*. *Procedia Eng.* 42, S. 144-562). Auf der experimentellen Validierungsebene wird die erweiterte SQMOM angewandt, um die stationäre Hydrodynamik und den (reaktiven) Stofftransport in Flüssig-Flüssig Extraktionskolonnen unter verschiedenen Betriebsbedingungen zu untersuchen. In diesem Zuge werden beide Modelle auf ihre Anwendbarkeit hinsichtlich des Scale-up (DN32, DN80 und DN150) von Flüssigextraktionskolonnen untersucht. Um die lokalen Wechselwirkungen zwischen den sich in Kontakt befindlichen Phasen besser zu beleuchten, wird ein reduziertes gekoppeltes Rahmenmodell aus PBE und CFD eingeführt, mit dem das hydrodynamische Verhalten von pulsierten Siebbodenkolonnen modelliert werden kann. Aus diesem Grund wird OPSOPM als spezifischer Anwendungsfall von SQMOM in die kommerziell erwerbliche Software FLUENT 18.2 implementiert. Die Tropfen-Tropfen-Wechselwirkungen (Bruch und Koaleszenz) werden durch OPOSPM berücksichtigt, während die notwendigen Informationen über das Geschwindigkeitsfeld und Energiedissipation durch CFD Modelle berechnet werden. Darüber hinaus wird

das vorgeschlagene gekoppelte OPOSPM-CFD-Rahmenmodell um den Einfluss des Stofftransports erweitert. Dieses Rahmenmodell wird numerisch getestet und die so erhaltenen Resultate in den Kontext zu veröffentlichten experimentellen Daten gestellt. Die für die 2D-CFD Simulation benötigten Bruch- und Koaleszenzparameter werden mittels PPBLab abgeschätzt, wobei eine 1D-CFD Simulation mit einem multi-sektionalen Gitter zugrunde gelegt wird. Hierbei wird eine hohe Übereinstimmung der experimentellen und numerischen Validierungsebenen erreicht.

Keywords: Flüssig-Flüssig-Extraktion, stationär, transient, Populationsbilanzen, SQMOM, SM-SQMOM, Hydrodynamik, Stoffaustausch, Reaktivextraktion, 1D-CFD, 2D-CFD, pulsierte und gerührte Kolonen.

Contents

List of publication	iii
List of oral and poster presentations	iv
List of symbols	v
An overview	1
1. Introduction	1
1.1 Population balance modeling and numerical solution methods.....	5
1.2 Motivation and aims of this work.....	
1.3 Thesis Outline.....	6
2. Detailed Population Balance Model (DPBM)	7
2.1 General Population Balance Equation.....	8
2.2 Spatially Distributed Population Balance Equation (SDPBE).....	9
2.3 Numerical solution methods of the PBE.....	10
2.3.1 Moments based methods.....	10
2.3.2 Quadrature Method Of Moments (QMOM).....	10
2.3.3 Quadrature Method Of Moments (QMOM).....	10
2.3.4 Direct Quadrature Method Of Moments (DQMOM).....	11
2.3.5 Sectional Quadrature Method Of Moments (SQMOM).....	12
2.3.6 Cumulative Quadrature Method Of Moments (CQMOM).....	17
2.3.7 The Differential Maximum Entropy Method (DMaxEntM).....	17
3. A nonhomogeneous bivariate extension of the SQMOM	18
4. The Spatially Mixed-SQMOM (SM-SQMOM)	21
5. A Coupled reduced OOSPM-CFD framework for modeling of liquid-liquid extraction columns	23
6. Conclusions	25
References	27
Chapter 1: One Dimensional Dynamic Modeling of Liquid-liquid Extraction Equipment using the SQMOM as a Reduced PBM	35
1.1 Introduction	35
1.2 Dynamic modeling of liquid-liquid extraction equipment using the SQMOM	36
1.2.1 Spatial Discretization of the SQMOM.....	36
1.3 Column hydrodynamics and mass transfer	38
1.3.1 Droplet rising velocity.....	38
1.3.2 Droplet breakage.....	39
1.3.3 Droplet coalescence.....	40
1.3.4 Interphase mass transfer.....	41
1.4 Analytical, numerical and experimental validation	38
1.4.1 Analytical validation.....	42
1.4.2 Numerical and experimental validation.....	43
1.5 Conclusions	46

References	51
Chapter 2: Steady State Modeling of Liquid-liquid Extraction Equipment using the Spatially Mixed-SQMOM as a Reduced PBM	51
2.1 Introduction	51
2.2 Steady state modeling of liquid-liquid extraction equipment using the SM-SQMOM	52
2.2.1 The SM-SQMOM implementation.....	52
2.3 Numerical and experimental validation	54
2.3.1 RDC liquid-liquid extraction column	54
2.3.2 Kühni liquid-liquid extraction column.....	58
2.4 Conclusions	60
References	61
Chapter 3: Steady State Modeling of Reactive Liquid-liquid Extraction of Zinc with D2EHPA using the SM-SQMOM	63
3.1 Introduction	63
3.2 Experimental investigations	64
3.2.1 Experimental procedure.....	64
3.2.2 Chemical reaction kinetics.....	65
3.3 Mathematical model: solute transport equations	66
3.4 Experimental validation	67
3.5 Conclusions	70
References	71
Chapter 4: CFD Modeling of Pulsed Sieve Liquid-liquid Extraction Columns the OPOSPM as Reduced DPBM	73
4.1 Introduction	73
4.2 The OPSOPM-CFD framework	75
4.3 Computational domain and boundary conditions	78
4.4 Analytical, numerical and experimental validation	79
4.4.1 Analytical validation.....	79
4.4.2 Pulsed sieve plate DN72 column: numerical and experimental validation.....	79
4.4.3 Pulsed sieve plate DN80 column: numerical and experimental validation.....	81
4.5 Conclusions	83
References	84

List of Publications

This thesis is based on the following publications that are referred to in the text using the standard literature citing employed in this overview.

- I. Alzyod, S., Attarakih, M., Bart, H.-J. (2018). CFD modelling of pulsed sieve plate liquid extraction columns using OPOSPM as a reduced population balance model: hydrodynamics and mass transfer. *Comput. Aided Chem. Eng.*, 43, 451-456.
- II. Alzyod, S., Attarakih, M., Hasseine, A., Bart H.-J. (2017a), Steady state modelling of a Kühni liquid extraction column using the Spatially-Mixed Sectional Quadrature Method Of Moments (SM-SQMOM). *Chem. Eng. Res. Des.*, 117, 549–556.
- III. Alzyod, S., Korb, C., Attarakih, M., Bart, H.-J. (2017b). Steady State Population Balance Modeling of Zinc Extraction in a Kühni Liquid-liquid Extraction Column, Proceedings of the International Solvent Extraction Conference (*ISEC2017*), 63-70. Miyazaki, Japan.
- IV. Alzyod, S., Attarakih, M., Bart, H.-J. (2017c). CFD Modelling of pulsed sieve plate liquid extraction columns using OPOSPM as a reduced population balance model, *Comput. Aided Chem. Eng.*, 40, 61-66.
- V. Korb, C., Alzyod, S., Attarakih, M., Bart, H.-J. (2017). SQMOM-Modellierung der Hydrodynamik in Kühni-Kolonnen bei der Reaktivextraktion, *Chem. Ing. Tech.*, 89, 1-11.
- VI. Alzyod, S., Attarakih, M., Bart H.-J. (2016a). Dynamic Modelling of Kühni Liquid Extraction Columns Using the Sectional Quadrature Method Of Moments (SQMOM). *Comput. Chem. Eng.*, 94, 1-12.
- VII. Alzyod, S., Attarakih, M., Bart H.-J. (2016b). The Sectional Quadrature Method of Moments (SQMOM): An extension to nonhomogeneous bivariate population balances. *Chem. Eng. Res. Des.*, 117, 549–556.
- VIII. Alzyod, S., Attarakih, M., Hasseine A., Bart H.-J. (2016c), Population Balance Modelling of Liquid Extraction Columns using the Sectional Quadrature Method of Moments (SQMOM), *Comput. Aided Chem. Eng.*, 38, 427-432.
- IX. Alzyod, S., Attarakih, M., Bart H.-J., (2016d). Detailed Modeling of an RDC liquid extraction column using the Sectional Quadrature Method Of Moments (SQMOM), In: Fraunhofer ITWM (Hg.): Young Researchers Symposium 2016 (YRS 2016). Proceedings: April, 14th-15th 2016, Fraunhofer-Zentrum Kaiserslautern. Stuttgart: *Fraunhofer Verlag*, 9-14.
- X. Hlawitschke M., Attarakih, M., Alzyod, S., Bart H.-J., (2016), CFD based extraction column design-Chances and challenges, *Chin. J. Chem. Eng.*, 24, 259-263.

List of Oral and Poster Presentations

- I. Alzyod, S., Attarakih, M., Bart, H.-J. CFD modelling of pulsed sieve plate liquid extraction columns using OPOSPM as a reduced population balance model: hydrodynamics and mass transfer. The 28th European Symposium on Computer-Aided Process Engineering (*ESCAPE-28*), 10-13 June 2018, Graz, Austria.
- II. Alzyod, S., Korb, C., Attarakih, M., Bart, H.-J. Steady State Population Balance Modeling of Zinc Extraction in a Kühni Liquid-liquid Extraction Column. The International Solvent Extraction Conference (*ISEC2017*), 5-9 November, 2017, Miyazaki, Japan.
- III. Alzyod, S., Attarakih, M., Bart, H.-J. Mathematical modelling of liquid-liquid extraction columns using the Sectional Quadrature Method of Moments (SQMOM). The annual meeting of the ProcessNet-Fachgruppen Extraktion (*ProcessNet*), 6-8 March 2017, Köln, Germany.
- IV. Alzyod, S., Attarakih, M., Bart, H.-J. CFD Modelling of pulsed sieve plate liquid extraction columns using OPOSPM as a reduced population balance model. The 27th European Symposium on Computer-Aided Process Engineering (*ESCAPE-27*), 1-5 October 2017, Barcelona, Spain.
- V. Attarakih, M., Alzyod, S., Bart H.-J. Process Intensification of the Distillation Section of the DiMethyl Ether (DME) Process Using CHEMCAD. The *CHEMCAD* user meeting, 15 September 2017, Berlin, Germany.
- VI. Attarakih, M., Alzyod, S., Bart H.-J. Steady State Modelling and Parametric Optimization Drying Oil Process using CHEMCAD and COCO Process Simulators. The *CHEMCAD* user meeting, 15 September 2017, Berlin, Germany.
- VII. Alzyod, S., Attarakih, M., Hasseine A., Bart H.-J. Population Balance Modelling of Liquid Extraction Columns using the Sectional Quadrature Method of Moments (SQMOM). The 26th European Symposium on Computer-Aided Process Engineering (*ESCAPE-26*), 12-15 Jun 2016, Portorož, Slovenia.
- VIII. Alzyod, S., Attarakih, M., Hasseine, A., Bart H.-J. Steady state modelling of a Kühni liquid extraction column using the Spatially-Mixed Sectional Quadrature Method Of Moments (SM-SQMOM). The 22nd International Congress of Chemical and Process Engineering (*CHISA-2016*) and the 19th Conference on Process Integration, Modelling and Optimisation for Energy Saving and Pollution Reduction (PRES 2016), 27-31 August 2016, Prague, Czech Republic.
- IX. Alzyod, S., Attarakih, M., Bart H.-J. Detailed Modelling of an RDC liquid extraction column using the Sectional Quadrature Method Of Moments (SQMOM). Young Researchers Symposium 2016 (*YRS-2016*), 14-15 April 2016, Fraunhofer-Zentrum Kaiserslautern, Germany.
- X. Alzyod, S., Attarakih, M., Dutta, A., Bart, H.-J. The Sectional Quadrature Method of Moments (SQMOM): An Application to Liquid-liquid Extraction Columns. Mathematics in (bio) Chemical Kinetics and Engineering (*MaCKiE-2015*), 2-3 July 2015, Ghent, Belgium.

List of Symbols

c	Solute concentration (kg/m^3)
D	Axial dispersion coefficients (m^2/s)
d, d_{30} , d_{32}	Droplet diameters (m)
f	Number density distribution function (s^{-1})
$F_{r,m}$	Two dimensional flux vector transformation
h	Source term as given by Eq.(2)
H	Column height (m)
$J(d, \gamma)$	Jacobian matrix as given by Eq.(10)
k_{od}	Overall mass transfer coefficient (m/s)
m	Solute distribution coefficient ($(\text{kg/m}^3)/(\text{kg/m}^3)$)
N	Droplets number concentration (m^{-3})
N_c	Number of numerical cells
N_{pp}	Number of sections
N_q	Number of quadrature points (-)
S	Source term as given by Eq.(5)
t	Time (s)
u	Velocity (m/s)
v	Droplet volume (m^3)
w	Quadrature weight
z	Space coordinate

Greek Symbols

μ	Moment transformation function
α	Dispersed phase volume fraction
Γ	Breakage frequency (1/s)
ρ	Source term as given by Eq.(26)
γ	Vector of external coordinate
δ	Driac delta function (m^{-1})
ϑ	Mean number of daughter droplets
λ_i	As given by Eqs.(55-59)
ξ	Mass transfer rate as given by Eq.(6)
τ	Residence time (s)
ω	Coalescence frequency (m^3/s)
Ω_d	Droplet diameter vector
ψ	Vector of internal coordinates

Subscripts

c	Continuous phase
d	Dispersed phase
j	Numerical cell index
m	Mass transfer index
r	Hydrodynamics index
s	Slip velocity
t	Terminal velocity

Superscripts

i	Section index
-	Mean value
r	Moment's index
in	Inlet

out

Outlet

Abbreviations

BvSDPBE	Bivariate Spatially Distributed Population Balance Equation
CFD	Computational Fluid Dynamics
CPU	Process time
CQMOM	Cumulative Quadrature Of Moments
D2EHPA	Di-(2-ethylhexyl)Phosphoric Acid
D2uQMoGeM	Direct Dual Quadrature Method of Generalized Moments
D2uQMoGeM	Direct Dual Quadrature Method of Generalized Moments
DAE-QMOM	Differential Algebraic Equations-Quadrature Method of Moments
DMaxEntM	Differential Maximum Entropy Method
DPBM	Droplet Population Balance Model
DQMOM	Direct Quadrature Method Of Moments
DQST	Direct Quadrature Spanning Tree
DSD	Droplet Size Distribution
DuQMoGeM	Dual-quadrature Method of Generalized Moments
EFPT	Extended Fixed Pivot Technique
EQMOM	Extended Quadrature Method Of Moments
FPM	Finite Point Set Method
GFP	Generalized Fixed-Pivot
GWA	Golub-Welsch Algorithm
JMT	Jacobian Matrix Transformation
LLEC	Liquid-liquid Extraction Column
LLECMOD	Liquid-Liquid Extraction Column MODule
LQMDA	The Long Quotient Modified Difference Algorithm
MaxEntM	Shannon Maximum Entropy Method
MOM	Method of Moments
MPSPM	Multi Primary and one Secondary Particle Method
MPT	Moving Pivot Technique
ODE	Ordinary differential equation
OPOSPM	One Primary One Secondary Particulate Method
PBE	Population Balance Model
PBM	Population Balance Model
PDA	Product Difference Algorithm
PDE	Partial Differential Equation
PPBLab	Particulate Population Balance Laboratory
QMOM	Quadrature Method Of Moments
RDC	Rotating Disk Contactor
SDPBE	Spatially Distributed Population Balance Equation
SM-SQMOM	Spatially Mixed- Sectional Quadrature Method of Moments
SQMOM	Sectional Quadrature Method of Moments
TEqWQ	Two-Equal Weight Quadrature
TUEQWQ	Two-Unequal weight Quadrature
VOF	Volume of Fluid

An Overview

A Coupled SQMOM-CFD Population Balance Framework for Modelling and Simulation of Liquid-liquid Extraction Equipment

1. Introduction

Liquid-liquid extraction is a mass transfer unit operation, which is commonly used in hydrometallurgy, pharmaceutical, and petroleum industries. The main idea behind liquid-liquid extraction is to separate the desired components based on their chemical structure rather than the relative volatility. Therefore, it has the priority when dealing with heat sensitive, small concentration, and close boiling point substances (Hanson, 1971; Treybal, 1993; Perry and Green, 2008; Ramaswamy et al., 2013). In this separation technique, one of the contacted phases is introduced as a discrete dispersed phase, while the other one is introduced as a continuous phase. The selection of the dispersed phase depends on the physical properties and operating conditions. As a rule of thumb, the dispersed phase should have a higher viscosity and a lower interfacial tension than the continuous phase to achieve a higher throughput operational range and to obtain better dispersion. Moreover, the available mass transfer interfacial area can be enhanced by introducing a higher inlet flow ratio between the dispersed and the continuous phases. In general, the available extraction columns are classified according to agitation into three major types: non-agitated, mechanically agitated, and pulsed liquid-liquid extraction columns. In these columns, the contacted phases are subjected to a continuous change in their identity due to the applied agitation or pulsation intensities. The applied agitation or pulsation characterizes the flow patterns inside the extraction column and increases the available interfacial area which enhances the mass transfer process. As a result of this, the dispersed phase internal properties (droplet size, and solute content) are distributed randomly and vary along the column height where the resulted droplet size distribution plays a decisive role in the design and operation of liquid-liquid extraction equipment (Attarakih and Bart, 2014). During droplets movement inside the extraction column, these droplets interact where coalescence among droplets of different or same sizes reduce the total number of droplets and the dispersed phase holdup (Gourdon et al., 1994; Mohanty, 2000; Garthe, 2006). These collisions mainly occur due to column internals and result in a droplet velocity distribution (Gourdon et al., 1994; Garthe, 2006; Drumm et al., 2010; Hlawitschka, 2013; Attarakih et al., 2015b). On the contrary, the breakage phenomenon takes place in liquid extraction columns due to shear forces and the turbulent continuous phase, which results in a higher number of droplets and dispersed phase holdup. Here, the physical properties (mainly the surface tension and viscosity), the droplets size, and the energy dissipation have a significant contribution to the breakage and coalescence phenomena (Coulaloglou and Tavlarides, 1977; Hamilton and Pratt, 1984; Garthe, 2006; Liao and Lucas, 2010; Maaß et al., 2012).

Due to the growing market demand, fast and accurate design and scale-up procedures of liquid-liquid extraction equipment are needed. In practice, the design of suitable extraction equipment is a challenging task, where a reliable design should take into account droplet-droplet interactions, the interphase mass transfer phenomena at droplets level, and the operating conditions. As a result of this, more attention is needed to model the coupled hydrodynamics and mass transfer phenomena inside the extraction equipment. In spite of decades of research, liquid-liquid extraction equipment design and scale-up procedures are still faced by the complex dynamic behavior of the dispersed phase. Accordingly, it is easier to design a chemical process, based on steady state behavior, which is practically uncontrollable (Skogestad, 1997). Therefore, the dynamic behavior of the dispersed phase should be also known. To shed more light on the dynamic behavior of the dispersed phase and to match the market demand, advanced mathematical models, which represent accurately the prevailing physical phenomena inside the extraction equipment, should be utilized (Steiner, 1994; Attarakih and Bart, 2014, 2015a). In this regard,

the reported mathematical models in literature for modeling of liquid-liquid extraction equipment include: empirical, differential, and stagewise models (Treybal, 1993; Steiner, 1994; Mohanty, 2000; Attarakih, 2004). In the empirical models, the dispersed phase integral properties (holdup and mean droplet diameter) are correlated based on experimental data in terms of column dimensions, operating conditions, and the physical properties. Indeed, these models are designed for specific column dimensions and physical properties ranges and hence they are not suitable for column design and scale-up purposes. In stagewise models, a series of completely mixed stirred tanks are used to represent the actual column height and the deviation from the ideal plug flow is taken into account by considering the forward and backward flow components (Treybal, 1993; Steiner, 1994; Mohanty 2000; Attarakih, 2004).

Unlike the aforementioned classical models, the differential models can be further classified based on the dispersed phase modeling approach into: pseudo-homogenous phase and the Detailed Droplet Population Balance Model (DPBM). These models are formulated by applying the conservation principles for both contacted phases inside the extraction equipment with the proper boundary conditions. Concerning the pseudo-homogenous models, a first attempt to design reactive liquid-liquid extraction equipment was presented by Veglio and Slater (1996). The authors proposed a numerical design procedure using a constant droplet diameter and concluded that, the most important design factor, which affects the column height, is the zinc ions mass transfer coefficient in the continuous phase. Wachs et al. (1997) presented a simplified empirical dynamic model for controlling Karr liquid-liquid extraction column. Weinstein et al. (1998) derived and solved a theoretical dynamic model to describe the hydrodynamic and mass transfer behavior of Karr and Kühni liquid-liquid extraction columns, where they assumed a constant average droplet diameter along the column height. In the same direction, Mjalli (2005) derived a non-equilibrium backflow mixing cell model to control product compositions of a Scheibel liquid-liquid extraction column using a neural network model. Ji et al. (2006) studied the role of kinetics of zinc extraction with D2EHPA in a packed bed liquid-liquid extraction column, where they used a simplified mathematical model based on the backmixing model. In addition to this, the authors assumed constant holdup and mean droplet diameter values along the column height. Goryunov and Mikhaylov (2012) derived and implemented a non-equilibrium dynamic model (based on the mass transfer diffusion kinetics for pulsed liquid-liquid extraction columns) and automatic control system using MATLAB/SIMULINK package. Neto and Mansur (2013) modeled the reactive extraction process of zinc with D2EHPA in a short Kühni liquid-liquid extraction column, operated in a batch mode, using back and forward mixing models. In their work, the required dispersed phase integral properties to conduct the simulation were calculated using lumped empirical correlations published by Kumar and Hartland (1996). Indeed, assuming constant dispersed phase integral properties is not realistic because the dispersed phase identity changes along the column height due to the breakage and coalescence phenomena as mentioned earlier. As a result of this, a detailed description of the dispersed phase behavior is required. Indeed, the aforementioned back-mixing and dispersion models used in industry ignore the permanent droplet-droplet interactions and hence they predict neither the correct steady state nor the actual dynamic behavior of the dispersed phase (Steiner, 1994; Schmidt et al., 2006; Attarakih et al., 2015a; Alzyod et al., 2016a). In addition to this, they neglect the discreet nature of the dispersed phase by assuming it to behave as a pseudo homogeneous phase and the deviation from the ideal plug flow is taken into account using the axial dispersion coefficient (Thornton, 1992; Steiner, 1994; Mohanty, 2000; Attarakih, 2004; Drumm, 2010). A promising approach to overcome some of these limitations is to utilize the DPBM as a mathematical framework.

1.1 Population balance modelling and numerical solution methods

Due to the growing computational power, the DPBM is accepted as an essential simulation framework for modeling of the steady state and dynamic behavior of multiphase flow unit operations. This behavior is characterized by the coupled interacting hydrodynamic and mass transfer phenomena such as: droplet breakage, coalescence, growth (or shrinking) and the interfacial physical and reactive mass transfer process. Such unit operations include: crystallization (Hulburt and Katz, 1964; Czaplá et al., 2009; Liu et al., 2010; Fysikopoulos et al., 2017), bubble columns (Deen et al., 2001; Petitti et al., 2010; Nauha and Alopaeus, 2013; Attarakih et al., 2016; Buffo et al., 2016), and liquid-liquid extraction columns (Weiss and Bart, 1993; Attarakih et al., 2004; Vikhansky and Kraft, 2004; Schmidt et al., 2006; Tiwari et al., 2008; Drumm et al., 2010; Sharma, 2009; Hlawitschka 2013; Wächtler et al., 2014; Attarakih et al., 2013a, 2014, 2015a, b; Alzyod, 2016a, 2017a, b, c, 2018). A first attempt to utilize the DPBM in chemical engineering applications was presented by Hulburt and Katz (1964), where they presented a mathematical formulation of the DPBM for crystallization process. Indeed, the DPBM is a geometrical dependent

integro-partial differential equation with highly nonlinear integral source terms and hence it has no general well known analytical solution except for a simplified special cases (Ramkrishna, 2000; Marchisio and Fox, 2005; Vikhansky, 2013; Attarakih and Bart, 2014). Accordingly, accurate numerical solution algorithms with low computational cost are required (Attarakih, 2004; Gimbun et al., 2009). In this regard, several numerical methods had been proposed to achieve these goals. In general, these methods can be classified into: method of characteristics, moment based methods, Monte Carlo simulation, finite difference method, and the recent differential maximum entropy method (McGraw, 1997; Ramkrishna, 2000; Mohanty, 2000; Attarakih, 2004; Marchisio and Fox, 2005; Dorao and Jakobsen, 2006; Lage, 2011; Attarakih and Bart, 2014). Among these methods, the moment based methods are fairly simple to be implemented and provide accurate results with moderate computational cost (Marchisio and Fox, 2005; Attarakih et al., 2009a; Vikhansky, 2013). Therefore, these methods are suitable to couple the DPBM with CFD codes to simulate complex column geometry (Tiwari et al., 2008; Drumm et al., 2010; Sharma, 2011; Wächtler et al., 2011; Hlawitschka, 2013; Attarakih et al., 2015b, 2016; Alzyod et al., 2017c, 2018). The main idea behind these methods is to reduce the detailed population balance equation into a set of Ordinary Differential Equations (ODE's) or Partial Differential Equations (PDE's), and then the particle size distribution can be tracked through the conserved moments. In this regard, Hulburt and Katz (1964) developed the Method Of Moments (MOM). This method is very attractive from computational point of view (Marchisio and Fox, 2005; Vikhansky, 2013). However, it doesn't provide any sufficient information about the required number of moments to get accurate results and to close the DPBM (Attarakih 2004; Marchisio and Fox, 2005; Lage, 2011; Vikhansky, 2013). In addition to this, the implementation of this method may be problematic when the equation contains general breakage, coalescence, and growth functions (Ramkrishna, 2000). To solve these problems, McGraw (1997) developed the Quadrature Method Of Moments (QMOM) and implement it to simulate the aerosols growth process. The principle of QMOM is to approximate the integral terms of the population balance equation by means of number of Gaussian quadrature points. Here, the required quadrature weights and nodes to approximate the integral terms are calculated by solving an eigenvalue problem based on the Product Difference Algorithm (PDA), which was developed by Gordon (1968). However, solving such a problem can be time consuming and usually the PDA is sensitive to small round-off errors as pointed out by many researchers (Attarakih et al., 2009a, b; John and Thein, 2012; Vikhansky, 2013). For example, Attarakih et al. (2009a, b) showed that the PDA suffers from a gradual increase in the round-off error when increasing the number of quadrature points due to the resulting large system of equations. In the same direction, John and Thein (2012) solved the QMOM for a batch process using three different eigenvalue algorithms: the Long Quotient Modified Difference Algorithm (LQMDA), the Product Difference Algorithm (PDA) and the Golub-Welsch Algorithm (GWA), where the authors concluded that the PDA was less efficient than the other algorithms and it may fail in certain applications. Another development in this research area is the Direct Quadrature Method Of Moments (DQMOM) which was introduced by Marchisio and Fox (2005). In this method, the quadrature weights and nodes are calculated directly by solving the governing transport equations. In spite of the DQMOM accuracy, this method could suffer from round-off errors as the number of quadrature points is increased (Vikhansky, 2013). In this regard, many researchers attempted to improve the available moments based methods. For example, Lage (2011) developed the Dual-quadrature Method of Generalized Moments (DuQMoGeM) and used the Gauss Christoffel quadrature rule to close the resulting model. Vikhansky (2013) proposed the Direct Quadrature Spanning Tree method (DQST) as a combination between the DQMOM and the Moving Pivot Technique (MPT). Attarakih et al. (2006a) extended the QMOM to model and simulate the coupled mass transfer and hydrodynamic behavior in a five compartments RDC liquid-liquid extraction column where they used the PDA to close the model. Gimbun et al. (2009) presented the Differential Algebraic Equations-Quadrature Method of Moments (DAE-QMOM), in which the solution proceeds by solving simultaneously the low order moments ODE's system and the nonlinear equations resulting from the quadrature approximation. Santos et al. (2013) developed The Direct Dual Quadrature Method of Generalized Moments (D2uQMoGeM) by combining the DQMOM and DuQMoGeM methods, where the quadrature weights and nodes are calculated as in the DQMOM. Unfortunately, these methods conserve the moments of the distribution but they are unable to reproduce the distribution itself which is needed in many engineering applications (Attarakih et al., 2009a; Souza et al., 2010; Yuan et al., 2012; Attarakih and Bart, 2014; Madadi-Kandjani and Passalacqua, 2015). Indeed, several reconstruction methods were proposed and coupled with the moments based methods to overcome this fundamental problem but without a general success. For example, Yuan et al. (2012) presented the Extended Quadrature Method Of Moments (EQMOM) followed by the work of Madadi-Kandjani and Passalacqua (2015) to solve the spatially homogeneous PBE, where the droplet size distribution is

approximated by a sum of nonnegative density functions. Actually, the work of Yuan et al. (2012) who presented the EQMOM and the work of Madadi-Kandjani and Passalacqua (2015) are based on the same idea of introducing a specified series of kernel density functions with a selected low-order moments to be preserved. Madadi-Kandjani and Passalacqua (2015) used the lognormal distribution as a kernel, while Yuan et al. (2012) used the gamma distribution function. The results obtained by Madadi-Kandjani and Passalacqua (2015) are compared to those provided by Yuan et al. (2012) with satisfactory results were obtained. The computational cost of the iterative solution is decreased using the lognormal density function due to the linear nature of this kernel. Unfortunately, these methods are computationally expensive, when using large number of tracked moments, due to the iterative solution procedure during the moments inversion step. On the other hand, John et al. (2007) proposed a reconstruction algorithm in which the droplet size distribution is approximated using a set of spline functions. This method has the advantage of reconstructing the distribution without any priori knowledge about the distribution shape. However, it fails to reconstruct the droplet size distribution accompanied by a local non-smooth behavior (Souza et al., 2010). Souza et al. (2010) improved this method by introducing the so called adaptive spline-based method algorithm. In the same direction, Attarakih (2013b) developed the Cumulative Quadrature Method Of Moments (CQMOM) to reconstruct the cumulative number density function, where the quadrature nodes and weights are calculated using the analytical solution of the extended product difference algorithm in terms of the droplet diameter as a continuous internal coordinate. Another development in this research area is the Sectional Quadrature Method Of Moments (SQMOM), which was introduced by Attarakih et al. (2009a). The SQMOM was developed, based on the primary and secondary particle concept, to solve the homogenous population balance equation by reducing it and conserving theoretically unlimited number of the droplet size distribution moments (Attarakih et al., 2009a). Within this framework, the internal coordinate (droplet diameter) is discretized into a finite number of sections and the droplets population is considered to behave as a single particle (primary particle) in each section. Unlike the classical moments based methods, the SQMOM is able to reconstruct the droplet size distribution without any assumptions concerning the distribution shape using only the first four low-order moment equations. This method is supplied with two analytical solutions to calculate the quadrature nodes and weights (in case of two quadrature points). Compared to the previous mentioned moment based methods, the SQMOM is considered as a comprehensive mathematical framework. This is because it combines the advantages of the method of classes and the QMOM and reduces their drawbacks (Attarakih et al., 2009a, 2014). In fact, the droplet size distribution can be reconstructed using the primary particles, while the secondary particles are responsible for breakage and coalescence events (Attarakih et al., 2009a). In order to study the real droplets hydrodynamic behavior, Attarakih et al. (2009a) used the SQMOM to simulate the hydrodynamics behavior in a continuous stirred tank vessel, where they concluded that the model equations are exact as those derived from the continuous DPBM for many popular droplet breakage and coalescence kernels. Moreover, the model accuracy can be easily increased by increasing the number of primary particles (sections). Attarakih et al. (2009a) showed that most of the available quadrature based methods are special cases from the general SQMOM and can be obtained by varying the number of primary and secondary particles. For example, if only one primary particle is used the QMOM and the DQMOM are obtained, while if only one secondary particle is used then the Moving Pivot Technique (MPT) is obtained. Another special case of the general SQMOM framework can be also obtained when using a finite number of primary particles and only one secondary particle. This method is called the Multi Primary one Secondary Particle Method (MPSPM). In this method, the droplets size distribution is divided into a specific number of subsections in which each primary particle is defined based on its number, volume, and mean concentration (Jaradat et al., 2012a). Jaradat et al. (2012a) extended MPSPM to include the momentum balance equation, where they modeled the hydrodynamics and mass transfer behavior of a pilot plant RDC DN80 liquid-liquid extraction column. The authors reported that the MPSPM is able to capture most of the relevant features of the continuous DPBM and it is a compromise between solution accuracy and CPU time requirements.

Another special case of the general SQMOM framework is obtained when using only one primary and one secondary particles. This method is called the One Primary One Secondary Particle Method (OPOSPM) (Attarakih et al., 2013a). In spite of its simplicity, OPOSPM retains most of the continuous DPBM features and hence it found many applications in CFD and online inverse problem research areas (Attarakih et al., 2012a; Jildeh et al., 2014; Mickler et al., 2014). For example, Attarakih et al., (2012a) developed a general optimization algorithm based on the OPOSPM to estimate the required coalescence model parameters using the experimental steady state holdup and mean droplet diameter profiles along the column height. Jildeh et al., (2014) followed the same procedure proposed by Attarakih et al., (2012a) to optimize Coulaloglou and Tavlarides (1977) coalescence model parameters for different Kühni column

geometries (DN80 and DN150) using different operating conditions. Mickler et al., (2014) developed an online monitoring and simulation tool based on OPOSPM within the context of model predictive control. Concerning CFD applications, Drumm et al. (2010) implemented OPOSPM using FLUENT 6.3 to simulate the hydrodynamic behavior of a pilot plant RDC liquid-liquid extraction column. In their work, the authors concluded that the coupled OPOSPM-CFD model is efficient from computational point of view since it reduces the CPU time by a factor of 5 compared to the classical method of classes. Hlawitschka (2013) extended the work of Drumm et al. (2010) to take into account the mass transfer process in both Kühni and RDC pilot plant liquid-liquid extraction columns using OpenFOAM software. In order to reduce the computational cost of the 3D-CFD simulation, another way for coupling the OPOSPM and CFD was introduced using the Finite Pointset Method (FPM) (Tiwari et al., 2008; Sharma, 2011). The new coupled OPOSPM-CFD model was found very attractive from a computational point of view. This is due to the fact that the FPM is able to predict the flow and velocity fields inside the extraction equipment, while OPOSPM is used to describe the nonlinear behavior of the dispersed phase. Wardle (2013) developed a hybrid multiphase CFD solver by combining the Eulerian multi-fluid method, the Volume Of Fluid (VOF) and OPOSPM to simulate an annular centrifugal liquid-liquid contactor used in processing of spent nuclear fuels. Attarakih et al. (2015b) implemented OPOSPM using FLUENT software to simulate the coupled hydrodynamics and mass transfer behavior of an RDC liquid-liquid extraction column with a height of 4.4 m. The required coalescence model parameters were optimized using PPBLab software (Attarakih et al., 2012b; 2017), which utilizes the extended fixed pivot technique as a one dimensional DPBM solver. In the same direction, Attarakih et al. (2015c) extended and coupled OPOSPM with the Shannon Maximum Entropy Method (MaxEntM) to simulate the hydrodynamics of bubble columns, where the extended model was found efficient to predict the bubble size distribution in the bubbly flow regime. Another development was introduced by Alzyod (2013) and Attarakih et al. (2015a), where they developed a MATLAB/SIMULINK module using OPOSPM as a reduced population balance model to simulate the steady state and dynamic behavior of Kühni liquid-liquid extraction columns. Recently, Kobert (2015) solved the kinetic Bhatnagar Gross Krook (BGK) model of gas dynamics by coupling the SQMOM and Finite Point Method (FPM). The new coupled OPOSPM-CFD model was found very attractive from a computational point of view.

Based on this condensed review, there are two different approaches to model liquid-liquid extraction columns using the DPBM framework. The first approach is to couple the DPB equation with 2D or 3D-CFD solvers (e.g. FLUENT, OpenFOAM), where the required information concerning the velocity field and the energy dissipation is obtained by CFD solvers as reported by the aforementioned studies. The second approach is to average flow field variables in each compartment and to solve the DPB equation in a 1D domain. In this approach, the required information concerning the velocity field and the energy dissipation is estimated using proper correlations. This approach appeared to be accurate and very efficient from computational point of view, where the required CPU time to perform the simulation is in order of minutes (Attarakih et al., 2012b, 2013a, 2017). Based on this approach, Attarakih et al., (2006b) developed the Liquid-Liquid Extraction Column MODule (LLECMOD) to simulate the hydrodynamics behavior of an RDC liquid extraction column as a first step and was extended later to simulate pulsed columns. In the same direction, Kalem et al., (2011) presented the Representative Drops (ReDrop) program, which is based on Monte Carlo approach. However, this approach requires large memory and computational power. Another development in this research area is the PPBLab (Particulate Population Balance Laboratory) software (Attarakih et al., 2012b; 2017). PPBLab is a MATLAB based environment for modeling of discrete flow processes in general and liquid-liquid extraction columns in particular using DPBM. PPBLab utilizes the recent PBE solution methods to model agitated, non-agitated and pulsed liquid extractions columns. These solution methods include: Mixed fixed-pivot and Quadrature Method Of Moments (QMOM), and the One Primary One Secondary Particle Method (OPOSPM). In a recent work, Attarakih et al. (2015b) showed that the 3D-CFD approach can be utilized to design proper correlations, which can be used later to perform the 1D-CFD simulation. Based on this, the authors concluded that the 1D-CFD simulation results using PPBLab software were found competitive with those obtained using 3D-CFD at both hydrodynamic and mass transfer levels.

1.2 Motivation and aims of this work

Up to date and due to advances in software engineering, the population balance framework added efficient modeling and simulation tools for two-phase flow problems. Accordingly, the two-phase flow behavior inside the extraction equipment is characterized by different factors. These factors include:

nonlinear interactions among droplets, different time scales due to the size distribution of the dispersed phase, and the micro time scale of the interphase diffusional mass transfer process (Attarakih et al., 2013a). In this regard, the DPBM flexibility makes it possible to take into account all of these factors and hence it is considered as a powerful mathematical tool for modeling of liquid-liquid extraction equipment. The growing market demand toward fast and accurate liquid-liquid extraction equipment simulation tools, calls for a special mathematical modeling approach based on more fundamental basis. Therefore, robust steady state and dynamic numerical algorithms, based on the DPBM, are of great importance. These algorithms should be able to increase the reliability of the liquid-liquid extraction equipment design, scale-up, and control procedures. In addition to this, recent advances in online measurements and model predictive control provide real-time access to system parameters, which are estimated based on the DSD (Maaß et al., 2012; Mickler et al., 2014). These parameters contain inherent information concerning droplet-droplet interactions such as breakage and coalescence phenomena (Attarakih et al., 2012a). In contrast to the aforementioned moments based methods, the SQMOM conserves the shape of the DSD, using only the first four low-order moments, and still keeps advantages of other moments based methods. The flexibility of the SQMOM makes it an attractive mathematical framework from computational point of view. For example, if only the dispersed phase mean integral properties are required, then the OPOSPM can be utilized a special case of the SQMOM. On the other hand, if the droplet size distribution is required, then more sections can be used, in compromise with the CPU time, to reconstruct distribution shape. In addition to this, the SQMOM avoids divergence problems arise when applying inversion eigenvalue algorithms to close the associated integral terms, which makes it a stable framework. Therefore, the SQMOM has the advantage over the other methods as a reduced DPBM for modeling of liquid-liquid extraction columns.

In this work the SQMOM is extended to solve the bivariate nonhomogeneous PBE in terms of the distribution marginal densities along the spatial domain to model the coupled hydrodynamic and physical/reactive mass transfer behavior of liquid-liquid extraction equipment (Alzyod et al., 2016a, b, c, d). As a first step, a one dimensional CFD model (1D-CFD) is introduced to explore the flexibility of the SQMOM in predicting of the droplet size distribution in agitated extraction columns (see chapters 1 and 2). These columns include: RDC and Kühni liquid-liquid extraction columns. In this regard, two different steady state and dynamic simulation algorithms, to model the coupled hydrodynamics and mass transfer behavior based on the SQMOM, are developed and tested (Alzyod et al., 2016a; 2017a, b). The dynamic framework is used for modeling of Kühni liquid-liquid extraction columns (see chapter 1), while the steady state algorithm is used to model the physical and reactive extraction processes inside RDC and Kühni extraction columns (see chapters 2 and 3). The availability of other PBE solvers such as the Extended-Fixed pivot Technique (EFPT) as implemented in PPBLab software (Attarakih et al., 2012b, 2017) aided to validate the proposed 1D-CFD SQMOM model prediction at the numerical level. In addition to this, an experimental validation using published data, at steady state and dynamic levels, has been done to explore the flexibility of the 1D-CFD framework to predict the actual coupled column hydrodynamic and the mass transfer behavior. In the second step, coupling of the SQMOM and the CFD-FLUENT software is believed to shed more light on the local interactions occurring among the dispersed phase droplets and the turbulent continuous phase. This can be achieved by utilizing the OPOSPM as a special case of the general SQMOM mathematical framework. Here, the OPOSPM is used to model the hydrodynamic behavior of pulsed sieve plate liquid-liquid extraction columns (Alzyod et al., 2017c). The droplet-droplet interactions (breakage and coalescence) are taken into account using the OPOSPM, while the required information about the velocity field and energy dissipation is estimated by the CFD solvers (see chapter 4). In addition to this, the proposed OPOSPM-CFD framework is extended to model the mass transfer behavior (Alzyod et al., 2018). In this regard, a specific DPBM-CFD framework for modeling the mass transfer process in pulsed sieve liquid-liquid extraction columns, to the best of authors' knowledge, is not published yet. Therefore, building such a coupled OPOSPM-CFD framework helps more to understand the effect of turbulence and local recirculation on the overall extraction efficiency. At the application level, the outcome of this work will provide a robust mathematical modeling approach for the coupled two-phase flow and interphase mass transfer in liquid-liquid extraction equipment.

1.3 Thesis outline

This overview is arranged as follows: in section 2 a general review concerning the DPBM is presented. In this regard, the spatially distributed bivariate PBE and the most commonly used moments based numerical methods for solving the PBE equation are reviewed. In Section 3 the bivariate extension

approach of the SQMOM is presented, where a general 1D-CFD dynamic framework for modeling of stirred liquid-liquid extraction equipment is developed. The proposed model predictions are validated at three different levels as presented in chapter 1. These validation levels include: analytical, numerical, and experimental levels. At the analytical level, the proposed 1D-CFD framework is validated using the published simplified analytical solutions (Attarakih et al., 2009a), while at the numerical level the framework predictions are validated using PPBLab software (Attarakih et al., 2012b, 2017). For the experimental validation, the model predictions are validated using published experimental data for a Kühni DN150 liquid-liquid extraction column. Section 4 is devoted to develop steady state 1D-CFD version of the SQMOM, which has the name of the Spatially Mixed-SQMOM (SM-SQMOM). The SM-SQMOM is used to model the physical and reactive flow inside stirred liquid-liquid extraction columns (RDC and Kühni) (see chapters 2 and 3). For the 2D-CFD modeling approach, a reduced coupled OPOSPM-CFD module to model the coupled hydrodynamics and mass transfer behavior of pulsed sieve plate liquid-liquid extraction column is developed and validated (see chapter 4). In this regard, the commercial CFD ANSYS/FLUENT is utilized for the coupling approach. In this work, each chapter has a short introduction concerning the related relevant topic. For more details concerning the theory and results, the reader can refer to the relevant publications.

2. Detailed population balance model (DPBM)

Fluid phases, which are discrete either at the molecular or particle levels, can be described by a general Boltzmann-type equation, typically referred to the Population Balance Equation (PBE) (Ramkrishna, 2000). A first effort to utilize the PBE in chemical engineering applications was given by Hulburt and Katz (1964), where they presented a mathematical formulation of the DPBM for the crystallization process. In this regard, the PBE is able to take the nonlinear behavior of the discrete dispersed phase into account to model multiphase flow unit operations. In such unit operations, the discrete phase elements (e.g. droplets) properties determine the overall equipment efficiency. In the context of the DPBM, elements of the dispersed phase are identified with respect to their internal and external coordinates. The internal coordinates include the information about the dispersed phase elements properties (e.g. size, and solute content), while the external coordinates retain the information about the spatial location of dispersed phase elements and time (Ramkrishna, 2000; Attarakih, 2004; Marchisio and Fox, 2005; Attarakih and Bart, 2014). Based on this, the population of elements of the dispersed phase, with respect to both internal and external coordinates, can be represented using a proper distribution density function. As a result of this, the PBE is able to track each element of the dispersed phase as represented by its own velocity and therefore the evolution of the density distribution function can be efficiently obtained. In the field of liquid-liquid dispersions in stirred tanks Valentas and Amundson (1966) developed a mathematical model based on the DPBM to study the droplet size distribution, where the proposed model takes the breakage and coalescence phenomena into account. In addition to this, the effect of the operating temperature on the drainage process during the coalescence phenomena was also studied. Shah and Ramkrishna (1972) used the DPBM to model the mass transfer phenomena in liquid-liquid dispersion in a continuous stirred tank. In their work, they formulated a trivariate PBE with respect to: the droplet size, the solute concentration, and the droplet age. However, this model assumes a low dispersed phase volume fraction and neglects the coalescence phenomena. Alopaeus et al., (2002) developed a model to simulate drop populations in stirred tanks. The model takes the breakage and coalescence phenomena into account, where the required fitting parameters to close the model kernels were obtained by fitting the model prediction with the online measured experimental data. In the field of liquid-liquid extraction columns, Casamatta and Vogelpohl (1985) proposed a differential mathematical model, based on the DPBM, using simplified breakage and coalescence kernels. Haverland et al. (1987) presented a model for the simulation of fluid dynamics of pulsed sieve plate columns based on the DPBM. The distribution density function was approximated using a normalized beta function and the model was validated using experimental results from studies performed using DN80 and DN225 pulsed sieve plate extraction columns. However, this model ignores the coalescence phenomena and hence it doesn't reflect the actual behavior of the discrete dispersed phase (Mohanty, 2000). Al Khani et al. (1989) used the DPBM to simulate the dispersed phase hydrodynamics and mass transfer behaviors of liquid extraction columns. The authors developed different iterative and numerical algorithms to solve the proposed steady state and dynamic models. However, these algorithms contain many adjustable parameters, which limit their applicability (Mohanty, 2000). In the same direction, Kronberger et al. (1995) presented a numerical algorithm, based on the Galerkin's method, to model the drop size distribution inside liquid-liquid extraction equipment.

Indeed, this algorithm is internally inconsistent and not efficient from computational of view because it contains many integrals in the source term (Attarakih, 2004). Mohanty and Vogelpohl (1997) presented a simplified stage-wise model, based on DPBM, to model the hydrodynamics of a pulsed sieve extraction column. The model takes into account the breakage and coalescence phenomena and represents each compartment as a single stage. Steiner et al., (1999) formulated a differential number balance equation, based on the DPBM, to model the hydrodynamic performance of a stirred Kühni liquid-liquid extraction column. The authors reported a mean average deviation of 20 percent between the simulated local drop size distribution and the experimental data. In the proposed model, the breakage and coalescence kernels were correlated empirically based on measurements obtained using a stirred cell. Indeed, these empirical kernels are only valid for a certain chemical system and certain column geometry. Therefore, new kernels must be developed using the same procedure when using other chemical systems and column geometries. Another development in this area was presented by Attarakih et al. (2006a), where they developed a general spatially distributed bivariate PBE with respect to droplet diameter and solute concentration to model the interacting hydrodynamic and mass transfer behavior of liquid-liquid extraction columns. In this regard, the Generalized Fixed-Pivot technique (GFP) and the Quadrature Method Of Moments (QMOM) were extended to include the solute concentration into account. The proposed mathematical framework was used to model a laboratory segment of a five compartments RDC liquid-liquid extraction column, where an experimentally validated breakage and coalescence kernels, based on single droplet models, were utilized. In this regard, both extended methods gave the same results and the reported CPU time was found acceptable from computational point of view. Based on this comprehensive mathematical framework, Attarakih et al, (2006b) developed the LLECMOD software to model and simulate agitated liquid extraction columns and was extended later to include pulsed packed bed and sieve plate columns by Jaradat et al. (2012b). In this chapter, the DPBM mathematical framework is introduced. Firstly, the general PBE, which describes the hydrodynamics behavior of liquid-liquid dispersions, as derived by Ramkrishna (2000), is presented. After that, the extended spatially distributed bivariate mathematical framework, as developed by Attarakih et al. (2006), for modeling of liquid-liquid extraction columns is briefly discussed. Finally, a condensed review of the most popular numerical methods for solving the PBE is presented. In spite of the importance of the other solution methods, the presented review only includes the most commonly used moments based methods and the maximum entropy method. These methods include: MoM, QMOM, DQMOM, SQMOM, CQMOM and the novel DMaxEntM (Hulburt and Katz, 1964; Marchisio and Fox, 2005; Attarakih et al., 2009a, b, 2013b; 2017).

2.1 The general population balance equation (PBE)

The PBE describing the hydrodynamics of a liquid dispersion system undergoing breakage and coalescence processes is given by (Ramkrishna, 2000):

$$\partial_t f(v; \gamma) + \nabla \cdot [\bar{u} f(v; \gamma)] = h\{f(v; \gamma), v\} \quad (1)$$

where v is the droplet volume, the vector $\gamma = [r, t]$ represents the spatial (r) and time (t) external coordinates, and $f(v; \gamma) \delta v = N(\gamma) f(v) \delta v$ is the average number density associated with droplets having a volume of $v \pm \delta v$ and a total number of $N(\gamma)$. The source term (h) a general volumetric term, which takes into account the breakage and coalescence phenomena. This term is given by (Valentas & Amundson, 1966):

$$\begin{aligned} h\{f(v; \gamma), v\} = & -\Gamma(v, \alpha_d) f(v; \gamma) + \int_v^{v_{\max}} \Gamma(v', \alpha_d) \beta(v/v') f(v', \gamma) \delta v' \\ & - f(v; \gamma) \int_v^{v_{\max}-v} \omega(v, v-v', \alpha_d) f(v-v'; \gamma) \delta v' \\ & + \frac{1}{2} \int_v^{v_{\max}} \omega(v, v-v', \alpha_d) f(v-v'; \gamma) f(v'; \gamma) \delta v' \end{aligned} \quad (2)$$

where α_d is the dispersed phase volume fraction, Γ and ω are the breakage and coalescence functions respectively, and β is the daughter droplet size distribution function. More information about these functions is given in the section 3. In the left side of Eq. (2), the first and third terms represent the rate at

which the droplets are lost due breakage and coalescence per unit volume respectively, while the second and the fourth terms account for the rate of formation of droplets by breakage and coalescence per unit volume respectively. The dispersed phase volume fraction is given by:

$$\alpha_d(v, \gamma) = \int_{v_{\min}}^{v_{\max}} v f(v; \gamma) \delta v \quad (3)$$

2.2 Spatially distributed population balance equation (SDPBE)

In order to model the coupled hydrodynamics and mass transfer behavior of liquid-liquid extraction equipment, Attarakih et al. (2006) developed a general mathematical framework based on the DPBM. The proposed Bivariate Spatially Distributed Population Balance Equation (BvSDPBE) is given by (Attarakih et al., 2006; 2012b; 2017):

$$\partial_t f(\psi; \gamma) + \nabla \cdot [u_d f(\psi; \gamma) - D_d \nabla f(\psi; \gamma) - \zeta f(\psi; \gamma)] = S\{f(\psi; \gamma), \psi\} \quad (4)$$

where u_d is the dispersed phase velocity, D_d is the dispersed phase axial dispersion coefficient, ζ is the particle growth rate due to solute transfer, and S is a volumetric source term. The first and second terms inside brackets describe the transport of liquid droplets along the spatial domain due to the rising velocity and axial dispersion respectively. The source term (S), is a general nonlinear integral term, which takes into account the net number of droplets produced by breakage and coalescence events, and it is given by:

$$S\{f(\psi; \gamma), \psi\} = B^b(\psi) - D^b(\psi) + B^c(\psi) - D^c(\psi) \quad (5)$$

The vector $\psi = [d, c_d]$ represents droplets internal coordinates which include: droplet diameter (d), and the solute concentration (c_d). Here, B_b and B_c are the rate of birth due to breakage and coalescence respectively, while D_b and D_c are the rate of death due to breakage and coalescence respectively. These rates are given in Table (1). In Eq. (4), the particle growth due to solute transfer process is represented by the rate of change of particle size with respect to time (t). In case of small solute concentrations, usually less than 10 percent, the growth rate can be safely neglected (Attarakih et al., 2006a, b). In addition to this, the solute mass transfer process between the contacted phases can be related to the convective solute transfer from the continuous phase. Based on this, the rate of change of solute concentration in each droplet is given by (Attarakih et al., 2012b):

$$\dot{c}_d = \partial_t c_d = \frac{6k_{od}}{d} (c_d^* - c_d) = \frac{6k_{od}}{d} (mc_c - c_d) \quad (6)$$

where k_{od} is the overall solute mass transfer coefficient, m is the solute distribution coefficient, c_d is the solute concentration in the dispersed phase, and c_c is the solute concentration in the continuous phase. Here, the overall mass transfer coefficient can be calculated using the two film resistance theory of Whitman (1923).

Table (1): The source term in Eq.(1.5) (Attarakih et al., 2006a, b, 2012b)

The rate of birth due to breakage (B^b):	$\int_d^{d_{\max}} \int_0^{C_{d,\max}} \Gamma(d', \alpha_d) \beta_n(d/d') f(d', C'_d; t, z) \delta(C'_d - C_d) \partial d' \partial C'_d$
The rate of birth due to coalescence (D^b):	$\Gamma(d', \alpha_d) f(d, C_d; t, z)$
The rate of death due to coalescence (B^c):	$\frac{1}{2} \int_0^d \int_{C'_{d,\min}}^{C'_{d,\max}} \omega(d', \eta, \alpha_d) (d/\eta)^5 f(d', C'_d; t, z) f(d', C''_d; t, z) \partial d' \partial C'_d$
The rate of death due to breakage (D^b):	$f(d, C_d; t, z) \int_d^{(d_{3\max} - d)^{1/3}} \int_0^{C_{d,\max}} \omega(d, d', \alpha_d) f(d', C'_d; t, z) \partial d' \partial C'_d$

2.3 Numerical solution methods of the PBE

The PBE is a differential equation with integral nonlinear source terms as presented in section 2.2. As results of this, it doesn't have a well known general analytical solution. As a result of this, numerical solution can't be avoided (Ramkrishna, 2000; Attarakih, 2004; Dorao and Jacobsen, 2005; Marchisio and Fox, 2005; Drumm, 2010; Lage, 2011; Favero et al, 2013; Attarakih and Bart, 2014; Buffo et al., 2014). During last years, several numerical methods had been proposed to insure accurate solution of the PBE with a reasonable computational cost. In general, all of the available numerical methods can be categorized into: direct discretization methods, Monte Carlo methods, moments based methods, and maximum entropy methods (Ramkrishna, 2000; Attarakih and Bart, 2014). A detailed review concerning advantages and disadvantages of these methods is given by Attarakih (2004) and Mohanty (2000). Among the aforementioned categorizes, moments based methods are more popular especially when coupling of the PBE with CFD codes. This is because they provide accurate results with moderate computational cost (Drumm et al., 2010; Favero et al, 2013; Attarakih and Bart, 2014). In spite of the importance of the other categorizes, only moments based methods are discussed in this section, where the most commonly used methods are presented.

2.3.1 Moments based methods

Hulburt and Katz (1964) were the first who utilized the framework of moments based methods to solve the PBE, where they introduced the method of moments. The idea behind this framework is to reduce the PBE by introducing a set of moment's functions to replace the population distribution function. Therefore, the PBE is reduced into a set of ordinary or partial differential system of equations, and the distribution is tracked through its moments. The method of moments, as a special case of weighted residuals, is based on the expansion of the unknown solution using test and weight functions. The general r th moment (μ_r) of the droplets density function is defined as follows:

$$\mu_r = \int_{\Omega_\gamma} f(\psi, \gamma) \gamma^r d\gamma \quad (7)$$

Based on this, the detailed PBE can be reduced by applying the transformation given by Eq. (7) and the resulting system of equations using the method of moments, in terms of moments of the droplet density function, can be written as follows:

$$\partial_t \mu_r = \int_{\Omega_\gamma} S \{f(\psi; \gamma), \psi\} \gamma^r d\gamma \quad (r = 0, 1, \dots, n) \quad (8)$$

where n is the order of moments equations. In this framework, the total number is given by the zero moment, while the total diameter, total area, and total volume are given by the first, second, and the third moments respectively. Indeed, Eq. (8) can't be directly solved unless the source terms are written as a function of the distribution moments. Hulburt and Katz (1964) presented different case studies to demonstrate the method of moments' ability to solve the PBE. These case studies include: nucleation, growth, and weak agglomeration kernels. These kernels were simplified in order to rewrite the source terms as a function of the distribution moments. However, in real engineering applications, formulating the source term in terms of the distribution moments is not always straight forward or even impossible. This is because the breakage and coalescence kernels, which are used to describe the dispersed phase interactions, are highly nonlinear and time dependent. Therefore, the method of moments suffers from a closure problem, which makes it limited to simplified ideal cases. Another disadvantage of this method is that, the required order of the distribution moments (n) to obtain accurate results is unknown. Therefore, several numerical methods were developed to avoid these fundamental problems and to improve the method of moments in general as discussed in the following subsections.

2.3.2 Quadrature Method Of Moments (QMOM)

The QMOM was developed by McGraw (1997) and it is considered as an extension of the MoM's. This method was used to solve the PBE in order to study the particle pure growth process. In this method,

moments of the density function are approximated using a set of Gaussian quadrature points along the internal coordinates. In contrast to the MoM's, the QMOM avoids the closure problem, arises when using the classical MoM's, and the degree of the distribution moments is known. In this method, the general k^{th} moment, with respect to the droplet diameter as internal coordinate, can be written as follows:

$$\mu_k = \int_0^{\infty} f(d, \gamma) d^k \partial d \approx \sum_{i=1}^N w_i d_i^k, \quad k = 2N - 1 \quad (9)$$

where N is the total number of quadrature points, w and d are the quadrature nodes and weights respectively. Using the QMOM, the source term of Eq. (8) is closed numerically using the Product Difference Algorithm (PDA), which was developed by Gordon (1968). The PDA is considered as an attractive method for obtaining the quadrature nodes and weights using the low-order moments of the droplet size density function. In this method, an arbitrary matrix (P) is generated and then the quadrature nodes and weights are calculated via a corresponding eigenvalue problem. The elements of the P matrix are given by:

$$P(d, \gamma) = \begin{bmatrix} \left[\delta_{i,1}, i = 1, \dots, 2N + 1 \right] \left[(-1)^{i-1} \mu_{i-1}, i = 1, \dots, 2N \right] \left[p_{1,j-1} p_{i+1,j-2} - p_{1,j-2} p_{i+1,j-1}, \begin{matrix} i = 1, \dots, 2N + 2 - j \\ j = 3, \dots, 2N + 1 \end{matrix} \right] \end{bmatrix} \quad (10)$$

where $\delta_{i,1}$ is the Kronecker delta. The required quadrature nodes and weights are calculated based on the eigenvectors of the Jacobian matrix ($J(d, \gamma)$) of $P(d, \gamma)$ as follows:

$$d_i = \text{eigenvalue}(J(d, \gamma)) \quad (11)$$

$$w_i = \mu_0 v_{i,1}^2 \quad (12)$$

where $v_{i,1}$ is denotes the first component of the i^{th} eigenvector, and μ_0 is the zero moment. In spite of the PDA efficiency, it is sensitive to small round-off errors accompanied by increasing the number of quadrature points (Marchisio and Fox, 2005; Attarakih et al., 2009; John and Thein, 2012). In addition to this, the PDA collapses when dealing with a very sharp distribution function (Attarakih, 2013). To avoid these fundamental problems, many efforts were spent to improve the PDA. For example, McGraw et al., (2003) developed the Jacobian Matrix Transformation (JMT) to provide an efficient procedure for evolving quadrature abscissas and weights. Attarakih et al. (2009) derived two analytical formulas, based on the PDA, using two quadrature points to close Eq. (9). These formulas include: the Two-Equal Weight Quadrature (TEqWQ) formula and the Two-Unequal weight Quadrature (TUEQWQ) formula. John and Thein (2012) compared the performance of three different eigenvalue algorithms: PDA, The Long Quotient Modified Difference Algorithm (LQMDA), and the Golub-Welsch Algorithm (GWA). In their work, the authors simulated a batch process and concluded that, the PDA was less efficient than the other algorithms and it may fail in certain applications due to the round-off errors. Alzyod et al. (2016a) compared the performance of three different algorithms: PDA, the Long Quotient Modified Difference Algorithm (LQMDA) (Sack and Donovan, 1972) and the analytical Two-Unequal weight Quadrature (TUEQWQ). The authors used the SQMOM to model a Kühni DN80 liquid-liquid extraction column and concluded that both the LQMDA and the PDA need more CPU time than the TUEQWQ. In addition to this, the PDA and LQMDA methods diverge after 80 and 30 spatial numerical cells respectively. As mentioned earlier, these eigenvalue based methods are sensitive small round off errors and hence they may diverge when solving large system of equations along the space. The QMOM proved to be an efficient method and suitable for coupling the PBE with CFD. However, this method destroys the shape of the density function, which is needed in many engineering applications. In addition to this, extending the QMOM to multivariate distributions is not straight forward and the extended method may lose efficiency as reported by Marchisio and Fox, (2005).

2.3.3 Direct Quadrature Method Of Moments (DQMOM)

The DQMOM was developed by Marchisio and Fox (2005) to overcome the QMOM limitations. In the classical QMOM, the required quadrature nodes and weights to close the set of moment's equations are

calculated by integrating the moments transport equations and then an inverse solution approach, based on the PDA as eigenvalue problem, is used to perform the calculation procedure. On contrast of the classical QMOM, the DQMOM tracks directly the required quadrature nodes and weights to close the governing integral source terms. This can be achieved by formulating proper transport equations to conserve the quadrature nodes and weights. Using the DQMOM, the density function can be approximated as follows (Marchisio and Fox, 2005):

$$f(d; \gamma) \approx \sum_{i=1}^N w_i(\gamma) \delta(d - d_i(\gamma)) \quad (13)$$

where $\delta(\cdot)$ is the Dirac delta function, which is used to locate the position. Based on this, the quadrature nodes and weights can be obtained by solving the following set of transport equations (Marchisio and Fox, 2005):

$$\partial_t w_i + \nabla \cdot [u_d w_i - D_d \nabla w_i] = \eta_1 \quad (14)$$

$$\partial_t w_i d_i + \nabla \cdot [u_d w_i d_i - D_d \nabla w_i d_i] = \eta_2 \quad (15)$$

where, η_1 and η_2 are the source terms. For more information concerning these terms, the reader can refer to Marchisio and Fox (2005). The DQMOM gained more attention during last years, mainly in CFD modeling and other different chemical engineering applications in general, as an improved moment's based method. For example, Fan et al., (2004) used the DQMOM to simulate the flow of a gas-solid fluidized bed. Fox (2005) extended the DQMOM to solve the bivariate PBE to study the evaporation and coalescence phenomena of liquid droplets in sprays. Silva et al. (2010) presented a study to compare the accuracy and the performance of the common available moments based methods. These methods include: DQMOM, QMOM, method of classes, and the parallel parent and daughter classes method. In their work, they examined different case studies, which include effects of particle breakage and aggregation, and concluded that the DQMOM was the most efficient method. Gupta and Roy (2013) developed a coupled CFD and DPBM mathematical framework for modeling a rectangular bubble column reactor, where they used the DQMOM as a reduced PBM. In spite of its accuracy, the DQMOM is not able to reconstruct the shape of the density function (Attarakih and Bart, 2004; 2009a; 2014). Moreover, this method could suffer from gradual increase of round-off errors as the number of quadrature points is increased (Attarakih et al., 2009a; Vikhansky, 2013).

2.3.4 Sectional Quadrature Method Of Moments (SQMOM)

The SQMOM was developed by Attarakih et al. (2009a) to overcome the aforementioned moments based methods limitations. In contrast to these methods, the SQMOM neither inverts badly scaled matrices nor solves time consuming eigenvalue algorithms in order to calculate the quadrature nodes and weights. In this method, the required quadrature nodes and weights are calculated analytically using the TEQWQ and TUEQWQ analytical formulas as derived by Attarakih et al. (2009a; 2013). These two analytical formulas are derived using two quadrature points to close the associated integral terms. In addition to this, the SQMOM conserves directly the shape of the density function using only the first four low-order moments of the distribution. As a result of this, the SQMOM is considered as a comprehensive mathematical framework, which combines advantages of the method of classes and the QMOM and reduces their drawbacks (Attarakih et al., 2009a; Drumm et al., 2010; Attarakih and Bart, 2014). The SQMOM is derived based on the concept of primary and secondary particles, where unlimited number of the distribution moments can be theoretically conserved. In this regard, the internal coordinate (here the droplet diameter) is discretized into a finite number of intervals (or sections and hence the name), which are used to track the evolution of the density function. Within this mathematical framework, the density function, in each i th section along the droplet diameter is given by (Attarakih et al., 2009a):

$$f^{(i)}(d; t) \approx \sum_{j=1}^{N_p} w_j^{(i)}(t) \delta(d - d_j^{(i)}(t)) \quad (16)$$

where N_{sp} is the number of secondary particles, and δ is the Dirac delta function placed at the secondary particle position. Indeed, applying Eq. (16) is equivalent, from mathematical point of view, for applying the QMOM in each individual section along the droplet diameter. The sectional moments of the density function as a function of positions (d) and weights (w) can be written as follows (Attarakih et al., 2009a):

$$\mu_r^{(i)} = \int_{d_{i-y/2}}^{d_{i+y/2}} f(d, t) d^r \delta d \approx \sum_{l=1}^{N_{sp}} w_j^{(i)} \left(d_j^{(i)} \right)^r, \quad r = 0, 1, \dots, 2N_{sp} - 1 \quad (17)$$

where $\mu_r^{(i)}$ is the r^{th} sectional moment of the droplet size distribution in the corresponding i^{th} section. Attarakih et al., (2009a) implemented the SQMOM to model the hydrodynamic behavior of liquid-liquid dispersions in a stirred tank vessel. In their work, five different case studies were presented and the SQMOM prediction was compared with available analytical solution using different breakage and coalescence kernels. The SQMOM proved to be able to reconstruct the distribution shape as compared with the analytical solution results. In this regard, Attarakih et al. (2009a) presented initially the TUEQWQ as an analytical closing quadrature rule. Using the TUEQWQ, the quadrature nodes and weight are given by (Attarakih et al., 2009a):

$$d_{1,2}^{(i)}(t) = -\frac{1}{2}\psi \mp \frac{1}{2}\sqrt{\psi^2 - 4\chi} \quad (18)$$

$$\omega_{1,2}^{(i)}(t) = \left(\frac{\sigma}{\hat{\mu}_1^{(i)} - d_{1,2}^{(i)}(t)} \right)^2 \frac{\hat{\mu}_0^{(i)}}{1 + [\sigma / \hat{\mu}_1^{(i)} - d_{1,2}^{(i)}(t)]^2} \quad (19)$$

where $\hat{\mu}_r^{(i)}$ is the normalized r^{th} moment in each section ($\hat{\mu}_r^{(i)} = \mu_r^{(i)} / \mu_0^{(i)}$), and parameters ψ , χ , and σ are given by:

$$\psi = \left(\frac{\hat{\mu}_1 \hat{\mu}_2 - \hat{\mu}_3}{\sigma^2} \right)_{(i)}, \quad \chi = \left(\frac{\hat{\mu}_1 \hat{\mu}_3 - \hat{\mu}_2^2}{\sigma^2} \right)_{(i)} \quad (20)$$

$$\sigma^2 = (\hat{\mu}_2 - \hat{\mu}_1^2)_{(i)} \quad (21)$$

Attarakih et al. (2009a) showed that the TUEQWQ formula may collapse under certain conditions. This is because the TUEQWQ is derived based on the PDA and therefore it collapses when dealing with a very sharp distribution function. To overcome this problem and to provide an unconditionally stable solution procedure, Attarakih et al. (2009a) introduced the TEqWQ formula as an alternative to the TUEQWQ. In the TEqWQ, the quadrature nodes are symmetric about the mean droplet diameter in each section and the quadrature nodes and weights are given by:

$$d_{1,2}^{(i)} = \hat{\mu}_1^{(i)} \mp \frac{1}{\sqrt{3}} \sqrt{\frac{\hat{\mu}_3^{(i)}}{\hat{\mu}_1^{(i)}} - \left(\hat{\mu}_1^{(i)} \right)^2} \quad (22)$$

$$w_{1,2}^{(i)} = \frac{1}{2} \hat{\mu}_0^{(i)} \quad (23)$$

Using the TEqWQ formula, the second moment of the density function can be directly calculated as a function of the zero, the first, and the third moments respectively. As a result of this, the set of low-order moment's equations and the CPU time are reduced. Based on this, the second normalized moment is given by:

$$\hat{\mu}_2^{(i)} = \left(\hat{\mu}_2^{(i)} \right)^2 + \frac{1}{\sqrt{3}} \sqrt{\frac{\hat{\mu}_3^{(i)}}{\hat{\mu}_1^{(i)}} - \left(\hat{\mu}_1^{(i)} \right)^2} \quad (24)$$

The TEqWQ formula was found superior to the TUEQWQ formula and able to locate the position of the two secondary particles correctly. The general reduced PBE, which describes the hydrodynamics behavior of the dispersed phase in a continuous stirred tank, as formulated by the SQMOM is given by (Attarakih et al., 2009a):

$$\partial_t \mu_r^{(i)}(t) = \frac{1}{\tau} \left(\mu_{r_{in}}^{(i)}(t) - \mu_r^{(i)}(t) \right) + \rho^{(i)} \{d'(t), w'(t)\} \quad (25)$$

where τ is the stirred tank time constant, and $\mu_{r_{in}}^{(i)}$ is the inlet moments of the density function. The source term ρ is a volumetric nonlinear term, which takes the breakage and coalescence phenomena into account. This source term is given by (Attarakih et al., 2009a):

$$\rho^{(i)} \{d'(t), w'(t)\} = S_b^{(i)} + S_c^{(i)} \quad (26)$$

where $S_b^{(i)}$ and $S_c^{(i)}$ are the breakage and coalescence hydrodynamics kernels in each section respectively. These kernels are given by (Attarakih et al., 2009a):

$$S_b^{(i)} = -D_r^{(i)} \left[\Gamma^{(i)} \bullet w^{(i)} \right]^T + \sum_{m=i}^{N_{sp}} C_r^{(i,m)} \left[\Gamma^{(i)} \bullet w^{(i)} \right]^T \quad (27)$$

$$S_c^{(i)} = \sum_{k=1}^{i \times N_{sp}} \left\{ \sum_{j=k}^{i \times N_{sp}} \Psi_{k,j,r}^{(i)} \omega_{j,k} w'_j w'_k - \eta_k \times \sum_{n=1}^{N_{sp} \times N_{sp}} (d'_j)^r \omega_{k,n} w'_k w'_n \right\} \quad (28)$$

Here, $C_r^{(i,m)}$ is the integral of the daughter droplet distribution function ($\beta(d/d_j^m)$), and $\Psi_{k,j,r}^{(i)}$ is a sparse aggregation matrix. The nonzero elements of the aggregation matrix represent the successful coalescence events between two droplets. These terms are given by (Attarakih et al., 2009a):

$$C_r^{(i,m)} = \pi_{r,j}^{(i,m)} = \int_{d_{i-1/2}}^{\min(d_{i+1/2}, d_j^{(m)})} d^r \beta(d/d_j^{(m)}) \partial d \quad (29)$$

$$\Psi_{k,j,r}^{(i)} = \begin{cases} \left(1 - \frac{1}{2} \delta_{k,j} \right) & \text{if } (d_{i-1/2})^3 \leq \left[(d'_k)^3 + (d'_j)^3 \right]^{r/3} < (d_{i+1/2})^3 \\ 0 & \text{otherwise} \end{cases} \quad (30)$$

Attarakih et al. (2009a) showed that all of the related sectional and quadrature methods appearing in the literature for solving the PBE are merely special cases of the SQMOM and can be obtained by varying the number of primary and secondary particles. These methods include: classes sectional methods, the fixed-pivot technique, the moving pivot technique, the QMOM, and the DQMOM. Fig. 1 shows the hierarchy of the SQMOM, where the continuous lines represent the special case derived using different number of primary particles and one secondary particle, where the dashed lines represent the special case derived using one primary particle and different number of secondary particles. Indeed, the SQMOM provides a hierarchy for different optimized reduced numerical solution methods (Attarakih et al., 2009a). For example, if the droplet size distribution is required, then the number of primary particles is increased to reconstruct the distribution shape. On the other hand, if only the integral properties of the dispersed phase are required, then one primary and secondary particles can be used as the simplest case of the SQMOM.

Based on this, different solution methods for solving the PBE, as special cases of the SQMOM, were recently developed. These methods include: the One Primary one Secondary Particle Method (OPOSPM), and the Multi Primary and one Secondary Particle Method (MPSPM) (Attarakih et al., 2009a, 2015b; Jaradat et al., 2012a). These two methods are briefly discussed in the following subsections.

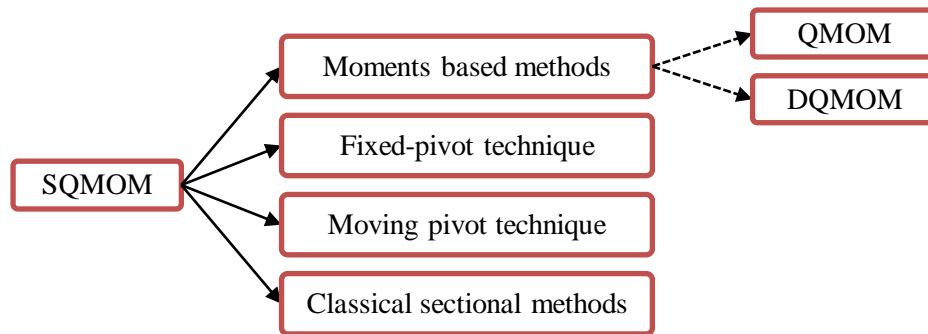


Fig. 1: The hierarchy of the SQMOM and the special derived from the SQMOM mathematical framework.

a) The One Primary One Secondary Particle Method (OPOSPM)

In the OPOSPM one section is used to represent the internal coordinate and the droplet size distribution is assumed to behave a single particle positioned at the middle of the interval. In addition to this, the integral terms are closed using one secondary particle. As a result of this, the SQMOM is reduced into two coupled equations, which conserve the zero and the third moments of the droplets density function. The OPOSPM was introduced by Attarakih et al., (2009c) as a reduced DPBM model and a special case of the general SQMOM mathematical framework. In their work, they used the OPOSPM to model liquid dispersions in a stirred tank operated in a batch mode. In this regard, the OPOSPM was able to reflect the actual hydrodynamics dispersed phase behavior. In addition to this, the model equations were found to be exact as those derived from the continuous PBE for many popular droplet breakage and coalescence models (Attarakih et al., 2009c). The OPOSPM is found to retain most of the dynamic features of the DPBM and the general SQMOM as shown in Fig. 2.

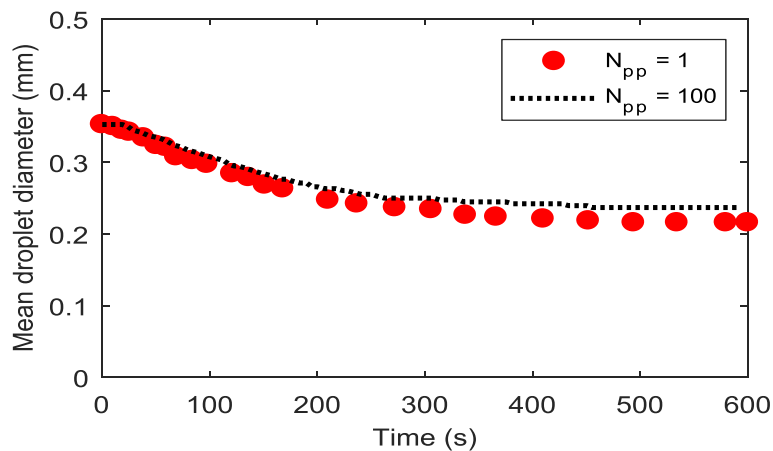


Fig. 2: Comparison between the OPOSPM prediction and the reference detailed SQMOM numerical solution (reproduced from Attarakih et al., 2009c).

Using the OPOSPM, the droplets density function is represented as follows (Attarakih et al., 2009c; 2013a; 2015b):

$$f(d;t) = N(t) \delta(d - d_{30}) \quad (31)$$

where N is the total number of droplets, and d_{30} is the mean mass droplet diameter. The mean mass droplet diameter is given by (Attarakih et al., 2009c):

$$d_{30} = \sqrt[3]{\frac{\mu_3}{\mu_0}} = \sqrt[3]{\frac{6}{\pi} \frac{\alpha_d}{N}} \quad (32)$$

Indeed, using the mean mass droplet diameter (d_{30}) as a closing quadrature rule, as proposed by Attarakih et al. (2009c), because it mathematically represents the quadrature node of the SQMOM integral terms. This is to avoid the accompanied integration error arises when using the Sauter mean droplet diameter (d_{32}) as a quadrature node. Indeed, this is a crucial issue when coupling this model with CFD solvers to model complex multiphase flow processes (Attarakih et al., 2009c; Drumm, 2010; Alzyod et al., 2017a, c, 2018). This is because the stability and the accuracy of these CFD solvers depend on the approximated source terms. Using the OPOSPM, the total number and dispersed phase volume fraction in a stirred batch vessel are given by (Attarakih et al., 2009c):

$$\partial_t N = (\mathcal{G}(d_{30}) - 1) \Gamma(d_{30}) N - \frac{1}{2} \omega(d_{30}, d_{30}) N^2 \quad (33)$$

$$\partial_t \alpha_d = \dot{v}(d_{30}) N \quad (34)$$

where \mathcal{G} is the number of daughter droplets produced due to the breakage process, and \dot{v} is the rate of droplet growth of contraction due to mass transfer. In spite of the OPOSPM simplicity, this method found intensive applications in CFD and adaptive online control as mentioned in the introduction in section 1. This is because it retains most of the dynamic features of the continuous PBE and it required less CPU time as compared with the other methods (Attarakih et al., 2009c; Drumm et al., 2010; Sharma, 2011; Hlawitschka, 2013; Alzyod et al., 2017c, 2018).

b) The Multi Primary one Secondary Particle Method (MPSPM)

In the MPSPM a different number of primary particles is used to discretize the internal coordinate, while only one secondary particle is used to take the hydrodynamics interactions (breakage and coalescence phenomena) in each section. Within the MPSPM framework, the droplet density function is defined as follows:

$$f^{(i)}(d;t) = N^i(t) \delta(d - d_{30}^{(i)}) \quad (35)$$

Unlike the OPOSPM, the MPSPM is able to reconstruct the distribution function shape. In addition to this, each secondary particle in each section has its own droplet rising velocity along the column height. As a result of this, this method is suitable to be coupled with CFD solvers to model multiphase flow problems, where different sections are required to reflect the velocity distribution.

Jaradat et al. (2012a) used MPSPM to model the hydrodynamics and mass transfer behavior of a pilot plant RDC DN80 liquid-liquid extraction column. In this regard, they couple the MPSPM model equations with the momentum balance equation. The authors reported that the MPSPM is able to capture most of the relevant features of the continuous DPBM and it is a compromise between solution accuracy and CPU time requirements. Moreover, the numerical error decreases when increasing the number of primary particles. The authors compared the predicted steady state profiles of the integral properties with the published experimental data and reported a good agreement. For more information, the reader can refer to Jaradat et al., (2012a).

2.3.5 Cumulative Quadrature Of Moments (CQMOM)

The SQMOM suffers from a numerical diffusion when dealing with growth problems. To overcome this fundamental problem, The CQMOM was introduced by Attarakih (2013b) as an alternative method to the SQMOM. In the CQMOM, a cumulative moment transformation is applied, where the cumulative r^{th} moment of the distribution function is directly conserved. In this regard, the quadrature nodes and weights are formulated as a continuous function of the particle property internal space. In addition to this, the resulting quadrature terms are approximated using Gauss-Christoffel quadrature formula. Based on this, the r^{th} cumulative moment transformation is given by (Attarakih, 2013b):

$$\mu_k(x, \gamma) = \int_{a=0}^x f(\xi, \gamma) \xi^r \partial \xi = \sum_{j=1}^{N_q} \lambda_j(x, \gamma) [\xi_j(x, \gamma)]^r, \quad r = 0, 1, \dots, 2N_q - 1 \quad (36)$$

where ζ and ξ are the continuous quadrature weights and nodes along the internal particle space. Using the CQMOM, only the first four cumulative moments are required to reconstruct the shape of the distribution. The CQMOM accuracy does not depend on sampling the continuous low-order cumulative moments. This is because the CQMOM is a mesh-free method and the accuracy depends on the quadrature nodes and weights of the cumulative quadrature rule. In this regard, Attarakih (2013b) extended the PDA to accommodate continuous low order cumulative moments in terms of droplet property space and derived the TUEQWQ and the TEQWQ analytical closure rules.

2.3.6 The Differential Maximum Entropy Method (DMaxEntM)

The DMaxEntM was introduced by Attarakih and Bart (2014) to overcome the distribution reconstruction fundamental problem while solving the PBE, which is accompanied by applying the classical QMOM method and its variants. In this method, a converging sequence of continuous approximations for the number concentration function, which are internally consistent, are introduced for the first time. The novel DMaxEntM is based on maximizing the Shannon's entropy to recover all of the missed information about the distribution function by solving a convex nonlinear programming problem. In this method, the sequence of continuous approximations, which contains the most missed information about the number concentration function is given by (Attarakih and Bart, 2014):

$$f_N^*(x, \lambda) = e^{-\sum_{r=0}^n \lambda_r x^r} \quad (37)$$

where λ is the Lagrange multiplier and x is the particle size. Initially, the authors introduced the MaxEntM to reconstruct the lost distribution and to provide a closed form for the PBE source terms (as a function of the expanded solution). However, the MaxEntM requires solving a convex nonlinear problem at each spatial point and time step, which is computationally expensive. To cure this problem, the authors developed differential form of the MaxEntM (DMaxEntM). Using the DMaxEntM the solution proceeds by solving a set of transport equations to calculate the conserved optimal Lagrange multipliers. Based on this, the PBE as formulated by DMaxEntM is given by (Attarakih and Bart, 2014):

$$\partial_t \lambda + \langle u \rangle \cdot \lambda = \psi_N \quad (38)$$

In this equation, u is the particle velocity and ψ_N is the solution of the following system of equations (Attarakih and Bart, 2014):

$$-M(\lambda) \psi_N = R_N(\lambda) + \langle D_d \rangle \nabla^2 \lambda \quad (39)$$

where M is the coded information matrix and R_N is a general term, which takes the breakage, coalescence, and the growth rate into account. The coded information matrix is a symmetrical real matrix, which includes the information about the moments of the distribution function. Attarakih and Bart (2014) presented different case studies to test and validate the DMaxEntM. These case studies include: numerical, analytical and experimental validation cases. At the experimental validation level, the authors used the bivariate form of the DMaxEntM to model the coupled hydrodynamic and mass transfer behavior of an

RDC liquid-liquid extraction column. The DMaxEntM was found able to predict the experimental data and to reconstruct the shape of the distribution function. In addition to this, the authors presented a numerical case study to compare the performance of the MaxEntM and the DMaxEntM from computation point of view. In this regard, they concluded that the DMaxEntM requires less CPU time than the MaxEntM and most of the CPU time is consumed to solve the double integrals of the coalescence source term. The differential form of the MaxEntM was found to predict the coupled hydrodynamics and mass transfer behavior of the column with a reasonable CPU time (around 15 s).

3. A nonhomogeneous bivariate extension of SQMOM

The SQMOM is considered as a robust mathematical framework for solving the DPBM (Attarakih et al., 2010; Jaradat et al., 2012a). The idea behind this framework depends on the local application of the QMOM in two dimensional spaces (w.r.t droplet diameter and solute concentration), where the two dimensional sectional moments are written as (Alzyod et al., 2016a, b, c, d; 2017a):

$$\mu_{r,m}^{(i)} = \int_{\Omega_d^{(i)}} \int_{\Omega_{c_d}} d^r c_d^m f(d, c_d) \partial d \partial c_d \quad (40)$$

In this formulation, the domains of integration: $\Omega_d^{(i)} = [d_{i-1/2}, d_{i+1/2}]$ and $\Omega_{c_d} = [0, \infty]$ are along the droplet diameter and solute concentration coordinates respectively, where are the left and right numerical cell interfaces along the droplet size. In each such section, low-order quadrature methods (based on the QMOM) are used to integrate any unclosed integral term (w.r.t. moments) such as (Alzyod et al., 2016a, b, c, d):

$$I_{r,m}^{(i)} = \int_{\Omega_d^{(i)}} \int_{\Omega_{c_d}} g(d, c_d) d^r c_d^m f(d, c_d) \partial d \partial c_d \quad (41)$$

where $g(d, c_d)$ is a given function (kernel). This formulation allows the control of the number of quadrature nodes along each coordinate depending on the variation of integrand as function of d and c_d . For example, if two quadrature nodes are taken along the droplet diameter and one node along the droplet concentration, one integrates the concentration and ends up with the TUEQWQ and the TEQWQ as derived by Attarakih et al. (2009a). By doing this, the extended SQMOM doesn't require solving large eigenvalue problems to calculate the required quadrature weights and nodes because they can be calculated analytically (in case of two quadrature points). The extension of the SQMOM starts by taking the sectional moments of Eq. (4) where integrals of the form of Eq. (40) are expressed in terms of $\mu_{r,m}^{(i)}$.

In addition to this, the unclosed integrals in the form of Eq. (41) are closed by selecting a proper quadrature rule. In this regard, the resulting unclosed integral terms are approximated using Gauss–Christoffel quadrature rule. Based on this, the SQMOM can be also extended to the physical spatial domain. The general PBE, as formulated by the SQMOM, can be derived by applying the mixed moment transformation given by Eq. (40) to Eq. (4). Based on this, the resulting transformed system of equations, in terms of the distribution mixed moments, is given by (Alzyod et al., 2016a, b, c, d; 2017a):

$$\partial_t \mu_{r,m}^{(i)} + \partial_z (\bar{F}_{r,m}^{(i)} - D_d \partial_z \mu_{r,m}^{(i)}) = u_y^{in} \mu_{in}^{(i)} c_{d,in}^m \delta(z - z_y) + S_{B,r,m}^{(i)} + S_{C,r,m}^{(i)} + S_{M,r,m}^{(i)} \quad (42)$$

where $i = 0, 1, \dots, N_{pp}$ is sections indices with as reflected by the number of primary particles (N_{pp}), $r = 0, 1, \dots, 2 \times Nq - 1$, $m = 0, 1, \dots, 2 \times Nq' - 1$ are moment indices, $\mu_{r,m}^{(i)}$ is a two dimensional moments transformed (with respect to r and m) for the i^{th} section, while $\bar{F}_{r,m}^{(i)}$ is the transformed numerical flux for each section and D_d is the mean dispersed phase axial dispersion coefficient. The transformed functions are given by (Alzyod et al., 2016a, b; 2017):

$$\mu_{r,m}^{(i)} = \int_{\Omega_d^{(i)}} \int_{\Omega_{c_d}} d^r c_d^m f(d, c_d) \partial d \partial c_d \approx \sum_{j=1}^{Nq} \sum_{n=1}^{Nq'} [d_j^r c_{d,n}^m w_{j,n}]^{<i> \quad (43)$$

$$\bar{F}_{r,m}^{(i)} = \int_{\Omega_d^i} \int_{\Omega_c^i} u_d(d, \alpha_d) f(d, c_d) d^r c_d^m \partial d \partial c_d \approx \sum_{j=1}^{N_q} \sum_{n=1}^{N_q} [u_y(d_{j,n}, \alpha_d) d_j^r c_{d,n}^m w_{j,n}]^{(i)} \quad (44)$$

where N_q is the number of quadrature nodes, u_d is the dispersed phase velocity, w is quadrature weight, and d is the quadrature node. In Eq. (42), u_d^{in} is the dispersed phase inlet superficial velocity, $\mu_{in}^{(i)}$ is inlet feed moments and $c_{d,in}$ is the dispersed phase inlet solute concentration. The first term on the right hand side represents the moments of the inlet feed modeled as a point source term at the dispersed phase inlet. The second and third terms are the transformed droplets breakage and coalescence functions respectively (see chapter 1 for more information). The mass transfer transformed source term is given by (Alzyod et al., 2016a, b; 2017):

$$S_{M,r,m}^{(i)} = m \sum_{n=1}^{N_{sp}} c_d^{m-1} \dot{c}_d W_n \quad (45)$$

In this equation, the rate \dot{c}_d is the mass transfer rate from the continuous phase to the dispersed phase and vice versa. More information concerning mass transfer rate is given in chapters 1 and 3. The solute concentration in the continuous phase is given by the solute concentration transport equation (Attarakih et al., 2006, 2012b, 2017; Alzyod et al., 2017):

$$\partial_t (\alpha_c c_c) - \partial_z (u_c \alpha_c c_c + D_c \partial_z (\alpha_c c_c)) = u_c^{in} c_c^{in} \delta(z - z_c) - \int_0^{\infty c_d^{\max}} \dot{c}_d v(d) n_{v,c_d}(d) \partial d \partial c_d \quad (46)$$

where c_c is the solute concentration in the continuous phase, u_c is the continuous phase velocity, D_c is the continuous phase axial dispersion coefficient, and is α_c the continuous phase holdup. It must satisfy the physical constrained: $\alpha_c + \alpha_d = 1$. Indeed, the integral term appearing in Eq. (46) is used to take the rate of mass transfer of all droplets into account. To close the mathematical model given by Eq. (42), the required quadrature nodes and weights are calculated analytically as given by Eqs. (18-23). It is worthwhile to mention here that, when using the TEqWQ formula as a closing rule then the number of moments preserved in each section is three (μ_0, μ_1 and μ_3). The realizability of the transported moments is checked by the quantity under the square root of Eq. (22) which also respects the Hankel determinants. Within this framework, the dispersed phase volume fraction (α_d) and the dispersed phase solute concentration are given by (Attarakih et al., 2006, Alzyod et al., 2016a, b, c, d; 2017a, b):

$$\alpha_d = \frac{\pi}{6} \sum_{i=1}^{N_{pp}} \mu_{3,0}^{(i)} \quad (47)$$

$$\bar{c}_d = \sum_{i=1}^{N_{pp}} \mu_{3,1}^{(i)} / \sum_{i=1}^{N_{pp}} \mu_{3,0}^{(i)} \quad (48)$$

Unfortunately, Eq. (42) can not be directly solved due to the strong coupling between the column hydrodynamics and mass transfer. Practically, the coupled column hydrodynamics and mass transfer behavior complicates the numerical treatment of the system of equations given by Eq. (42). Actually, Eq. (42) is solved using a segregated approach (Patankar, 1980). To overcome this problem, both hydrodynamic and mass transfer behavior should be decoupled. Firstly, the pure column hydrodynamic equation is solved (by $m = 0$), then the mass transfer equation is solved (by setting $m = 1$). This assumption is valid for liquid extraction equipment since the breakage and coalescence terms are weak functions of the solute concentration and the operating solute concentration is usually less than 10 percent (Garthe, 2006; Schmidt et al., 2006; Attarakih et al., 2006, 2013a, 2015a). In this regard, the required breakage and coalescence kernels, which are used to describe droplets interaction, are geometrical dependent functions. Therefore, suitable breakage and coalescence functions should be utilized for each

column geometry. The required breakage and coalescence functions to close the hydrodynamics transport equation are discussed and presented in chapter 1. In addition to this, a stable space-time numerical scheme to solve the governed transport equations is required. This numerical scheme should be able to handle the discontinuous events, resulted from the breakage and coalescence phenomena, and the continuous mass transfer phenomena. To achieve this, a semi-implicit finite volume scheme, based on the flux vector splitting technique is developed and implemented. This numerical scheme is fifth order accurate with respect to time and first order accurate with respect to space. After introducing the sliding average cell, the discreet form of Eq. (42) can be written as follows (see chapter 1):

$$\frac{\partial \mu_{r,m}^{(i)}}{\partial t} \Big|_j + \frac{\bar{F}_{r,m}^{(i)} \Big|_{j+1/2} - \bar{F}_{r,m}^{(i)} \Big|_{j-1/2}}{\Delta z_j} = \frac{\left(D_d \partial_z \mu_{r,m}^{(i)} / \partial z \right) \Big|_{j+1/2} - \left(D_d \partial_z \mu_{r,m}^{(i)} / \partial z \right) \Big|_{j-1/2}}{\Delta z_j} + S_{B,r,m}^{(i)} \Big|_j \quad (49)$$

where j is the spatial numerical cell index. It is worthwhile to mention here that the convection numerical flux vector is split in order to capture the droplets swarm in case of flooding or small entrainment (negative droplet velocity). To achieve this goal, the splitting approach of Patankar (1980) is implemented in this work as given in details in chapter 1. The required quadrature nodes and weights to close Eqs. (40-45) are calculated the one of the analytical formulas as given by the TEqWQ and the TUEQW, (with $N_q = 1$ and $N'_q = 1$) as given by Eqs. (18-23). These analytical formulas provide a stable numerical solution with a reasonable CPU time. Fig. 3 shows a comparison between three different methods for calculating the quadrature weights and nodes. These are the product difference algorithm (McGraw, 1997), the Long Quotient Modified Difference Algorithm (LQMDA) (Sack and Donovan, 1972) and TUEQWQ, which was derived by Attarakih et al. (2009a). Here a pilot plant Kühni DN150 liquid-liquid extraction column is considered (see chapter 1), where the effect of changing the number of spatial numerical cells on the numerical stability and the CPU is examined. The PDA uses ordinary moments of the population density function, the LQMDA uses modified moments, and the TUEQWQ uses analytical solution for the quadrature weights and nodes. Both the PDA and LQMDA use the inversion of an eigenvalue problem, which might become ill-conditioned due to the increase in the size of the problem (practically beyond four nodes) (Marchisio and Fox, 2005; Attarakih et al., 2006). In terms of the CPU time, it is clear that the TUEQWQ has lower computational cost than the other methods. In addition to this, the PDA and LQMDA methods diverge after 80 and 30 spatial numerical cells respectively. As mentioned earlier, these eigenvalue based methods are sensitive to small round off errors and hence they may diverge for large system of equations.

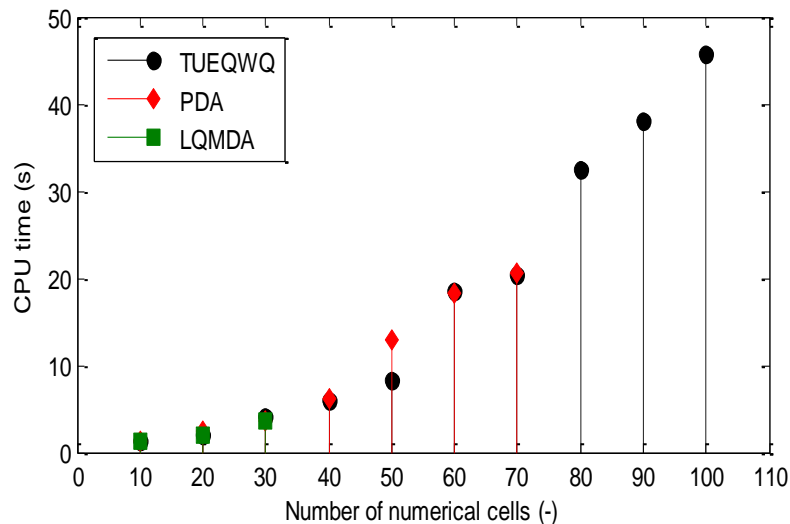


Fig. 3: Comparison between three different methods for calculating the quadrature weights and abscissas: PDA, LQMDA and the TUEQWQ in terms of CPU time as a function of the spatial numerical cells (Intel Core i5-2430M CPU 2.4 GHz, RAM 4 GB).

4. The Spatially Mixed-SQMOM (SM-SQMOM)

The steady state moment's system of equations which describe the coupled hydrodynamics and mass transfer along the spatial domain can be formulated and written, based on Eq.(42), as follows (Alzyod et al., 2017a, b):

$$\partial_z \left(\bar{F}_{r,m}^{(i)} - D_d \partial_z \mu_{r,m}^{(i)} \right) = u_y^{in} \mu_{in}^{(i)} c_{d,in}^m \delta(z - z_y) + S_{B,r,m}^{(i)} + S_{C,r,m}^{(i)} + S_{M,r,m}^{(i)} \quad (50)$$

Indeed, from experimental point of view, the Reynolds number in Kühni extraction column compartment is usually high and the breakage frequency is dominant due to the high flow in each compartment (Gomes et al., 2009). Accordingly, the axial dispersion coefficient has a little influence on the mass transfer process inside the extraction column and hence it can be safely neglected (Schmidt et al., 2006). The same procedure was proposed by many researchers to simplify the calculations (2013a, 2015a; Schmidt et al., 2006; Alzyod, 2013). Using the SM-SQMOM, Eq. (50) is written for column hydrodynamics (by setting $m = 0$) and the resulting numerical flux vector is closed using the MPSPM as follows (Alzyod et al., 2017a, b):

$$\partial_z \bar{F}_{r,0}^{(i)} = \partial_z \left(u_d^{(i)} \left(d_{30}^{(i)}, \alpha_d, P \right) \mu_{r,0}^{(i)} \right) = \hat{S}_{r,0}^{(i)} \quad r = 0, \dots, 2 \times N_q - 1 \quad (51)$$

Where α_d is the dispersed phase volume fraction, $d_{30}^{(i)}$ is the mean mass droplet diameter for each individual section and P is the physical properties vector. The mean mass droplet diameter is given by:

$$d_{30}^{(i)} = \sqrt[3]{\frac{\mu_{3,0}^{(i)}}{\mu_{0,0}^{(i)}}} = \sqrt[3]{\frac{\bar{F}_{3,0}^{(i)} \left(d_{30}^{(i)} \right)}{\bar{F}_{0,0}^{(i)} \left(d_{30}^{(i)} \right)}} \quad (52)$$

Here, the mean mass droplet diameter (d_{30}) is used to close the integral terms since it mathematically represents the quadrature node of the given integrals. The same procedure was used by Attarakih et al. (2015c) to avoid the integration error arising when using the Sauter mean droplet diameter (d_{32}). It is also worthwhile to mention here that each section has its own rising velocity along the column height as represented by its mean diameter. Indeed, this is a crucial issue when coupling this model with CFD solvers. To close the hydrodynamics source terms, the quadrature nodes and weights are calculated analytically using the TEqWQ as given by Eqs. (18-23). Based on this, the second moment based numerical flux vector is calculated as follows (Alzyod et al., 2017a, b):

$$\bar{F}_{2,0}^{(i)} = \bar{F}_{0,0}^{(i)} \cdot \left[\hat{F}_{1,0}^{2(i)} + \frac{1}{\sqrt{3}} \sqrt{\frac{\hat{F}_{3,0}^{(i)}}{\hat{F}_{1,0}^{(i)}} - \hat{F}_{1,0}^{2(i)}} \right] \quad (53)$$

Indeed, the required dispersed phase mean droplet velocity to close the model hydrodynamics equations can't be directly calculated using the algebraic velocity model and the numerical solution can't be avoided (see chapter 2). This is because the Eq. (51) conserves directly the numerical flux and as a result of this the dispersed phase holdup can't be directly retrieved. To overcome this problem, the algebraic velocity model can be rewritten in terms of the third moment numerical flux vector and the dependency on the dispersed phase holdup can be eliminated. Based on this and after a long mathematical treatment procedure, an analytical solution for calculating the droplet rising velocity based on the algebraic velocity is derived and is given by (Alzyod et al., 2017a, b) (see chapter 2):

$$u_d^{(i)} \left(F_{3,0}^{(i)}, d_{30}^{(i)} \right) = \frac{1}{3} \cdot \lambda_1^{(i)} - \lambda_2^{(i)} \quad (54)$$

where $\lambda_1^{(i)}$ and $\lambda_2^{(i)}$ are functions of the mean mass droplet diameter and they are given by (Alzyod et al., 2017a, b):

$$\lambda_1^{(i)} = \left[u_r^{(i)} + \frac{\pi}{6} \cdot \sum_{i=1}^{Mx} F_{3,0}^{(i)} - u_c^{in} \right] \quad (55)$$

$$\lambda_2^{(i)} = \frac{1}{9(\lambda_3^{(i)})^{1/3}} \left[\pi u_r^{(i)} \cdot \sum_{i=1}^{Mx} F_{3,0}^{(i)} - (\lambda_1^{(i)})^2 + 9 \cdot (\lambda_3^{(i)})^{2/3} \sum_{i=1}^{Mx} F_{3,0}^{(i)} \right] \quad (56)$$

$$\lambda_3^{(i)} = \lambda_4^{(i)} + \sqrt{(\lambda_4^{(i)})^2 + (\lambda_5^{(i)})^3} \quad (57)$$

$$\lambda_4^{(i)} = \frac{1}{54} \left[27 u_r^{(i)} \left(\frac{\pi}{6} \cdot \sum_{i=1}^{Mx} F_{3,0}^{(i)} \right)^2 + 2 \lambda_1^{(i)} \cdot \left((\lambda_1^{(i)})^2 - \frac{\pi}{6} u_r^{(i)} \cdot \sum_{i=1}^{Mx} F_{3,0}^{(i)} \right) \right] \quad (58)$$

$$\lambda_5^{(i)} = \frac{1}{9} \left[\left(\pi u_r^{(i)} \cdot \sum_{i=1}^{Mx} F_{3,0}^{(i)} \right) - (\lambda_1^{(i)})^2 \right] \quad (59)$$

Fig. 4 shows a comparison between the numerically calculated dispersed phase velocity along the column and the analytical solution, where a very good agreement is obtained. In this validation, a Kühni DN80 pilot plant liquid-liquid extraction column is used at two different operating conditions (see chapter 2 for more details concerning the experimental data sets and the validation).

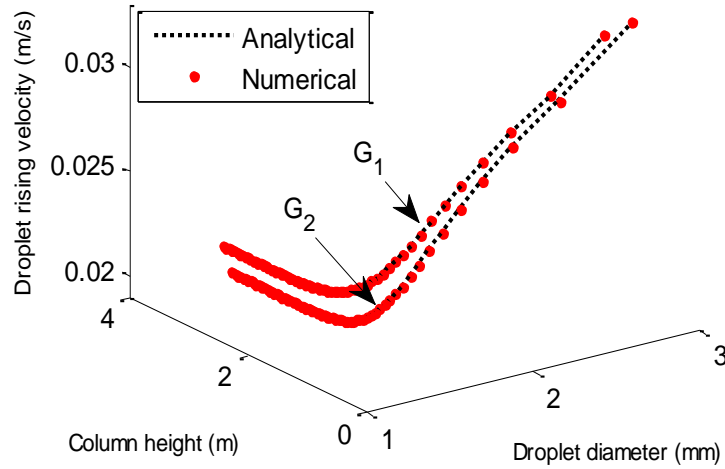


Fig. 4: Comparison between the calculated dispersed phase rising velocity along the column height and the analytical solution as given by Eq.(54).

To model the mass transfer behavior inside the column, the dispersed phase solute concentration conservation equation can be obtained from Eq. (51) by setting $r = 0$ and $m = 1$. Based on this, the following dispersed phase solute concentration transport equation can be derived using one primary and one secondary particles to approximate the distribution function as follows:

$$\partial_z (u_d c_d \alpha_d) = u_d^{in} c_d^{in} \partial (z - z_y) + S_{M,0,1}^{(i=1)} \quad (60)$$

where m' is the modified distribution coefficient ($m' = m\alpha_d/\alpha_c$). The mass transfer source term $S_{M,0,1}^{(i=1)}$ takes into account the physical and reactive transfer effects. This term is explained in details in chapters 1 and 3. The solute concentration in the continuous phase is given by the following solute concentration transport equation:

$$-\partial_z (u_c \alpha_c c_c) = u_c^{in} c_c^{in} \delta(z - z_c) - S_{M,0,1}^{(i=1)} \quad (61)$$

In this equation, u_c is the continuous phase velocity, c_c^{in} is the continuous phase inlet solute concentration and Z_c is the continuous phase inlet height. The negative sign here is used to take into account the flow direction (in the opposite direction of the dispersed phase toward the column bottom ($Z = 0$)). More information about the steady state model discretization and the numerical implementation is given in chapter 2.

5. A coupled reduced OOSPM-CFD framework for modeling of liquid-liquid extraction columns

In this research thesis, the OOSPM is utilized and coupled with the CFD commercial software FLUENT, as a special case of the SQMOM, by implementing the OOSPM as a User Defined Function (UDF). The proposed coupled 2D-CFD framework is able to predict the hydrodynamic and the mass transfer behavior of liquid-liquid extraction columns (see chapter 4 for more details). In this regard, the coupled reduced OOSPM-CFD framework is used to model the hydrodynamic and mass transfer behavior of a pulsed sieve plate liquid-liquid extraction column. Using the OOSPM, two transport equations are solved to track the total number of droplets and the dispersed phase volume fraction (see section 2.3.4). Indeed, the CFD solver already solves the dispersed phase volume transport equation through the continuity equation and hence only the number balance equation should be solved, which reduces the computational cost. Within this framework, the droplet-droplet interactions (breakage and coalescence) are taken into account using the OOSPM, while the required information about the velocity field and energy dissipation is estimated by the CFD models and solvers as shown in Fig. 5. The required breakage and coalescence models parameters are optimized using the 1D-CFD PPBLab software, where the 1D and 2D CFD simulation efforts are combined in order to minimize the computational efforts as shown in Fig. 6 (see chapter 4 for more details). The first step is to provide PPBLab with the case description and proper energy dissipation correlation. The description includes the column geometry, the operating condition and the physical properties. After that, a 1D-CFD simulation is carried using PPBLab to obtain the breakage and coalescence parameters. These parameters are given then to FLUENT in order to perform more detailed 2D-CFD simulation to predict the column hydrodynamic integral properties (holdup and mean droplet diameter) and the solute mass transfer profiles. In addition to this, PPBLab can benefit from the 2D-CFD model to correlate the energy dissipation if needed.

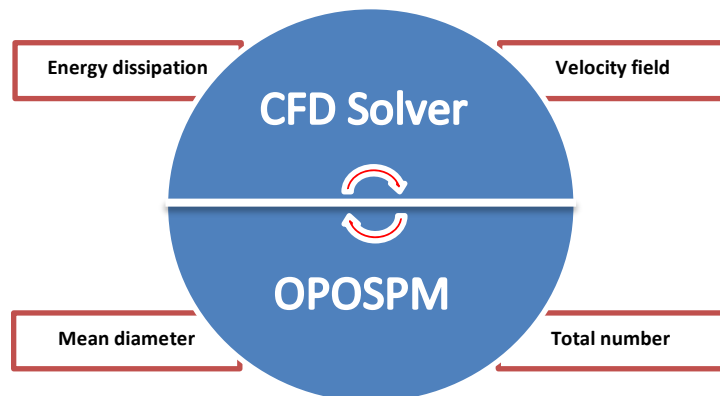


Fig. 5: Two way coupling approach of the reduced OOSPM-CFD framework.

Based on the dispersed phase volume fraction value, one can select between two different approaches to model the two phase flow behavior inside a unit operation namely: Euler-Euler and Euler-Lagrange approaches. In the Euler-Euler approach both phases are treated as interpenetrating continua and they both can coexist in each cell in the computational domain. On the other hand, within the Euler-Lagrange approach the dispersed phase is treated as discrete entities with a specific number of particles. Therefore, the Euler-Lagrange approach is suitable for low dispersed phase volume fraction values, where the interaction between the continuous and dispersed phases can be safely neglected. For high dispersed phase volume fraction values, the hydrodynamics interaction among the contacted phases can't be neglected and hence the Euler-Euler approach should be utilized as a modeling approach.

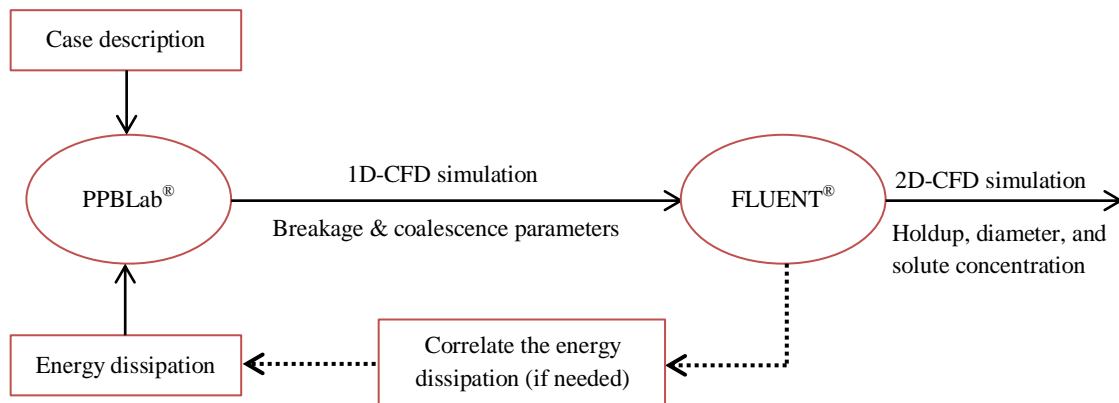


Fig. 6: Estimation procedure of the required breakage and coalescence model parameters to perform the 2D CFD simulation.

As a result of this, a two way coupling is obtained, where both phases are allowed to interact in order to correct the flow field variables. In this regard, the Euler-Euler approach is considered suitable to model liquid-liquid extraction equipment. This is because the dispersed phase volume fraction is usually larger than 10% (Weiss and Bart, 1993; Rieger et al., 1996; Drumm and Bart, 2006; Retieb et al., 2007; Yadav and Patwardhan, 2009; Drumm, 2010; Hlawitschka, 2013; Attarakih et al., 2015b; Sen et al., 2016; Alzyod et al., 2017c, 2018). Therefore, only the Euler-Euler approach is considered and used in this work. Indeed, the Euler-Euler approach is considered as the most general multiphase flow framework (Rieger et al., 1996). Using this approach, the transport equations of each phase are solved and coupled through the pressure and the momentum exchange coefficients. Therefore, this approach utilizes the available interphase drag coefficient models and takes into account all of the possible forces (e.g. lift and virtual forces). The Euler-Euler approach was extensively used by many researches for modeling of liquid-liquid extraction equipment. For example, Rieger et al. (1996) employed the Euler-Euler approach to simulate the flow field inside an RDC liquid-liquid extraction column. In this regard, the simulation results were validated using Laser-Doppler velocity measurements at the experimental validation level. Retieb et al. (2007) presented and applied a CFD model, based on Euler-Euler approach, to study the hydrodynamics behavior of pulsed disc and doughnut columns. The CFD model was validated using the experimental average hold-up, where the authors reported a deviation of 12% from the experimental data. Drumm et al. (2010) presented a coupled reduced population balance model with CFD to study the hydrodynamics behavior of an RDC liquid-liquid extraction column. In the same direction, Hlawitschka (2013) utilized the Euler-Euler approach to couple the population balance model with CFD using OpenFOAM software. Attarakih et al. (2015b) presented a coupled hydrodynamics and mass transfer PBM-CFD framework, based on Euler-Euler approach, to model a pilot plant RDC liquid-liquid extraction column. Amokrane et al. (2016) presented a coupled PBM-CFD Euler-Euler framework to study the hydrodynamic behavior of a pulsed disc and doughnut column. The authors presented different test cases to study the effect of the applied pulsation intensity on the size distribution and the mean droplet diameter. In this regard, the κ - ϵ turbulence model was utilized and the CFD predictions of the energy dissipation values were experimentally validated. In addition to this, in the proposed coupled PBM-CFD model the hydrodynamic predictions were experimentally validated using the Sauter mean droplet diameter (d_{32}) and the dispersed phase volume fraction, where a very good agreement was reported.

6. Conclusions

- Based on the literature review of the available most commonly used moments based methods for solving the PBE, the SQMOM is considered as a comprehensive mathematical framework because it combines the advantages of the classes methods and the moments based methods and minimizes their drawbacks. In this regard, the SQMOM conserves directly the distribution function shape using only the first four low order moments. In addition to this, the SQMOM is considered as a stable mathematical framework because it avoids solving time consuming eigenvalue problems (e.g. PDA) to close the model transport equations. The robustness and stability is assured by utilizing the analytical closure formulas as given by the TUEQWQ and the TEqWQ analytical solutions. As a general mathematical framework, the SQMOM provides a hierarchy of different solution methods. Therefore, many optimized reduced numerical schemes can be implemented as a special case of the SQMOM to handle different modeling and simulation challenges. As a result of this, the required solution accuracy and CPU time can be efficiently optimized. Based on this, the SQMOM is the most candidate method to model the coupled hydrodynamic and mass transfer behavior of liquid-liquid extraction equipment. In such equipment, the dispersed phase identity changes along the spatial domain and time due to the discrete breakage and coalescence phenomena. To handle this physical challenges, in this work the SQMOM is extended and adapted to model liquid-liquid extraction equipment reflecting the internal (droplet diameter and concentration) and the external (space and time) dependency.
- Based on the extended version of the SQMOM, two different 1D-CFD dynamic and steady state algorithms are developed and implemented for modeling and the simulation of stirred liquid-liquid extraction columns. To provide a stable numerical solution, a first order upwind finite volume numerical scheme with flux vector splitting technique is developed. This numerical scheme is first order accurate in space and fifth order accurate with respect to the time. The numerical case studies showed that the spatial dependency has a substantial effect on the numerical scheme stability. This is because the size of the system of transport equations is proportional to the number of the numerical spatial cells used to reflect the actual column height and is equal to $8 \times N_q \times N_c$, where N_c is the number of numerical spatial cells. Moreover unlike the TUEQWQ and the TEqWQ, the classical inversion algorithms (e.g. PDA) are rapidly diverging when increasing the number of numerical spatial cells and therefore the numerical scheme may collapse. The proposed numerical scheme is validated at the numerical level using the extended fixed pivot technique as implemented in PPBLab software, where a very good agreement is obtained.
- At the steady state modeling level, a Spatially Mixed-SQMOM (SM-SQMOM) numerical scheme is developed and implemented for modeling of the hydrodynamics and reactive/nonreactive mass transfer phenomena of liquid-liquid extraction columns. The proposed SM-SQMOM conserves directly the numerical flux vector, where the mean mass droplet diameter is used as a closure quadrature point to close the numerical flux. On the other hand, the analytical TEqWQ is utilized as a closure rule to close the breakage and coalescence source terms. Therefore, the SM-SQMOM is a unconditionally stable numerical scheme. To reduce the size of the required transport equations, the second moment numerical flux based vector is directly calculated using the TEqWQ and one primary and one secondary particle (as in the OOSPM) are used to derive the solute mass transfer transport equations. In this regard, the resulting mixed ordinary differential equation system is solved using the adaptive fifth order (w.r.t spatial domain) Runge–Kutta method, where the size of the system of equations depends on the size step (w.r.t. space). On the other hand, In case of using a first order scheme with a fixed number of spatial numerical cells the resulting size of the transport equations is reduced as compared with the dynamic algorithm and is equal to $(3 \times N_q + 1) \times N_c$.
- The droplet velocity can't be directly calculated using the SM-SQMOM due to the dependency of the algebraic velocity model on the third moment of the DSD (holdup). To cure this problem an analytical solution based on the algebraic velocity model is derived to facilitate the source term implementation and to provide an explicit form of the droplet rising velocity. Indeed, this

problem arises because the SM-SQMOM conserves only the moments based flux vectors and hence the third moment can't be directly calculated. Therefore, the proposed analytical solution is formulated using the third moment based flux vector rather than the third moment.

- The OPOSPM, as a special case of the general SQMOM, is coupled with the CFD FLUENT commercial software to model the coupled hydrodynamics and mass transfer behavior of pulsed sieve plate liquid-liquid extraction columns for the first time. Such a coupled OPOSPM-CFD framework for modeling of both hydrodynamic and mass transfer behaviors, to the best the authors' knowledge, is not published yet. In this framework, the required information about the velocity field and energy dissipation to close the OPOSPM is provided by the CFD solver, while the required mean droplet diameter to close the momentum balance equation and correct the flow field variables is calculated by the OPOSPM.
- To provide a stable numerical solution, the OPOSPM source terms are linearized and implemented as a UDF and the model equations are implemented as user defined scalars. At the numerical and experimental validation levels, the developed 2D OPOSPM-CFD framework is found fixable and able to predict both the experimental and the numerical solution results. In this regard, the OPOSPM as a reduced population balance model, compromises between CPU time and accuracy. To minimize the simulation efforts at the validation level, the required breakage and coalescence model parameters to do the 2D-CFD simulation are estimated using 1D-CFD simulation as given by PPBLab software.

References

- Al Khani, S.D., Gourdon, C., Casamatta, G., (1989). Dynamic and steady state simulation of hydrodynamics and mass transfer in liquid-liquid extraction column. *Chem. Eng. Sci.*, 44, 1295-1305.
- Alopaeus, V., Koskinen, J., Keskinen, K.I. (2002). Simulation of the population balances for liquid-liquid systems in a nonideal stirred tank. Part 2 parameter fitting and the use of the multi-block model for dense dispersions. *Chem. Eng. Sci.* 57, 1815-1825.
- Alzyod, S. (2013). A one primary one secondary particle method simulink module for the steady state and dynamic modeling of Kühni extraction column, master thesis. The University of Jordan, Jordan.
- Alzyod, S., Attarakih, M., Bart H.-J. (2016a), Dynamic Modeling of Kühni Liquid Extraction Columns Using the Sectional Quadrature Method Of Moments (SQMOM). *Comput. Chem. Eng.* 94, 1-12.
- Alzyod, S., Attarakih, M., Bart H.-J. (2016b), The Sectional Quadrature Method of Moments (SQMOM): An extension to nonhomogeneous bivariate population balances. *Chem. Eng. Res. Des.* 117, 549–556.
- Alzyod, S., Attarakih, M., Bart H.-J., (2016d), Detailed Modeling of an RDC liquid extraction column using the Sectional Quadrature Method Of Moments (SQMOM), In: Fraunhofer ITWM (Hg.): Young Researchers Symposium 2016 (YRS 2016). Stuttgart: Fraunhofer Verlag, 9-14.
- Alzyod, S., Attarakih, M., Bart, H.-J. (2017c). CFD Modeling of pulsed sieve plate liquid extraction columns using OPOSPM as a reduced population balance model, *Comput. Aided Chem. Eng.* 40, 61-66.
- Alzyod, S., Attarakih, M., Bart, H.-J. (2018). CFD modeling of pulsed sieve plate liquid extraction columns using OPOSPM as a reduced population balance model: hydrodynamics and mass transfer. *Comput. Aided Chem. Eng.* 43, 451-456.
- Alzyod, S., Attarakih, M., Hasseine A., Bart H.-J , (2016c), Population Balance Modeling of Liquid Extraction Columns using the Sectional Quadrature Method of Moments (SQMOM), *Comput. Aided Chem. Eng.* 38, 427-432.
- Alzyod, S., Attarakih, M., Hasseine, A., Bart H.-J. (2017a), Steady state modeling of a Kühni liquid extraction column using the Spatially-Mixed Sectional Quadrature Method Of Moments (SM-SQMOM). *Chem. Eng. Res. Des.* 117, 549–556.
- Alzyod, S., Korb, C., Attarakih, M., Bart, H.-J. (2017b). Steady State Population Balance Modeling of Zinc Extraction in a Kühni Liquid-liquid Extraction Column, *Proceedings of the International Solvent Extraction (ISEC2017)*, Miyazaki, Japan, 63-70.
- Amokrane, A., Maaß, S., Lamadie, F., Puel, F., Charton, S. (2016). On droplets size distribution in a pulsed column. Part I: In-situ measurements and corresponding CFD–PBE simulations. *Chem. Eng. J.*, 296, 366-376.
- Attarakih M., Alzyod S., Fricke A. (2017). Population balance modeling of pulsed packed bed extraction columns using PPBLab software. *Comput. Aided Chem. Eng.* 40, 67-72.
- Attarakih, M. (2004). Solution methodologies for the population balance equations describing the hydrodynamics of liquid–liquid extraction contactors. Dissertation. Technische Universität Kaiserslautern, Germany.
- Attarakih, M. M., Drumm, C., Bart, H.-J. (2009a). Solution of the population balance equation using the Sectional Quadrature Method of Moments (SQMOM). *Chem. Eng. Sci.* 64, 742-752.
- Attarakih, M., (2013b), Integral formulation of the population balance equation: application to particulate systems with particle growth. *Comput. Chem. Eng.* 48, 1-13.
- Attarakih, M., Abu-Khader, M., Bart, H.-J. (2013a). Modeling and dynamic analysis of an RDC extraction column using OPOSPM. *Chem. Eng. Sci.* 91, 180-196.

- Attarakih, M., Al-Slaihat, F., Hlawitschka, M., Bart, H.-J. (2015c). Modeling the hydrodynamics of bubble columns using coupled OPOSPM-maximum entropy method. *Comput. Aids. Chem. Eng.* 37, 203–208.
- Attarakih, M., Al-Zyod, S., Abu-Khader, M., Bart, H.-J. (2012b). PPBLAB: A new multivariate population balance environment for particulate system modeling and simulation. *Procedia Eng.* 42, pp. 144-562.
- Attarakih, M., Alzyod, S., Hlawitschka, M., Bart, H.-J. (2015a). OPOSSIM: a population balance-SIMULINK module for modeling coupled hydrodynamics and mass transfer in liquid extraction equipment. *Comput. Aided Chem. Eng.* 37,257-262.
- Attarakih, M., Bart, H.-J. (2014). Solution of the population balance equation using the differential maximum entropy method (DMaxEntM). *Chem. Eng. Sci.*, 108, 123-133.
- Attarakih, M., Bart, H.-J., Faqir, N. (2006a). Numerical solution of the bivariate population balance equation for the interacting hydrodynamics and mass transfer in liquid-liquid extraction columns. *Chem. Eng. Sci.*, 61, 113-123.
- Attarakih, M., Bart, H.-J., Faqir, N. (2006b), LLECMOD: A windows-based program for hydrodynamics simulation of liquid-liquid extraction columns. *Chem. Eng. Process*, 45(2), 113-123.
- Attarakih, M., Hasseine, A., Bart, H.-J. (2016). CFD modeling of bubbly gas flow using coupled OPOSPM two-fluid model. *Comput. Aided Chem. Eng.* 38, 403-408.
- Attarakih, M., Hlawitschka, M., Abu-Khader, M., Alzyod, S., Bart, H.-J. (2015b). CFD-population balance modeling and simulation of coupled hydrodynamics and mass transfer in liquid extraction columns. *Appl. Math. Model.* 39, 5105–5120.
- Attarakih, M., Jaradat, M., Bart, H.-J., Kuhnert, J., Drumm, C., Tiwari, S., et al. (2010). A multivariate Sectional Quadrature Method of moments for the Solution of the Population Balance Equation. *Comput. Aided Chem. Eng.* 28, 1551-1556.
- Attarakih, M., Jaradat, M., Drumm, C., Bart, H.-J., Tiwari, S., Sharma, V. Kuhnert, J., Klar, A. (2009c). Solution of the population balance equation using the One Primary and One Secondary particle Method (OPOSPM), *Comput. Aided Chem. Eng.*, 26, 1333-1338.
- Attarakih, M., Jaradat, M., Drumm, C., Bart, H.-J., Sudarshan Tiwari, S., Sharma, V., Kuhnert, J., Klar, A. (2009b). A multivariate population balance model for liquid extraction columns. *Comput. Aided Chem. Eng.* 26, 1339-1344.
- Attarakih, M., Jildeh, H. B., Mickler, M., and Bart, H.-J. (2012a). The OPOSPM as a nonlinear autocorrelation population balance model for dynamic simulation of liquid extraction columns. *Comput. Aided Chem. Eng.* 31, 1216-1220.
- Buffo, A., Vanni, M., Renze, P., Marchisio, D. (2016). Empirical drag closure for polydisperse gas-liquid systems in bubbly flow regime: Bubble swarm and micro-scale turbulence. *Chem. Eng. Res. Des.* 113, 284-303.
- Casamatta, G., Vogelpohl, A. (1985), Modeling of Fluid Dynamics and Mass Transfer in Extraction Columns, *Ger. Chem. Eng.* 8 (2): 96–103.
- Coulaloglou, C. A., Tavlarides, L.L. (1977). Description of interaction processes in agitated liquid-liquid dispersions. *Chem. Eng. Sci.* 32, 1289–1297.
- Czaplá, F., Haida, H., Elsner, M. P., Lorenz, H., Briesen, H., Seidel-Morgenstern, A. (2009). Parameterization of population balance models for polythermal auto seeded preferential crystallization of enantiomers. *Chem. Eng. Sci.* 64, 753-763.
- Deen, N., Solberg, T., Hjertager, B. (2001). Large eddy simulation of the gas-liquid flow in a square cross-sectioned bubble column. *Chem. Eng. Sci.* 56, 6341-6349.
- Dorao, C., Jakobsen, H., (2006). Numerical calculation of the moments of the population balance equation. *J. Comput. Appl. Math.* 196, 619-633.
- Drumm, C. (2010). Coupling of computational fluid dynamics and population balance modeling for liquid-liquid extraction, Dissertation. Technische Universität Kaiserslautern, Germany, Kaiserslautern.

- Drumm, C., Bart, H.-J. (2006). Hydrodynamics in a RDC Extractor: Single and Two-Phase PIV Measurements and CFD Simulations, *Chem. Eng. Technol.*, 29, 1297-1302.
- Fan, R., Marchisio, D., Fox, R. (2004). Application of the direct quadrature method of moments to polydisperse gas–solid fluidized beds, *Powder Technol.*, 139, 7-20.
- Favero, J., Silva, L., F., Lage, P. L. C., (2014), Comparison of methods for multivariate moment inversion-introducing the independent component analysis. *Comput. Chem. Eng.*, 60, 41-56.
- Fysikopoulos, D., Borsos, A., Li, W., Onyemelukwe, I., Benyahia, B., Nagy, Z. K., Rielly, C. D. (2017). Local vs Global Estimability Analysis of Population Balance Models for Crystallization Processes. *Comput. Chem. Eng.* 40, 55-60.
- Garthe, D. (2006). Fluid dynamics and mass transfer of single particles and swarms of particles in extraction columns. Dissertation. Technische Universität München, Germany.
- Gimbut, J., Nagy, Z.K., Rielly, C.D. (2009). Simultaneous quadrature method of moments for the solution of population balance equations, using a differential algebraic equation framework. *Ind. Eng. Chem. Res.* 48, 7798–7812.
- Gomes, L.N, Guimaraes, M.L, Stichlmair, J., and Cruz-Pinto, J.J, (2009). Effects of mass transfer on the steady state and dynamic performance of a Kuhni column-experimental observations. *Ind. Eng. Chem. Res.* 48, 3580-3588.
- Gordon, R. G. (1968). Error bounds in equilibrium statistical mechanics. *J. Math. Phys.* 9, 655-663.
- Goryunov, A. G., Mikhaylov, V. S. (2012). The automatic control system of a multi-component nonequilibrium extraction process in the pulse column. *J Process Control.* 22, 1034-1043.
- Gourdon, C., Casamatta, G., Muratet, G. (1994). Population Balance Based Modeling. In: Godfrey & Slater (Ed). *Liquid-liquid extraction equipment.* (pp.140-226), New York: Eds. John Wiley and Sons.
- Gupta, A., Roy, S. (2013). Euler–Euler simulation of bubbly flow in a rectangular bubble column: Experimental validation with Radioactive Particle Tracking. *Chem. Eng. J.*, 225, 818-836.
- Hamilton, J. A., Pratt, H., R., C. (1984). Droplet Coalescence and Breakage Rates in a Packed Liquid Extraction Column. *AIChE J.*, 30, 442-450.
- Hanson, C. (1971). *Recent Advances in Liquid-Liquid Extraction.* Pergamon Press, Oxford, United Kingdom.
- Haverland, H., Vogelpohl, A., Gourdon, C., Casamatta, G. (1987), Simulation of fluid dynamics in a pulsed sieve plate column, *Chem. Eng. Technol.* 10 (1): 151–157.
- Hlawitschka, M. (2013). Computational fluid dynamics aided design of stirred liquid-liquid extraction columns, Dissertation, Technische Universität Kaiserslautern, Germany.
- Hulburt, H., Katz, S. (1964). Some problems in particle technology. A statistical mechanical formulation. *Chem. Eng. Sci.* 19, 555-574.
- Jaradat, M. M., Attarakih, M. M., Steinmetz, T., Bart, H.-J. (2012b), LLECMOD: A Bivariate Population Balance Simulation Tool for Pulsed Liquid-Liquid Extraction Columns, *Open Chem. Eng. J.* 6: 8–31.
- Jaradat, M., Attarakih, M., Bart, H.-J. (2012a). RDC extraction column simulation using the multi-primary one secondary particle method: coupled hydrodynamics and mass transfer. *Comput. Chem. Eng. J.* 37, 22–32.
- Ji, J., Mensforth, K. H., Perera, J. M., Stevens, GW. (2006). The role of kinetics in the extraction of zinc with D2EHPA in a packed column. *Hydrometallurgy.* 84, 139-148.
- Jildeh, H.B., Attarakih, M.M., Mickler, M. & Bart, H.-J. (2014). Parameter optimization and validation for droplet population balances. *Can. J. Chem. Eng.* 92, 210-219.
- John, V., Angelov, I., Oncul, A.A., Thevenin, D. (2007). Techniques for the reconstruction of a distribution from a finite number of its moments. *Chem. Eng. Sci.* 62, 2890-2904.
- John, V., Thein, F. (2012). On the efficiency and robustness of the core routine of the quadrature method of moments (QMOM). *Chem. Eng. Sci.* 75, 327–333.

- Kalem, M., Buchbender, F., Pfennig, A. (2011). Simulation of hydrodynamics in RDC extraction columns using the Simulation Tool "ReDrop". *Chem. Eng. Res. Des.*, 8, 1-9.
- Kobert, M. (2015). Application of the Finite Pointset Method to Moving Boundary Problems for the BGK Model of Rarefied Gas Dynamics. Dissertation. Technische Universität Kaiserslautern, Germany.
- Kronberger, T., Ortner, A., Zulehner, W., and Bart, H.-J. (1995). Numerical Simulation of Extraction Columns using a Drop Population Model. *Comput. Chem. Eng.*, 19, 639-644.
- Kumar A., Hartland, S. (1985). Gravity Settling in Liquid/Liquid Dispersions, *Can. J. Chem. Eng.*, 63, 368-376.
- Kumar, A., Hartland, S. (1996). Unified correlations for the prediction of drop size in liquid-liquid extraction columns. *Ind. Eng. Chem. Res.*, 35, 2682-2695.
- Lade, V., Rathod, V., Bhattacharyya, S. Manohar, S., Wattal, P. (2013). Comparison of normal phaseoperation and phase reversal studies in a pulsed sieve plate extraction column. *Chem. Eng. Res, Des*, 91, 1133-1144.
- Lage, P. (2011). On The Representation of QMOM as a weighted-residual method-the dual-quadrature method of generalized moments. *Comput. Chem. Eng.* 35, 2186-2203.
- Liao Y., Lucas D. (2010). A literature review on mechanisms and models for the coalescence process of fluid particles. *Chem. Eng. Sci.* 65, 2851-2864.
- Liu, J., Ma, C., Hu, Y., Wang, X. (2010). Effect of seed loading and cooling rate on crystal size and shape distributions in protein crystallization-A study using morphological population balance simulation. *Comput. Chem. Eng.* 34, 1945-1952.
- Maaß, S., Paul, N., Kraume., M. (2012). Influence Of the dispersed phase fraction on experimental and predicted drop size distributions in breakage dominated stirred systems. *Chem. Eng. Sci.* 76, 140-153.
- Madadi-Kandjani, E., Passalacqua, A. (2015). An extended quadrature-based moment method with log-normal kernel density functions. *Chem. Eng. Sci.* 131, 323-339.
- Marchisio, D., Fox, R. (2005). Solution of population balance equations using the Direct Quadrature Method of Moments. *Aerosol Sci.* 36, 43-73.
- McGraw, R. (1997). Description of aerosol dynamics by the quadrature method of moments. *Aerosol Sci. Tech.*, 27, 255-265.
- Mickler, M., Jildeh, H.B., Attarakih, M.M., Bart, H.-J. (2014). Online monitoring, simulation and prediction of multiphase flows. *Can. J. Chem. Eng.* 92, 307-317.
- Mjalli F. (2005). Neural network based predictive control of liquid-liquid extraction contactors. *Chem. Eng. Sci.* 60, 239-253.
- Mohanty, S. (2000). Modeling of liquid-liquid extraction column: a review. *rev. Chem. Eng.* 16, 199-248.
- Mohanty, S., Vogelpohl, (1997). A simplified hydrodynamic model for a pulsed sieve-plate extraction column, *Chem. Chem. Eng. Process.*, 36, 385-395.
- Nauha, E., Alopaeus, V. (2013). Modeling method for combining fluid dynamics and algal growth in a bubble column photobioreactor. *Chem. Eng. J.* 229, 559-568.
- Neto, P., Mansur M.B. (2013). Transient modeling of zinc extraction with D2EHPA in a Kühni column. *Chem. Eng. Res. Des.* 91, 2323-2332.
- Patankar, S. (1980). *Numerical Heat Transfer and Fluid Flow*. Taylor & Francis, Bristol, PA.
- Perry, R. H., Green, D. W. (2008). *Perry's Chemical Engineers' Handbook*. 8th Edition, McGraw-Hill.
- Petitti, M., Nasuti, A., Marchisio, D.L., Vanni, M., Baldi, G., Mancini, N., Podenzani, F. (2010). Bubble size distribution modeling in stirred gas-liquid reactors with QMOM augmented by a new correction algorithm. *AIChE J.* 56, 36-53.

- Ramaswamy, S., Huang, H., J., Ramarao, B., V. (2013). Separation and purification technologies in bio-refineries. 1th Edition, John Wiley, New York.
- Ramkrishna, D. (2000). Population balances: Theory and applications to particulate systems in engineering. Academic Press, San Diego.
- Retieb, S., Guiraud, P., Angelov, G., Gourdon C. (2007). Hold-up within two-phase countercurrent pulsed columns via Eulerian simulations, *Chem. Eng. Sci.*, 62, 4558-4572.
- Rieger, R., Weiss, C., Wigley, G., Bart, H.-J., Marr, R., (1996). Investigating the Process of Liquid-Liquid Extraction by Means of Computational Fluid Dynamics, *Comput. Chem. Eng.* 20(12), pp. 1467-75.
- Santos, F., Favero, J., Lage, P. (2013). Solution of the population balance equation by the direct dual quadrature method of generalized moments. *Chem. Eng. Sci.* 101, 663-673.
- Schiller, L., Naumann, A., (1935). A drag coefficient correlation, *Zeitschrift des Vereins Deutscher Ingenieure* 77, 318–320.
- Schmidt, S., Simon, M., Attarakih, M., Lagar, L., Bart, H.-J. (2006). Droplet population balance modeling - hydrodynamics and mass transfer. *Chem. Eng. Sci.* 61, 246-256.
- Sen, N., Singh, K., Patwardhan, A., Mukhopadhyay S., Shenoy, K. (2016). CFD simulation of two-phase flow in pulsed sieve-plate column – Identification of a suitable drag model to predict dispersed phase hold up, *Sep. Sci. & Tech.* 51, 2790-2803.
- Shah, B.H., Ramkrishna, D. (1972). A population balance model for mass transfer in lean liquid-liquid dispersions, *Chem. Eng. Sci.*, 28, 389-399.
- Sharma, V. (2011). Multi-Phase Flow Model Incorporated with Population Balance Equation in a Meshfree Framework. Dissertation. TU Kaiserslautern, Germany.
- Sharma, V.K., Tiwari, S., Attarakih, M.M., Jaradat, M., Klar, A., Kuhnert, J., Bart, H.-J. (2009). A meshfree CFD-PBM coupled model. *Comput. Aided Chem. Eng.* 26, 345-1350.
- Silva, L., Rodrigues, R., Mitre, J., Lage, P. (2010). Comparison of the accuracy and performance of quadrature-based methods for population balance problems with simultaneous breakage and aggregation. *Comput. Chem. Eng.*, 34, 286-297.
- Skogestad, S. (1997). Dynamics and Control of Distillation Columns - A Critical Survey. *Modeling, Identification and Control.* 18, 177-217.
- Souza, L., Janiga, G., John, V., Thevenin, D. (2010). Reconstruction of distribution from a finite number of moments with an adaptive spline-based algorithm. *Chem. Eng. Sci.* 65, 2741-2750.
- Steiner, L. (1994). In: Godfrey, Slater (Eds.), *Computational Procedures for Column Simulation and Design. In Liquid-liquid Extraction Equipment.* John Wiley and Sons, New York, pp. 116–136.
- Steiner, L., Bamelli, M., Hartland, S. (1999). Simulation of hydrodynamic performance of stirred extraction column. *AIChE J.*, 45, 257-267.
- Thornton, D. (1992). *Science and practice of liquid-liquid extraction 2*, Oxford University Press, New York.
- Tiwari, S., Christian Drumm, Attarakih, M., Kuhnert, J., Bart, H.-J. (2008). Coupling of the CFD and the droplet population balance equation with the finite pointset method, *Notes in Computational Science and Engineering*, Vol. 65, Griebel, Michael; Schweitzer, Marc Alexander (Eds.).
- Treybal, R., (1963). *Liquid Extraction.* McGraw-Hill, New York.
- Valentas, K.J.; Bilous, O.; Amundson, N.R., (1966). Analysis of breakage in dispersed phase systems. *Ind. Eng. Chem. Fundam.*, 5, 271-279.
- Veglio F., Slater, M. J. (1996). Design of liquid-liquid extraction columns for the possible test system Zn/D2EHPA in n-dodecane. *Hydrometallurgy*, 42. 177-195.
- Vikhansky A. (2013). Direct Quadrature Spanning Tree Method for Solution of the Population Balance Equations. *Journal of Aerosol Science*, 55, 78-88.

- Vikhansky, A., Kraft, M. (2004). Modeling of a RDC using a combined CFD-population balance approach. *Chem. Eng. Sci.* 59, 2597-2606.
- Wachs, A., Benyamin, J., Semiat, R., Lewin, D. R. (1997). Control of a pilot scale Karr liquid-liquid extraction column. *Comput. Chem. Eng.* 21, 601-606.
- Wächtler, T. (2014). Numerical simulation of turbulent dispersions in liquid-liquid extraction columns. Dissertation, TU Kaiserslautern, Germany.
- Wächtler, T.F., Kuhnert, J., Attarakih, M., Tiwari, S., Klar, & Bart, H.-J. (2011). The normalized quadrature method of moments coupled with finite pointset method, II International Conference on Particle-based Methods. Barcelona, Spain.
- Wardle K., (2013). Hybrid multiphase CFD simulation for liquid-liquid interfacial area prediction in annular centrifugal contactors, Salt Lake City, Utah, USA, September 29-October 3.
- Weinstein, O., Semiat, R., Lewin, D. R. (1998). Modeling simulation and control of liquid-liquid extraction columns. *Chem. Eng. Sci.* 53, 325-339.
- Weiss, C., Bart, H.-J. (1993). Calculation of Flow Patterns in an RDC Based on Computational Fluid Dynamic Methods. In Longsdail, D.H. & Slater, M.J. (eds.) *Solvent Extraction in the Process Industry*. London: Elsevier Applied Science. 1191-1197.
- Whitman, W.G., (1923). The film theory of absorption, *Chem. Met. Eng.* 29, 147-151.
- Yadav, R., Patwardhan, A. (2009). CFD modeling of sieve and pulsed-sieve plate extraction columns. *Chem. Eng. Res. Des.*, 87, 25-35.
- Yuan, C., Laurent, F., Fox, R. (2012). An extended quadrature method of moments for population balance equations. *J. Aerosol Sci.* 51, 1-23.

Chapter 1

One Dimensional Dynamic Modelling of Liquid-liquid Extraction Equipment using the SQMOM as a Reduced PBM

1.1 Introduction

The DPBM proved to be an efficient mathematical framework for modelling of multiphase flow problems in general and liquid-liquid extraction equipment in particular. In liquid-liquid extraction equipment, the mass transfer process is characterized by the dispersed phase hydrodynamics interactions which include: breakage and coalescence phenomena. This is because they determine the available interfacial mass transfer area. In such processes, the rate of growth due to mass transfer can be safely neglected, which reduces the problem complexity. This is due to the weak dependency of the column hydrodynamic on the mass transfer process inside the extraction equipment (Schmidt et al., 2006; Perry and Green, 2008). Therefore, the effect of the mass transfer rate on the growth process can be neglected from practical point of view (Jaradat et al., 2012a, b; Jildeh et al., 2012; Attarakih et al., 2012a, b, 2015a, 2017; Alzyod et al., 2016a, b, c, 2017, a, b). In addition to this, the overall extraction equipment efficiency depends on the size distribution, which determines the final product properties. As a result of this, a robust numerical scheme based on the DPBM, which is able to track the distribution shape and predict the mass transfer behavior, is needed. In this regard, the SQMOM has the advantage over the other moment's solution methods for modelling of liquid-liquid extraction equipment. This is because the SQMOM provides an unconditionally stable numerical scheme, which is able to track the droplets distribution shape. Indeed, the SQMOM was introduced by Attarakih et al. (2009a) to solve the homogenous PBE. Therefore, the SQMOM should be extended to solve the nonhomogeneous PBE. However, in this chapter the SQMOM is extended to solve the spatially distributed nonhomogeneous PBE and adapted for modelling and the simulation of liquid-liquid extraction equipment. The extended SQMOM requires sufficient information about the velocity field and the energy dissipation in order to close the resulting model equations. In this regard, two different approaches can be used to close the SQMOM model equations using the required flow field variables. In the first approach, the required velocity field and energy dissipation values are estimated using proper correlations, where these values are averaged in each single compartment along the column height. This approach proved to be very efficient and accurate from practical and computational point of views as reported by many researchers (Schmidt et al., 2006; Steinmetz, 2007; Drumm, 2010; Jaradat et al., 2012a, b; Alzyod, 2013; Hlawitschka, 2013; Jildeh et al., 2014; Attarakih et al., 2015a; Alzyod et al., 2016a, b, c, d, 2017a, b). This is because the dispersed phase integral properties (holdup and mean diameter) can be accurately estimated with a low CPU time. In the second approach, the required flow field and turbulence variables are obtained by performing a detailed CFD simulation. Unlike the first approach, this approach provides local information about the flow field variables and hence it releases the averaging assumption mentioned before. In addition to this, this approach doesn't require lab scale experiments to estimate the flow field variables (Drumm, 2010). However, this approach is very expensive from computational point of view and needs huge computational efforts when modelling industrial scale equipment (Attarakih et al., 2012a, b, 2015a, b, 2017; Drumm, 2010; Sharama et al., 2011; Hlawitschka, 2013; Alzyod et al., 2017a, 2018). Indeed, both modelling approaches can be combined to make use of their advantages and minimize their drawbacks (Hlawitschka, 2013; Attarakih et al., 2015b). More information concerning the combined approach is given in Chapter 4. In this chapter, the SQMOM is extended to model the dynamic behavior of liquid-liquid extraction equipment in a one dimensional domain (1D). In this regard, the first approach is used to estimate the required flow field variables to close the mathematical model equations, where proper correlations are used. Indeed, this step is crucial because the 1D framework provides a fundamental basis to understand and to study the effect of the hydrodynamics and mass transfer mechanisms and their contributions to the extraction equipment efficiency. This chapter is organized as follows: firstly, the extended SQMOM framework, for modelling

of liquid-liquid extraction equipment, is presented. After that, the extended framework is validated at three different levels namely: analytical, numerical, and experimental validation levels. In this regard, the validation procedure is carried out in a 1D domain using a Kühni liquid-liquid extraction column, where different case studies are used to demonstrate the ability of both algorithms to predict and capture the prevailing physical phenomena inside the extraction equipment. These case studies include hydrodynamics mass transfer cases. In this regard, the required flow field and turbulence variables are estimated using proper correlations as disused in the following subsections.

1.2 Dynamic modelling of liquid-liquid extraction equipment using the SQMOM

The general extended SQMOM to solve the nonhomogeneous PBE in a 1D domain is written as follows (Alzyod et al., 2016a, b, c, d; 2017a):

$$\partial_t \mu_{r,m}^{(i)} + \partial_z \left(\bar{F}_{r,m}^{(i)} - D_d \partial_z \mu_{r,m}^{(i)} \right) = u_y^{in} \mu_{in}^{(i)} c_{d,in}^m \delta(z - z_y) + S_{B,r,m}^{(i)} + S_{C,r,m}^{(i)} + S_{M,r,m}^{(i)} \quad (1)$$

where $i = 0, 1, \dots, N_{pp}$ is sections indices with as reflected by the number of primary particles (N_{pp}), $r = 0, 1, \dots, 2 \times Nq - 1$, $m = 0, 1, \dots, 2 \times Nq' - 1$ are moment indices, $\mu_{r,m}^{(i)} = \sum_{j=1}^{Nq} \sum_{n=1}^{Nq'} [d_j^r c_{d,n}^m w_{j,n}]^{<i>$ is a two dimensional moments transformed (with respect to r and m) for the i^{th} section, while $\bar{F}_{r,m}^{(i)}$ is the transformed numerical flux for each section and D_d is the mean dispersed phase axial dispersion coefficient. The first term in the right hand side takes into account the inlet moments of the dispersed phase at the dispersed phase inlet point. For more information concerning each term of Eq. (1) see the overview section.

1.2.1 Spatial discretization of the SQMOM

In this section, the SQMOM is implemented and solved in the physical space using MATLAB software. This model consists of four population balance equations (based on first four low-order moments), while the fifth equation is the continuity equation of the solute concentration in the continuous phase. Indeed, these equations are coupled through the source terms, which complicate the analytical and numerical solutions. Moreover, this system of equations is dominant by convection (Attarakih et al., 2013). As a result of this, a special numerical treatment to handle such a highly nonlinear system of equations is required. In this regard, both hydrodynamic and mass transfer behavior should be decoupled as pointed out in the previous section. The same procedure was done by Attarakih et al. (2006), where they extended the QMOM to solve the bivariate PBE to model hydrodynamic and mass transfer behavior of an RDC column. Based on this, the solution proceeds as follows: first, the column pure hydrodynamics is solved (setting $m = 0$ in Eq. (1)) and then the mass transfer equations are solved (setting $m = 1$ in Eq.(1)). In this regard, a semi-implicit finite volume scheme with vector flux splitting technique is developed and coupled with the standard MATLAB ordinary differential equation solvers. To speed up the system approach to steady state and to ensure numerical stability, the present numerical scheme is fifth order accurate in time and first order accurate in space. On the other hand, the use of second-order spatial discretization scheme was shown to be only necessary for sharp moving dynamic profiles along space (for more discussion on this topic, the reader may refer to Attarakih, (2004). In this work, the column height (z) is discretized into n spatial numerical cells $I_j = [z_{j-1/2}, z_{j+1/2}]$ of size $\Delta z = z_{j+1/2} - z_{j-1/2}$, with $j = 1, 2, 3, \dots, n$. The control volume is given by $V = I_j \times [t^n, t^{n+1}]$ as shown in Fig. 1. Let the sliding cell average for the conserved quantity $\mu_{r,m}^{(k)}$:

$$\mu_{r,m}^{(i)} = \frac{1}{\Delta z} \int_{z_{j-1/2}}^{z_{j+1/2}} \mu_{r,m}^{(i)}(\xi, t) d\xi \quad (2)$$

Using the cell sliding average for the conserved quantity the system given by Eq. (1) can now be integrated over the j^{th} control volume to get the following semi- discrete form:

$$\frac{d\mu_{r,m}^{(i)}}{dt} \Big|_j + \frac{1}{\Delta z} \left[\bar{F}_{r,m}^{(i)} \Big|_{j+1/2} - \bar{F}_{r,m}^{(i)} \Big|_{j-1/2} \right] = \bar{S}(U)_{r,j}, \quad j = 1, \dots, n \quad (3)$$

where n , is the number of numerical cells used to discretize the physical spatial domain, and $\bar{F}_{r,m}^{(i)} \Big|_{j+1/2}$ and $\bar{F}_{r,m}^{(i)} \Big|_{j-1/2}$ are the right and left fluxes at the cell interface respectively. Finally, using Patankar (1980) compact notation, the numerical flux could be written as follows:

$$\bar{F}_{r,m}^{(i)} \Big|_{j+1/2} = \left\langle \bar{F}_{r,m}^{(i)} \Big|_j, 0 \right\rangle - \left\langle -\bar{F}_{r,m}^{(i)} \Big|_{j+1}, 0 \right\rangle \quad (4)$$

$$\bar{F}_{r,m}^{(i)} \Big|_{j-1/2} = \left\langle \bar{F}_{r,m}^{(i)} \Big|_{j-1}, 0 \right\rangle - \left\langle -\bar{F}_{r,m}^{(i)} \Big|_j, 0 \right\rangle \quad (5)$$

where the symbol $\langle \cdot, 0 \rangle$ is defined as $\langle \cdot, 0 \rangle = \max(\cdot, 0)$ and the definition of $\bar{F}_{r,m}^{(i)}$ is given by:

$$\bar{F}_{r,m}^{(i)} = \sum_{j=1}^{N_d} \sum_{n=1}^{N_d} [u_y (d_{j,n}, \alpha_d) d_j^r c_{d,n}^m w_{j,n}]^{<i>} \quad (6)$$

It should be mentioned that the presented finite-volume scheme, which is given by Eqs. (3-5) is only first-order accurate in space, is sufficient to capture the transient behavior of the column hydrodynamics and mass transfer by simply increasing the number of the spatial numerical cells. This is can be easily achieved since these transient profiles are not sharp along the column height with no sharp moving front.

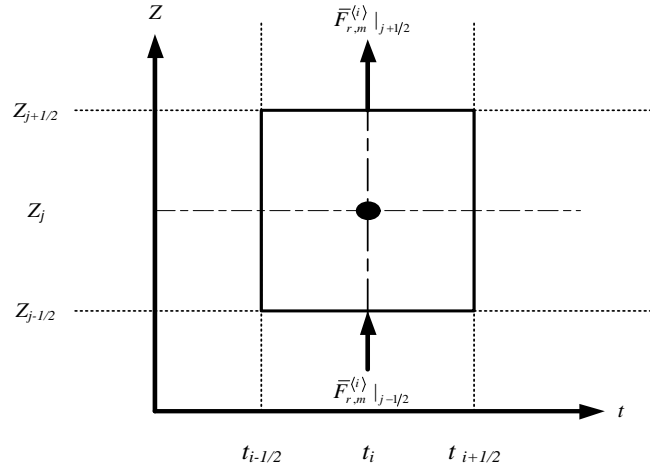


Fig. 1: Two-dimensional representation of the space-time grid.

For more information concerning the application of higher order numerical schemes, the reader can refer to Attarakih (2004). The initial conditions of Eq. (1) are zero for all quantities derived from the droplet population density, while the boundary conditions are given by:

$$\left[\bar{F}_{r,j}^{(i)} - D_d \partial_z \mu_{r,j}^{(i)} \right] \Big|_{z=0} = 0 \quad (7)$$

$$\left[D_d \partial_z \mu_{r,j}^{(i)} \right] \Big|_{z=H} = 0 \quad (8)$$

where H is the extraction column height. Based on the decoupling approach, the solution algorithm for solving the hydrodynamic moments transport equations is as follows:

- 1) Start with given initial conditions for specified value of N_q , number of spatial cells (n) and final simulation time: $\mu_{r,j} = 0, \forall r = 0, 1, \dots, N_q, j = 1, 2, \dots, n$.
- 2) For all $\mu_{r,j} > \varepsilon$ (ε is a small number \approx machine epsilon) calculate the quadrature weights and nodes using the TUEQWQ or the TEQWQ.
- 3) Calculate the numerical fluxes as given by Eqs. (4, 5, 6).
- 4) Calculate the dispersed phase holdup.
- 5) Calculate the source term $S_{r,j} = 0, \forall r = 0, 1, \dots, N_q, j = 1, 2, \dots, n$ using as given by Attarakih et al. (2009a, b) supplement by the breakage and coalescence frequencies.
- 6) Solve the set of ordinary differential equations given by Eq. (3) along with the boundary conditions given by Eqs. (7 & 8) using the MATLAB ordinary differential equation solver ode45.

1.3 Column hydrodynamics and mass transfer

In this section, the required hydrodynamic and mass transfer models and correlations for closing the mathematical model as given by Eq. (1) are presented and briefly discussed. These correlations are used to estimate the required flow field variables inside Kühni liquid extraction column as discussed in section 1 and include: the droplet rising velocity, the energy dissipation, and the breakage, and coalescence kernels as well as the mass transfer correlations.

1.3.1 Droplet rising velocity

Liquid droplet moves through the extraction column in the continuous phase due to the difference in densities between the two phases. Then it accelerates until the buoyancy force is balanced by the drag force (Gourdon et al., 1994). This steady state velocity is called the droplet rising velocity. The rising velocity of a single droplet depends on the physical properties of the liquid system and the droplet diameter (Garthe, 2006). In general, droplet rising velocity is given by (Gourdon et al., 1994):

$$u_d(\alpha_d, d) = u_s(\alpha_d, d) - \frac{u_c^{in}}{(1 - \alpha_d)} \quad (9)$$

Where u_s is the slip velocity, and u_c^{in} is the continuous phase superficial velocity. Here, the slip velocity of a single droplet is modified to take into account the interactions occurring among the other droplets in the swarm. Moreover, the slip velocity is related to the slowing factor (k_s), which takes into account the effect of the column internal geometry on the droplet terminal velocity (Garthe 2006; Steinmetz, 2007). In this work, the slip velocity is given by (Gourdon et al., 1994):

$$u_s(\alpha_d, d, P) = k_s(d, P) \cdot (1 - \alpha_d) \cdot u_t(\alpha_d, d, P) \quad (10)$$

where u_t is the droplet terminal velocity of a single droplet, which depends on the droplet internal state. Actually, the terminal velocity is one of the most important parameters used in liquid-liquid extraction equipment design and scale-up (Garthe, 2006). This is because it aides in getting the required information about the actual dispersed phase velocity inside the column. Following Attarakih et al. (2012a, b; 2015a), the terminal velocity law of Wesselingh and Bollen (1999) is implemented, which covers small and large droplet regimes (Wesselingh and Bollen, 1999):

$$u_t = \left[\left(\frac{g |\rho_c - \rho_d| d^2}{18\mu_c} \right)^{-0.85} + \left(1.74 \frac{g |\rho_c - \rho_d| d}{\rho_d} \right)^{-0.85} \right]^{-1/0.85} \quad (11)$$

In this equation, the first term takes into account the viscous force on the rising droplet and the inertia of droplet is taken into account by the second term. Wesselingh and Bollen (1999) combined these two terms in the above equation where interpolation between these two regimes is allowed. Attarakih et al. (2012a, b) examined the validity of this equation using a general droplet terminal velocity model with a drag coefficient, following Drumm (2010), this coefficient was calculated using the well-known correlation of Schiller and Naumann (1935) where a good agreement between the Wesselingh and Bollen (1999) and the terminal velocity with a drag coefficient, was found. The slowing effect due to internal column geometry is given by Steinmetz (2007):

$$k_s = 0.0028 \cdot \left(\frac{D_s - D_R}{d} \right) + 0.7227 \cdot \frac{D}{H_c} \cdot \exp \left(-0.5 \left(\frac{Ne - 1.703}{0.3105} \right)^2 \right) \quad (12)$$

Here, D_s is the stator diameter, D_R is the rotor diameter, H_c is the compartment height, and N_e is Newton's number. This correlation results in positive slowing factors over the whole operating and simulation ranges, which is an obvious advantage when compared to the correlation of Garthe (2006).

1.3.2 Droplet breakage

Droplet breakage takes place in agitated liquid extraction columns due to the shear forces of the rotating shafts and the turbulent continuous phase (Gourdon et al., 1994; Garthe, 2006; Hlawitschka, 2013). In general, the physical properties (mainly the surface tension and viscosity), droplets size and the energy dissipation have a significant contribution to the breakage frequency inside the column (Garthe, 2006). The droplet breakage frequencies required by the population balance model is given by (Gourdon et al., 1994):

$$\Gamma(d, \alpha_d) = P(d) / \tau_m \quad (13)$$

where $P(d)$ is the breakage probability and τ_m is the droplet mean residence time. During the last decades many researchers proposed droplet breakage frequency models. Coualoglou and Tavlarides (1977) studied the droplets breakage rate in a turbulent velocity field where they assumed that the droplet breakage frequency is induced by the drop-eddy collisions. Although the proposed model by Coualoglou and Tavlarides (1977) provides an experimental approach toward testing the models and their behavior (Zedel, 2010). It has the drawback of neglecting the viscosity effect (Maaß et al., 2012). To overcome this limitation, another breakage model was developed by Alopaeus et al. (2002). In the same direction, Maaß et al. (2012) extended the model of Alopaeus et al. (2002) by including a damping factor. This factor takes into account the damping of the flow field turbulence due to dispersed phase volume fraction. In order to study the breakage rate for high viscous systems, Schmidt (2006) developed a breakage probability correlation based on the modified Weber number for stirred LLEC's (Schmidt, 2006):

$$\frac{p_B}{1 - p_B} = c_1 \cdot \left(\frac{W_{\text{mod}}}{1 + c_2 \cdot \eta_d \cdot [W_{\text{mod}} / (\gamma \cdot d_m \cdot \rho_d)]^{0.5}} \right)^{c_3} \quad (14)$$

where the modified Weber number W_{mod} is given by (Garthe, 2006):

$$We_{\text{mod}} = \frac{\rho_c^{0.8} \eta_c^{0.2} d_m D_R^{1.6} (2\pi)^{1.8} [N^{1.8} - N_{\text{crit}}^{1.8}]}{\sigma} \quad (15)$$

The critical rotational speed N_{crit} is the rotational speed below which no breakage occurs and it is given by (Garthe, 2006):

$$n_{R,\text{crit}} = c_4 \cdot \frac{d_A^{-2/3} \cdot \eta_d \cdot d_m^{-4/3}}{2 \cdot (\rho_c \cdot \rho_d)^{0.5}} + \left[\left(c_4 \cdot \frac{d_A^{-2/3} \cdot \eta_d \cdot d_m^{-4/3}}{2 \cdot (\rho_c \cdot \rho_d)^{0.5}} \right)^2 + c_5 \cdot \frac{\sigma}{\rho_c \cdot d_A^{4/3} \cdot d_m^{5/3}} \right]^{0.5} \quad (16)$$

The parameters c_i , appearing in Eqs. (14 & 16) depend on the column geometry (see Table 1). These parameters are estimated by a regression analysis against the experimental data.

Table 1: Correlation parameters for Eqs. (3.14 & 3.16)

Column type	Author	C_1	C_2	C_3	C_4	C_5
RDC	Garthe (2006)	1.29×10^{-6}	0.33	2.78	0.020	0.13
	Modes (2000)	6.04×10^{-4}	0.00	1.595	0.020	0.13
Kühni	Garthe (2006)	1.63×10^{-3}	0.48	3.05	0.13	1.21×10^{-2}
	Fang et al., (1994)	4.60×10^{-3}	0.68	3.19	0.739	4.7×10^{-2}

1.3.3 Droplet coalescence

During droplets movement in the extraction column, they collide with each other with a certain specific efficiency. As a result of these collisions, there will be coalescence among the droplets (of different or same sizes) which results in total holdup reduction (Gourdon et al., 1994). These collisions mainly occur under the column stators and cause a droplet velocity distribution. Based on the film drainage theory and kinetic theory of gases, Coualoglou and Tavlarides (1977) developed a coalescence model for stirred liquid-liquid vessels. The coalescence frequency is given by the product of collision rate $h(d, d', \alpha_d)$ and coalescence efficiency $\lambda(d, d', \alpha_d)$ between two droplets of diameters d and d' :

$$\omega(d, d', \alpha_d) = h(d, d', \alpha_d) \cdot \lambda(d, d', \alpha_d) \quad (17)$$

This coalescence model was modified by Tsouris and Tavlarides (1994) and the expression of the collision rate is given by:

$$h(d, d', \alpha_d) = C_1 \cdot \left(\frac{\pi}{6} \right)^{7/9} \cdot \left(\frac{\varepsilon^{1/3}}{1 + \alpha_d} \right) \cdot (d^2 + d'^2) \cdot (d^{2/3} + d'^{2/3})^{1/2} \quad (18)$$

In Eq. (19), ε is the energy dissipation and it is correlated for agitated columns as follows (Kumar and Hartland, 1996):

$$\varepsilon = \frac{4P}{\pi D_c^2 H_c \rho_c} \quad (19)$$

Where P is the power input per unit mass and it is a function of the rotational speed (N_s) and power number (N_p). Based on the film drainage theory, the coalescence efficiency $\lambda(d, d', \alpha_d)$ depends on the liquid system physical properties, the droplet diameter and the energy dissipation. The coalescence efficiency is given by (Coualoglou and Tavlarides, 1977):

$$\lambda(d, d', \alpha_d) = \exp\left(-\left(\frac{\pi}{6}\right)^{4/3} \cdot \frac{C_2 \eta_c \rho_c \varepsilon}{\sigma^2 (1 + \alpha_d)^3} \cdot \left(\frac{dd'}{d + d'}\right)^4\right) \quad (20)$$

1.3.4 Interphase mass transfer

The solute transfer rate across the droplet interface may be controlled by molecular diffusion or by the motion of eddies (Slater, 1994; Kumar and Hartland, 1999). To date, the actual mechanism of the mass transfer across the interface is not well known yet (Slater, 1994). In general, the mass transfer rate inside the extraction equipment depends mainly on the overall mass transfer coefficient (k_{od}), where the rate of change of droplet contents in terms of the overall mass transfer coefficient is given by:

$$\frac{\partial c_d}{\partial t} = \frac{6k_{od}}{d} (mc_c - c_d) \quad (21)$$

In the above equation, m is the distribution coefficient, and c_d and c_c are the solute concentration in the dispersed and continuous phases respectively. In this work, the distribution coefficient is correlated as a function of solute mass fraction in the continuous phase (c_c) based on the experimental work of Garthe (2006) and it is given by (Alzyod et al., 2016a, b, c; 2017):

$$m = \exp(a \times c_c + b) \quad (22)$$

The parameters a and b were estimated using the PPBLab activity model optimization tool (Attarakih et al., 2012a; 2017). The values of these parameters are shown in Table 2 (see Fig. 2).

Table 2: Distribution coefficient correlation parameters (see Eq. (22))

Chemical system	a	b
Water–acetone–toluene	2.660	-0.41040
Water–acetone–butyl acetate	1.121	-0.09792

In this work, the two film theory of Whitman is the most commonly used. In this theory, the overall mass transfer coefficient is the reciprocal of the overall resistance and is given by:

$$k_{od} = (m/k_c + 1/k_d)^{-1} \quad (24)$$

Where k_c and k_d are the individual mass transfer coefficients in the heavy and light phases respectively. These coefficients are described in detail in the following sections.

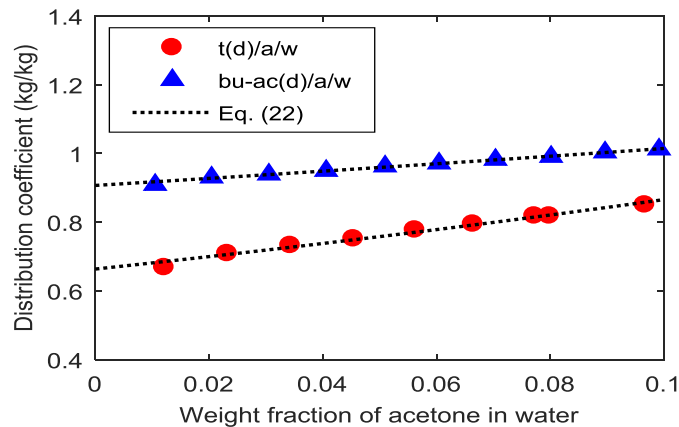


Fig. 2: Comparison between the calculated distribution coefficient values using Eq. (22) and the experimental data of Garthe (2006).

1.4 Analytical, numerical and experimental validation

In this section, the SQMOM is validated at three different levels: analytical, numerical and experimental levels. At the analytical level, the SQMOM is validated against a simplified analytical solution for the population balance equation in a batch stirred tank for particle breakage and aggregation. The analytical solution for this simplified case is given by McCoy and Madras (2003). At the second level, the SQMOM results are compared with the PPBLab (Attarakih et al., 2012a, 2017) software as a detailed population balance solver. Finally, at the experimental level, the SQMOM is validated using the available published transient experimental data by Zamponi (1996). The chemical test system used here is water (c)-acetone-toluene (d). The physical properties are taken from Garthe (2006). The column used in all simulations is a pilot plant Kühni DN150 liquid-liquid extraction column where its detailed dimensions are shown in Table 3.

Table 3: Kühni column geometry (all dimensions are in mm) (Zamponi, 1996).

Active height	Column diameter	Rotor diameter	Compartment height
2.520	150	85	70

1.4.1 Analytical validation

This section is devoted to test the accuracy of the developed numerical scheme presented in the previous section, where the results are compared with the analytical solution of McCoy and Madras (2003) for a stirred batch vessel. In this validation, the required number of sections is set to one. As a case study, only a single Kühni compartment is simulated, where the initial condition is given by (Attarakih et al., 2009a):

$$f(d, t=0) = 3d^2 \exp(-d^3) \quad (24)$$

The minimum and maximum droplet diameters are 0.01 and 3 mm respectively. The inlet flow rates for both phases are set to zero to approach a stirred batch vessel.

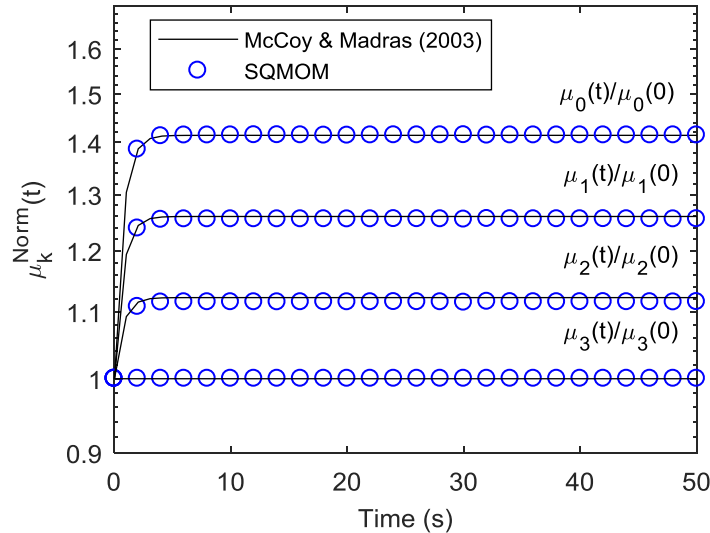


Fig. 2: Comparison between the analytical (McCoy and Madras, 2003) and predicted normalized moment's ($\mu_r^{norm}(t) = \mu_r(t)/\mu_r(0)$) evolution in a batch stirred vessel.

Here, a power breakage frequency is used ($\Gamma = 0.01 \times d^3$), while the coalescence frequency is taken as a constant value ($\omega = 0.01$). The daughter droplets distribution is given by (Attarakih et al., 2009a):

$$\beta(d/d') = \begin{cases} 6d^2/d'^3, & 0 < d < d' \\ 0, & \text{Otherwise} \end{cases} \quad (25)$$

Fig. 2 shows a comparison between the simulated normalized low order moments and the analytical solution. It can be clearly observed that one section is enough to predict accurately the hydrodynamic source terms. As a result of this, the number of sections is fixed at one in the experimental validation.

1.4.2 Numerical and experimental validation

This section is devoted to validate the extended SQMOM at numerical and experimental levels. At the numerical level, the SQMOM model prediction is validated using PPBLab software. In this regard, the extended pivot technique, as implemented in PPBLab, with a multi-sectional grid with respect to droplet diameter and solute concentration is used. At the experimental validation level, the SQMOM is validated against the transient experimental data published by Zamponi (1996) using Kühni extraction column. The effect of changing the inlet feed flow rates and inlet solute concentration on the hydrodynamics and mass behavior are investigated. Here, the droplet velocity model is given by Wesselingh and Bollen (1999), while the breakage probability and the coalescence frequency are given by Fang et al., (1995) and Coulaloglou and Tavlarides (1977) respectively. The mean inlet diameter is taken 1.80 mm as an average value for all cases based on the reported experimental data of Zamponi (1996). Table 4 shows the operating conditions for the dynamic experimental validation. The adjusted correlation parameters of Coulaloglou and Tavlarides (1977) model (C_1 and C_2) are estimated by fitting the simulated column hydrodynamics (dispersed phase holdup and mean droplet diameter) to the experimental data and found to be $C_1 = 0.01$ and $C_2 = 1.33 \times 10^{10} \text{ m}^{-2}$ respectively.

Table 4: Operating conditions for dynamic validation (Zamponi, 1996)

Exp. set	Q_c^{in} (L/h)	Q_d^{in} (L/h)	C_c^{in} (kg/kg)%	C_d^{in} (kg/kg)%
D ₂	125.0	160.0	5.0	0.0
D ₃	137.5	175.0	0.0	0.0
D ₄	112.5	144.0	0.0	0.0

These values are in the same order of magnitude as those used by Attarakih et al. (2015a) and Alzyod (2013) for a Kühni extraction column where they implemented OPOSPM as a reduced population balance model to simulate the same geometry under the same operating conditions. Table 5 shows a comparison between the adjusted coalescence model parameters and the published values by Attarakih et al. (2015a) and Alzyod (2013).

Table 5: Comparison between the adjusted coalescence model parameters and the published values

Author	Attarakih et al. (2015a)	Alzyod (2013)	Current work
C_1 (-)	0.03	0.03	0.01
C_2 (m ⁻²)	1.33×10^{10}	1.33×10^{10}	1.33×10^{10}

The slight reduction in the value of C_1 in the present work is attributed to the difference in the used population balance models. In this work the SQMOM is used with two quadrature nodes, while Attarakih et al. (2015a) and Alzyod (2013) used OPOSPM as a special case of SQMOM with only one quadrature node. Fig. 3 shows the effect of combined (positive and negative) step changes of the total throughput on the dynamic response of the dispersed phase holdup. The simulation was carried out at a total throughput of $16 \text{ m}^3/\text{m}^2 \cdot \text{s}$ without mass transfer. At $t = 200 \text{ s}$ a positive step change in the total throughput was carried out from 16 to $17.6 \text{ m}^3/\text{m}^2 \cdot \text{s}$ followed by two negative step changes from 17.6 to $16 \text{ m}^3/\text{m}^2$ and finally from 16 to $14 \text{ m}^3/\text{m}^2$ respectively. It is clear that the dispersed phase holdup is increased in the first positive step. This is because of increasing the dispersed phase inlet flow rate (Oliveira et al., 2008). Moreover, by increasing the continuous phase inlet flow rate, the drag force between the continuous

phase and dispersed phase droplets increases, which reduces the dispersed phase velocity and increases the residence time inside the column (Oliveira et al., 2008; Gomes et al., 2009).

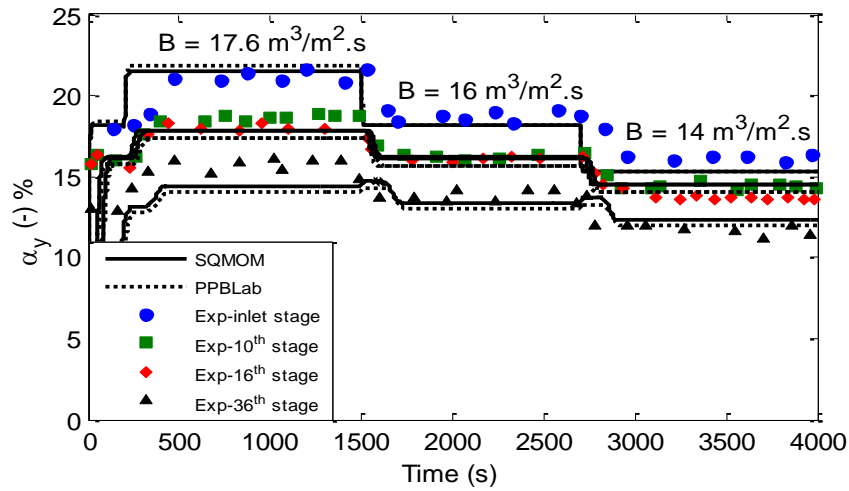


Fig. 3: Comparison between simulated and experimental (Zamponi et al., 1996) dynamic response of the holdup profile due to combined step changes in the total throughput.

After 1500 s the holdup was reduced and brought back to its original value due to the second negative step change. Finally, the holdup values decrease again and reach the final steady state value due to the last negative step change. A very good agreement between the simulated and experimental data is obtained using the SQMOM and PPBLab software. It is worthwhile to mention here that the adjusted coalescence parameter (C_1) was found the same for the whole combined steps. Again, this indicates that C_1 is insensitive to change in flow rate. Based on the holdup dynamics validation using the adjusted droplet coalescence model parameter (C_1), the converged holdup profiles are used to predict the column mass transfer profiles. This approach was proposed by many researchers and proved to be successful for mini-plant simulation and industrial cases (Alzyod et al., 2013; Attarakih et al., 2012a, 2013, 2015a). Fig. 4 shows the variation of the solute concentration in the continuous phase at five different measuring points along the column height (see Table 6) due to positive step change in the continuous phase inlet flow rate from 125 to 150 liter/h after reaching the steady state conditions using D_2 experimental data set.

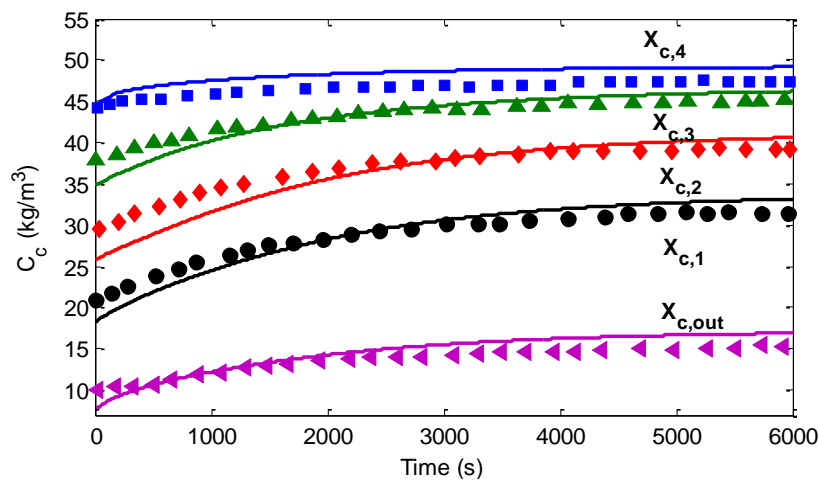


Fig. 4: Comparison between simulated and experimental (Zamponi et al., 1996) dynamic evolution of the solute mass fraction in the continuous phase due to positive step change in the continuous phase flow rate from 125 to 150 liter/h after reaching steady state conditions using D_2 experimental data set.

Table 6: Location of measuring points along the extraction column height

Symbol	$X_{c,out}$	$X_{c,1}$	$X_{c,2}$	$X_{c,3}$	$X_{c,4}$
Stage	Bottom	8 th	14 th	23 rd	32 nd

Both simulation and experimental results indicate that the solute concentration increases with time. Moreover, it is clear that the lag time along the column height is almost negligible. This is because of the homogeneity nature of the continuous phase where any disturbance occurs in the continuous phase will rapidly affect the entire column. Fig. 5 shows the variation of the solute mass fraction in the continuous phase due to a positive step change in the dispersed phase inlet flow rate from 160 to 190 liter/h after reaching the steady state conditions using D_2 experimental set. It is clear that increasing the dispersed phase inlet flow rate results in a higher holdup values as shown in Fig. 3 ($t \in [200 \ 1000]$), which reduces the solute mass fraction in the continuous phase. Moreover, the speed of response for the solute mass fraction in this case is slow (has a lag time) especially in the upper stages of the column (away from the disturbance stage). This is again due to the velocity distribution of the droplets inside the column as mentioned earlier.

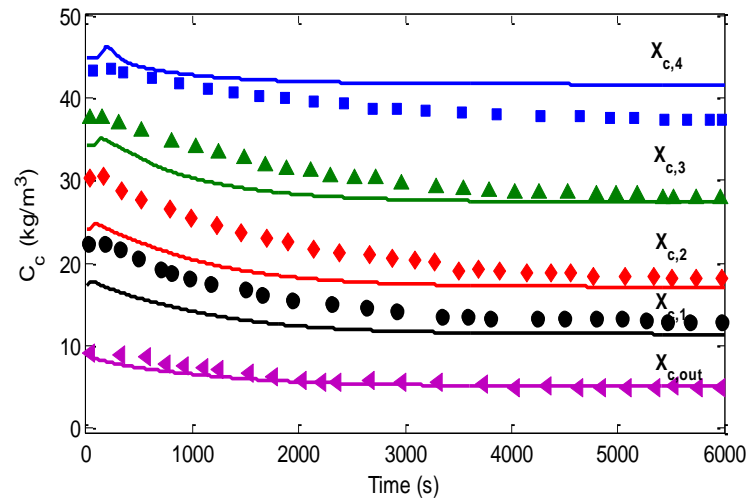


Fig. 5: Comparison between simulated and experimental (Zamponi et al., 1996) dynamic evolution of the solute mass fraction in the continuous phase due to positive step change in the dispersed phase inlet flow rate from 160 to 190 liter/h after reaching steady state conditions using D_2 experimental data set.

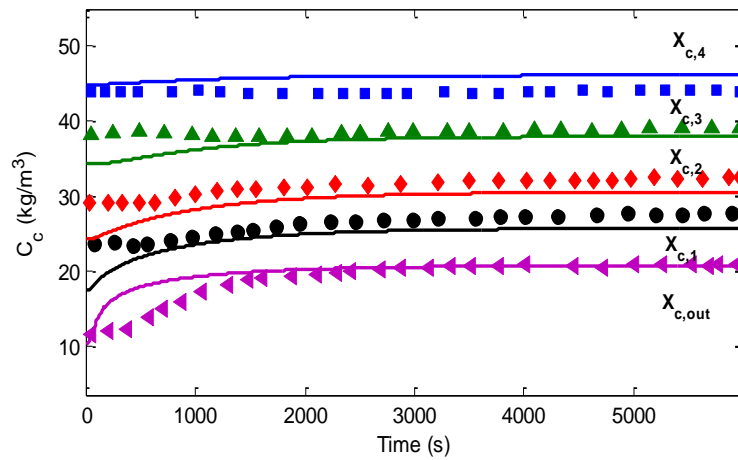


Fig. 6: Comparison between simulated and experimental (Zamponi et al., 1996) dynamic evolution of the solute mass fraction in the continuous phase due to positive step change in the dispersed phase inlet flow rate from 160 to 190 liter/h after reaching steady state conditions using D_2 experimental data set.

Fig. 6 shows the dynamic response of the solute mass fraction in the continuous phase due to positive step change in the dispersed phase inlet concentration from 0 to 0.01 kg/m³ after reaching the steady conditions. Moreover, it can be observed that the model response is faster than the experimental data response especially at the disturbance stage (dispersed phase inlet stage). The reason behind this dynamic behavior of the simulated data is that the step change was performed at the dispersed phase inlet point since we don't have any information about the actual mixing point position (pipe length).

1.5 Conclusions

The SQMOM is extended to solve the nonhomogeneous PBE and adapted to model the hydrodynamic and mass transfer dynamic behavior of liquid-liquid extractions columns. A stable numerical scheme based on the finite volume method and the flux vector splitting technique is developed and implemented. The proposed numerical scheme is first order accurate in space and fifth order accurate with respect to the time. The extended SQMOM mathematical framework is able to capture the dynamic behavior of liquid-liquid extraction equipment as demonstrated by different case studies. These case studies include: analytical, numerical, and experimental studies. At the numerical level, the extended model is validated using the extended fixed pivot technique solver as implemented in PPBLab software. For the experimental case study the model is used to simulate the dynamic behavior of a Kühni and validated using the published experimental data. In this regard, at both validation levels, the model prediction shows very good agreement with the numerical and experimental results.

Nomenclature

C	Solute concentration (kg/m ³)
d	Droplet diameter (m)
D _c	Column diameter (m)
D _R	Rotor diameter (m)
D _S	Stator diameter (m)
Eö	Eötvös number (-)
F	Flux vector as given by Eq. (7)
g	Acceleration of gravity (m/s ²)
h	Coalescence frequency (s ⁻¹)
H _c	Compartment height (m)
k _{oy}	Overall mass transfer coefficient (m/s)
k _s	Slowing factor (-)
m	Solute distribution coefficient
N _{pp}	Number of sections (-)
N _q	Number of quadrature points (-)
N _s	Rotational speed (s ⁻¹)
P	Power number (-)
Q	Flow rate (L/h)
S	Source term
t	Time (s)
u	Velocity (m/s)
We	Weber number (-)
z	Space coordinate
x	Mass fraction (kg/kg)

Greek Symbols

λ	Coalescence efficiency (m ³)
μ _{r,k}	Two dimensional moment
α	Volume fraction (-)
Γ	Breakage frequency (1/s)
δ	Dirac delta function (m ⁻¹)
ε	Energy dissipation (m ² /s ³)
η	Viscosity (Pa.s)
ρ	Density (kg/m ³)
σ	Interfacial tension (n/m)
τ _m	Droplet residence time (s)
ω	Coalescence frequency (m ³ /s)

Subscript

c,d	Continuous and dispersed phases respectively
r	Relative velocity
s	Slip velocity
t	Terminal velocity

References

- Alopaeus, V., Koskinen, J., Keskinen, K.I. (2002). Simulation of the population balances for liquid-liquid systems in a nonideal stirred tank. part 2 parameter fitting and the use of the multi-block model for dense dispersions. *Chem. Eng. Sci.* 57, 1815-1825.
- Alzyod, S., Attarakih, M., Bart H.-J. (2016a), Dynamic Modelling of Kühni Liquid Extraction Columns Using the Sectional Quadrature Method Of Moments (SQMOM). *Comput. Chem. Eng.* 94, 1-12.
- Alzyod, S., Attarakih, M., Hasseine, A., Bart H.-J. (2017a), Steady state modelling of a Kühni liquid extraction column using the Spatially-Mixed Sectional Quadrature Method Of Moments (SM-SQMOM). *Chem. Eng. Res. Des.* 117, 549–556.
- Alzyod, S., Korb, C., Attarakih, M., Bart, H.-J. (2017b). Steady State Population Balance Modelling of Zinc Extraction in a Kühni Liquid-liquid Extraction Column, *Proceedings of the International Solvent Extraction Conference (ISEC2017)*, 63-70. Miyazaki, Japan.
- Alzyod, S., Attarakih, M., Bart, H.-J. (2017c). CFD Modelling of pulsed sieve plate liquid extraction columns using OPOSPM as a reduced population balance model, *Comput. Aided Chem. Eng.* 40, 61-66.
- Alzyod, S. (2013). A one primary one secondary particle method simulink module for the steady state and dynamic modelling of Kühni extraction column, master thesis. The University of Jordan.
- Alzyod, S., Attarakih, M., Bart H.-J. (2016b), The Sectional Quadrature Method of Moments (SQMOM): An extension to nonhomogeneous bivariate population balances. *Chem. Eng. Res. Des.* 117, 549–556.
- Alzyod, S., Attarakih, M., Hasseine A., Bart H.-J. (2016c), Population Balance Modelling of Liquid Extraction Columns using the Sectional Quadrature Method of Moments (SQMOM), *Comput. Aided Chem. Eng.* 38, 427-432.
- Alzyod, S., Attarakih, M., Bart H.-J., (2016d), Detailed Modelling of an RDC liquid extraction column using the Sectional Quadrature Method Of Moments (SQMOM), In: *Fraunhofer ITWM (Hg.): Young Researchers Symposium 2016 (YRS 2016)*. Stuttgart: Fraunhofer Verlag, 9-14.
- Alzyod, S., Attarakih, M., Bart, H.-J. (2018). CFD modelling of pulsed sieve plate liquid extraction columns using OPOSPM as a reduced population balance model: hydrodynamics and mass transfer. *Comput. Aided Chem. Eng.* 43, 451-456.
- Attarakih M., Alzyod S., Fricke A. (2017). Population balance modelling of pulsed packed bed extraction columns using PPBLab software. *Comput. Aided Chem. Eng.* 40, 67-72.
- Attarakih, M., Al-Zyod, S., Abu-Khader, M., Bart, H.-J. (2012a). PPBLAB: A new multivariate population balance environment for particulate system modelling and simulation. *Procedia Eng.* 42, 144-562.
- Attarakih, M., Albaraghtli, T., Abu-Khader, Hamamre, Z., Bart, H.-J. (2012b). Mathematical modelling of high-pressure oil-splitting reactor using a reduced population balance model. *Chem. Eng. Sci.*, 84, 276-291.
- Attarakih, M., Jildeh, H. B., Mickler, M., and Bart, H.-J. (2012a). The OPOSPM as a nonlinear autocorrelation population balance model for dynamic simulation of liquid extraction columns. *Comput. Aided Chem. Eng.* 31, 1216-1220.
- Attarakih, M. M., Drumm, C., Bart, H.-J. (2009a). Solution of the population balance equation using the Sectional Quadrature Method of Moments (SQMOM). *Chem. Eng. Sci.* 64, 742-752.
- Attarakih, M., Jaradat, M., Drumm, C., Bart, H.-J., Sudarshan Tiwari, S., Sharma, V., Kuhnert, J., Klar, A. (2009b). A multivariate population balance model for liquid extraction columns. *Comput. Aided Chem. Eng.* 26, 1339-1344.
- Attarakih, M., Hlawitschka, M., Abu-Khader, M., Alzyod, S., Bart, H.-J. (2015b). CFD-population balance modelling and simulation of coupled hydrodynamics and mass transfer in liquid extraction columns. *Appl. Math. Model.* 39, 5105–5120.

- Attarakih, M., Alzyod, S., Hlawitschka, M., Bart, H.-J. (2015a). OPOSSIM: a population balance-SIMULINK module for modelling coupled hydrodynamics and mass transfer in liquid extraction equipment. *Comput. Aided Chem. Eng.* 37,257-262.
- Attarakih, M., Bart, H.-J., Faqir, N. (2006). Numerical solution of the bivariate population balance equation for the interacting hydrodynamics and mass transfer in liquid-liquid extraction columns. *Chem. Eng. Sci.*, 61, 113-123.
- Attarakih, M. (2004). Solution methodologies for the population balance equations describing the hydrodynamics of liquid-liquid extraction contactors. Dissertation. Technische Universität Kaiserslautern, Germany.
- Attarakih, M., Abu-Khader, M., Bart, H.-J. (2013). Modelling and dynamic analysis of an RDC extraction column using OPOSPM. *Chem. Eng. Sci.* 91, 180-196.
- Coulaloglou, C. A., Tavlarides, L.L. (1977). Description of interaction processes in agitated liquid-liquid dispersions. *Chem. Eng. Sci.* 32, 1289-1297.
- Drumm, C. (2010). Coupling of computational fluid dynamics and population balance modelling for liquid-liquid extraction, Dissertation. Technische Universität Kaiserslautern, Germany.
- Fang, J., Godfrey, Z.-Q., Slater, M. J., Gourdon, C., (1995), Single liquid drop breakage probabilities and characteristic velocities in Kühni columns. *Chem Eng. Technol.* 18, 41-48.
- Garthe, D. (2006). Fluid dynamics and mass transfer of single particles and swarms of particles in extraction columns. Dissertation. Technische Universität München, Germany.
- Gomes, L.N., Guimaraes, M.L., Stichlmair, J., Cruz-Pinto, J.J., 2009. Effects of mass transfer on the steady state and dynamic performance of a Kuhni column experimental observations. *Ind. Eng. Chem. Res.* 48, 3580-3588.
- Gourdon, C., Casamatta, G., Muratet, G. (1994). Population Balance Based Modelling. In: Godfrey & Slater (Ed). *Liquid-liquid extraction equipment.* (pp.140-226), New York, John Wiley and Sons.
- Hlawitschka, M. (2013). Computational fluid dynamics aided design of stirred liquid-liquid extraction columns, Dissertation. Technische Universität Kaiserslautern, Germany.
- Jaradat, M., Attarakih, M., Bart, H.-J. (2012a). RDC extraction column simulation using the multi-primary one secondary particle method: coupled hydrodynamics and mass transfer. *Comput. Chem. Eng. J.* 37, 22-32.
- Jaradat, M. M., Attarakih, M. M., Steinmetz, T., Bart, H.-J. (2012b), LLECMOD: A Bivariate Population Balance Simulation Tool for Pulsed Liquid-Liquid Extraction Columns, *Open Chem. Eng. J.* 6: 8-31.
- Jildeh, H.B., Hlawitschka, M., Attarakih, M.M., Bart, H.-J. (2012). Solution of Inverse Problem with the One Primary and One Secondary Particle Model (OPOSPM) Coupled with Computational Fluid Dynamics (CFD). *Procedia Eng.* 42, 1692-1710.
- Jildeh, H.B., Attarakih, M.M., Mickler, M. & Bart, H.-J. (2014). Parameter optimization and validation for droplet population balances. *Can. J. Chem. Eng.* 92, 210-219.
- Kumar, A., Hartland, S., (1996). Unified correlations for the prediction of drop size in liquid-liquid extraction columns, *Ind. Eng. Chem. Res.* 35, 2682-2695.
- Kumar, A. and Hartland, S. (1999). Correlations for prediction of mass transfer coefficients in single drop systems and liquid-liquid extraction columns. *Trans. Inst. Chem. Eng.*, 77 (Part A), 372-384.
- Maaß, S., Paul, N., Kraume, M. (2012). Influence Of the dispersed phase fraction on experimental and predicted drop size distributions in breakage dominated stirred systems. *Chem. Eng. Sci.* 76, 140-153.
- McCoy, J., Madras, G. (2003). Analytical solution for a population balance equation with aggregation and fragmentation. *Chem. Eng. Sci.* 58, 3049-3051.
- Modes, G. (2000). Grundsätzliche Studie zur Populationsdynamik einer Extraktionskolonne auf Basis von Einzeltropfenuntersuchungen. Dissertation, Shaker Verlag, Aachen

- Oliveira, N.S., Silva, D.M., Gondim, M.P.C., Mansur, M.B. (2008). A study of the drop size distributions and hold-up in short Kuhni columns. *Braz. J. Chem. Eng.* 25, 729–741.
- Patankar, S. (1980). *Numerical Heat Transfer and Fluid Flow*. Taylor & Francis, Bristol, PA.
- Perry, R. H., Green, D. W. (2008). *Perry's Chemical Engineers' Handbook*. 8th Edition, McGraw-Hill.
- Schiller, L., Naumann, A., (1935). A drag coefficient correlation, *Zeitschrift des Vereins Deutscher Ingenieure* 77, 318–320.
- Schmidt, S., Simon, M., Attarakih, M. , Lagar, L., Bart, H.-J. (2006). Droplet population balance modelling-hydrodynamics and mass transfer. *Chem. Eng. Sci.* 61, 246-256.
- Sharma, V. (2011). *Multi-Phase Flow Model Incorporated with Population Balance Equation in a Meshfree Framework*. Dissertation. Technische Universität Kaiserslautern, Germany.
- Slater, M.J. (1994). Rate coefficients in liquid-liquid extraction systems. In: Godfrey & Slater (Ed), *Liquid-liquid extraction equipment*. (pp.47-94), New York: Eds. John Wiley and Sons.
- Steinmetz, T., (2007), Tropfenpopulationsbilanzgestütztes Auslegungsverfahren zur Skalierung einer gerührten Miniplant Extraktionskolonne, Dissertation, Düsseldorf: VDI Verlag GmbH.
- Tsouris, C., Tavlarides, L.L., (1994). Breakage and coalescence models for drops in turbulent dispersions. *AIChE J.* 40, 395-406.
- Wesselingh, J.A., Bollen, A.M. (1999). Single particles: bubbles and drops: their velocities and mass transfer coefficients. *Chem. Eng. Res. Des.* 77, 89-96.
- Whitman, W.G., (1923), The film theory of absorption, *Chem. Met. Eng.* 29, 147–151.
- Zamponi, G., 1996. *Das Dynamische Verhalten Einer Gerührten Solventextraktionskolonne*. Shaker Verlag, Aachen.
- Zedel, D., (2010). *Experimental Investigations on the Influence of the System Properties and the Drop Diameter on Drop Breakage*. Dissertation. Technische Universität Berlin, Germany.

Chapter 2

Steady State Modelling of Liquid-liquid Extraction Equipment using the Spatially Mixed-SQMOM as a Reduced PBM

2.1 Introduction

Due to the growing market demand, mathematical modelling tools of liquid-liquid extraction equipment are required. These tools should be able to describe the actual hydrodynamic and mass transfer behavior inside the extraction equipment. Therefore, recent mathematical models should be utilized to present a more fundamental design and scale up basis. As a result of this, robust steady state and dynamic numerical algorithms, based on the PBE, are of great importance. To shed more light on the steady state modelling, we present a new steady state algorithm for modelling of the hydrodynamic and mass transfer behavior of liquid-liquid extraction equipment based on the SQMOM in a one dimensional domain. In this regard, the SQMOM is extended to solve the nonhomogeneous spatially distributed population balance equation (w.r.t. droplet diameter and the solute concentration) at steady state. The integral spatial numerical flux is closed using the mean mass droplet diameter (d_{30}) as in the MPSPM, while the hydrodynamics integral source terms are closed using the TEqWQ analytical formula. Therefore, the presented numerical scheme has the name of Spatially Mixed-SQMOM (SM-SQMOM). To facilitate the source terms implementation, an analytical solution based on the algebraic velocity model is derived to calculate the required dispersed phase mean droplet velocity. In addition to this, the hydrodynamics moment transport equations are coupled with the OPOSPM to close the mass transport equations. The required flow field variables and energy dissipation to close the resulting mathematical model equations are estimated using proper correlations as described in detailed in chapter 1. The resulted discreet hydrodynamics system of ordinary differential equations is solved using the adaptive fifth order Runge-Kutta method in the spatial domain. Concerning the mass transfer, the coupled solute transport equations are solved simultaneously due to the boundary conditions constrains. This is due to the existence of two contacted waves, which carry the information about the solute concentration in the continuous and dispersed phases (Attarakih et al., 2013). Therefore, a first order finite volume numerical scheme is developed to solve the mass transfer transport equation. Based on this, the column hydrodynamics transport equations are solved first, and then the mass transfer profiles are predicted independently as will be described in the following subsections. At the validation level, two column geometries are used to check the proposed mixed model predictions. These column geometries include: RDC and Kühni DN80 liquid-liquid extraction columns. In this regard, the published experimental data of Garthe (2006) and Modes (2006) is used at the experimental validation level, while the extended fixed pivot technique solver as implemented in PPBLab is used at the numerical validation level. In this regard, the SM-SQMOM is found able to found able to predict the column hydrodynamics as well as the nonreactive mass transfer profiles as compared with the experimental data. In addition to this, the ability of reconstructing the shape droplet size distribution is successfully examined.

This chapter is organized as follows: in section 2.2 the general framework of the SM-SQMOM is introduced. After that, the discreet model hydrodynamic and mass transfer numerical implementation algorithms are presented. Finally, a 1D numerical and experimental validation is presented using RDC and Kühni columns.

2.2 Steady state modelling of liquid-liquid extraction equipment using the SM-SQMOM

The steady state moment's system of equations which describe the coupled hydrodynamics and mass transfer along the spatial domain can be formulated and written (Alzyod et al., 2017a, b):

$$\partial_z \bar{F}_{r,0}^{(i)} = \partial_z \left(u_d^{(i)} \mu_{r,0}^{(i)} \right) = u_y^{in} \mu_{in}^{(i)} c_{d,in}^m \delta(z - z_d) + S_{B,r,m}^{(i)} + S_{C,r,m}^{(i)} + S_{M,r,m}^{(i)} \quad r = 0, \dots, 2 \times N_q - 1 \quad (1)$$

In this equation, the term on the left hand side is the convection term. As pointed out in the section 2.1, the mean mass droplet diameter is used to close this term and therefore the droplet velocity appears here and the mixed moment can be directly retrieved. Indeed, this is a crucial step to calculate the dispersed phase holdup and to provide an explicit analytical form to calculate the dispersed phase velocity in order to close the model equations. The first term in the left hand side takes in the inlet moments at the dispersed phase inlet point into account, while the second, third, and fourth terms are the breakage, coalescence, and mass transfer source terms. These terms are described in details in chapter 1. Based on Eq. (1), the required quadrature weights and nodes to close the hydrodynamic source terms can be directly calculated using the conserved numerical flux based on the TEqWQ as follows (Alzyod et al., 2017a):

$$d_{1,2}^{(i)} = \hat{F}_{1,0}^{(i)} \mp \frac{1}{\sqrt{3}} \sqrt{\frac{\hat{F}_{3,0}^{(i)}}{\hat{F}_{1,0}^{(i)}} - \left(\hat{F}_{1,0}^{(i)} \right)^2} \quad (2)$$

$$w_{1,2}^{(i)} = \frac{1}{2} F_{0,0}^{(i)} \quad (3)$$

where $d_{1,2}$ and w are the analytical quadrature nodes weights respectively. These quantities were derived from the product difference algorithm using two quadrature points (Attarakih et al., 2009). Here, $\hat{F}_r^{(i)}$ is the normalized r^{th} moment based numerical flux and it is given by:

$$\hat{F}_{r,0}^{(i)} = \frac{\bar{F}_{r,0}^{(i)} \left(d_{30}^{(i)} \right)}{\bar{F}_{0,0}^{(i)} \left(d_{30}^{(i)} \right)} \quad (4)$$

For more information concerning the model mass transfer equations and the analytical dispersed phase velocity solution, the reader can refer to section 4 in the overview section.

2.2.1 The SM-SQMOM implementation

As described in the previous section, the solution proceeds by solving the column hydrodynamics equations first, then the solute mass transfer profiles along the column height are calculated. Fig. 1 shows the calculation sequences of the column hydrodynamics equations, where the solid lines represent the flow of information in one direction, while the dashed lines represent the loops. First, the mean mass droplet diameter and the quadrature nodes and weights are calculated using the initial conditions. After that, the dispersed phase velocity and the dispersed phase volume fraction (α_d) are calculated. Finally, the hydrodynamics source terms are calculated for each section and the flux's conservation equations are calculated and updated for each spatial numerical cell.

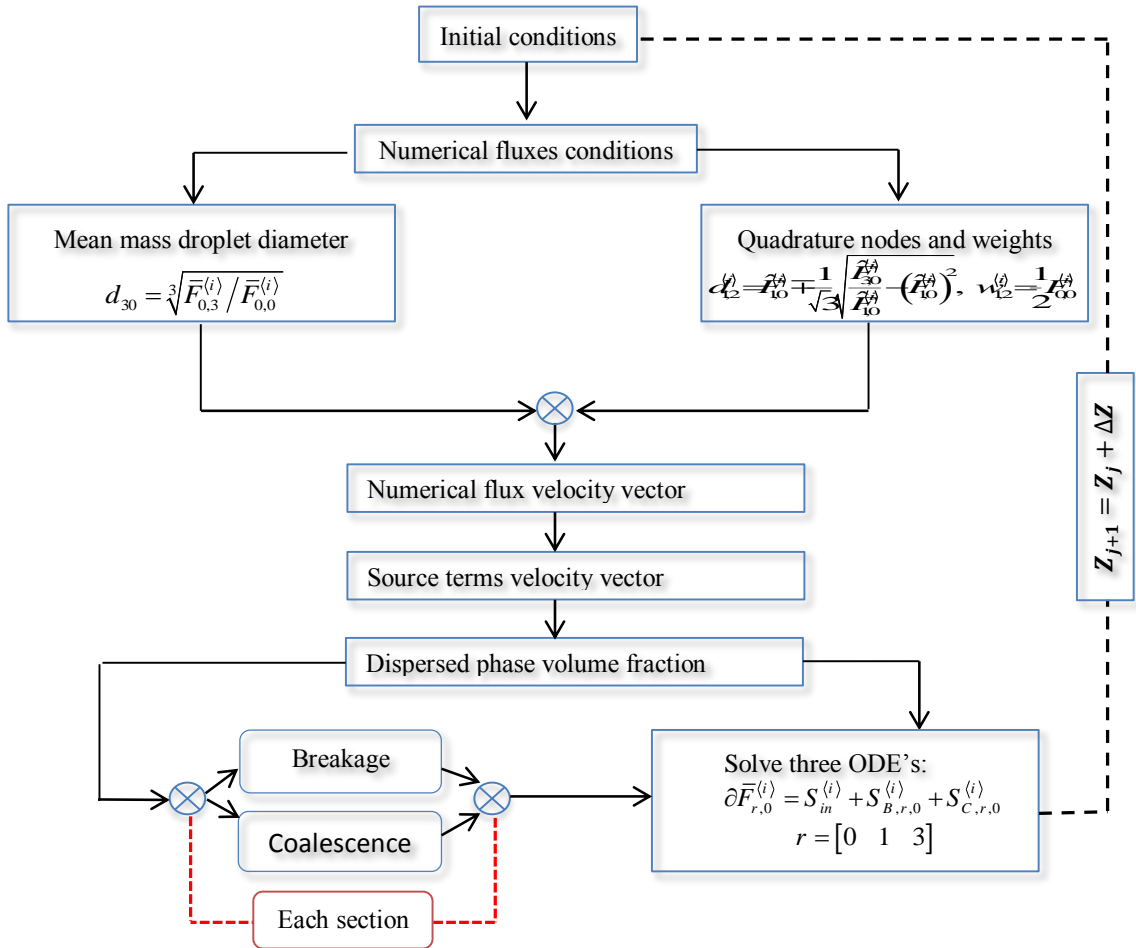


Fig. 1: Column hydrodynamics transport equations solution algorithm.

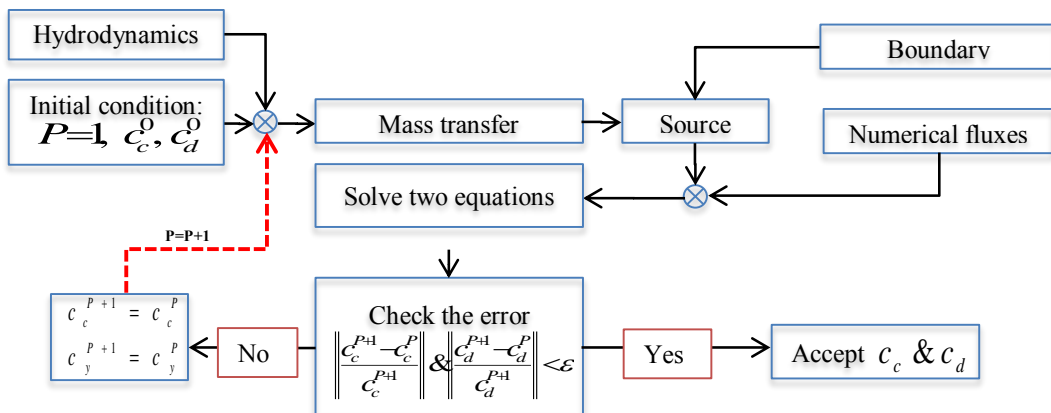


Fig. 2: Solute mass transfer transport equations solution algorithm.

The size of the Ordinary Differential Equation (ODE) system in each spatial numerical cell is proportional to the number of the droplet's sections (N_{pp}) and is equal to $3 \times N_{pp}$. Indeed, each single droplet has its own spatial scale inside the column (Attarakih et al., 2012; 2013; 2015). These different scales call for a special ODE solver to ensure numerical stability. In this work, the MATLAB ODE solver ode45, which is based on the adaptive fifth order Runge-Kutta is used. Following the solution algorithm proposed by Attarakih et al. (2015) and Alzyod (2013), the solute mass transfer profiles are obtained using the converged hydrodynamics integral properties as shown in Fig. 2. Actually, this algorithm is based on the finite volume method, where the first order upwind scheme is implemented here. The solution proceeds by calculating the overall mass transfer coefficient first, and then the mass transfer source term is calculated. After that, the governed transport equations are solved along the column height to calculate the solute concentration in both phases.

2.3 Numerical and experimental validation

This section is devoted to test the proposed SM-SQMOM mixed model accuracy. In this regard, two column geometries are considered: RDC and Kühni extraction columns for the sake of numerical and experimental validation. In the first part of this section, the SM-SQMOM is used to model the hydrodynamics and mass transfer behaviors of an RDC liquid extraction column. Here, the SM-SQMOM ability to reconstruct the shape of the distribution is successfully examined. In the second part of this section, the SM-SQMOM is used to model a Kühni liquid-liquid extraction column. In this regard, two different case studies are presented to demonstrate the SM-SQMOM to predict the mass transfer profiles along the column height.

2.3.1 RDC liquid-liquid extraction column

In this section the SM-SQMOM results are analyzed and compared with the steady state experimental data published by Modes (2006) and Garthe (2006). The chemical systems used are the EFCE (European Federation of Chemical Engineering) test systems: water-toluene and water-acetone-toluene, where the physical properties are taken from Garthe (2006). The column used in simulation is a pilot plant RDC liquid-liquid extraction column where the detailed dimensions are shown in Table 1.

Table 1: RDC column geometry (all dimensions are in m)

Author	Column height	Column diameter	Rotor diameter	Compartment height
Modes (2000)	2.55	0.15	0.090	0.03
Garthe (2006)	4.40	0.08	0.045	0.05

A) RDC DN150 liquid-liquid extraction column

The construction of the distribution function based on a limited number of low-order moments (which is the usual case) is confronted by ill-conditioning and uniqueness problems (John et al., 2007; Attarakih et al., 2009, 2012a, 2012b, 2014). To resolve these problems, Attarakih et al. (2009) introduced the SQMOM which can be viewed as a hybrid method of sectional and QMOM methods. The method comes to resolve the two main problems associated with QMOM (ill-conditioned when large number of moments used) and the moment inconsistency problem of the sectional methods. The first problem was solved by using only few moments which range from two to four local moments in each section of the particle property space.

To avoid the product-difference inversion problem required for abscissa and weights calculations, an analytical solution was derived by Attarakih et al. (2009) to overcome the usually encountered ill-conditioned eigenvalue problem (especially when large number of moments is used). The second problem (uniqueness) associated with constructing the distribution from its low-order moments is solved by the classical

discretization problem which guarantees the uniqueness of the reconstructed distribution (see Ramkrishna, 2000; Attarakih et al., 2009). In this section the ability of SQMOM to reconstruct the experimental droplet size distribution is tested with thorough convergence analysis. The simulation was conducted using water-toluene chemical system. The dispersed phase (toluene) flow rate is 100 liter/h, while the continuous phase flow rate is 112 liter/h. The rotational speed is fixed at 300 rpm. To check the model convergence, the number of required sections to discretize the internal coordinate (d) is varied and the model prediction for the droplet size distribution is compared with the measured experimental data (Modes, 2000) in the middle of the column as shown in Fig. 3. It is clear that the deviation between the simulated and the experimental data (since no analytical solution is available for such case) remains almost the same after 15 sections. Therefore, the same number of sections is used to simulate the other cases.

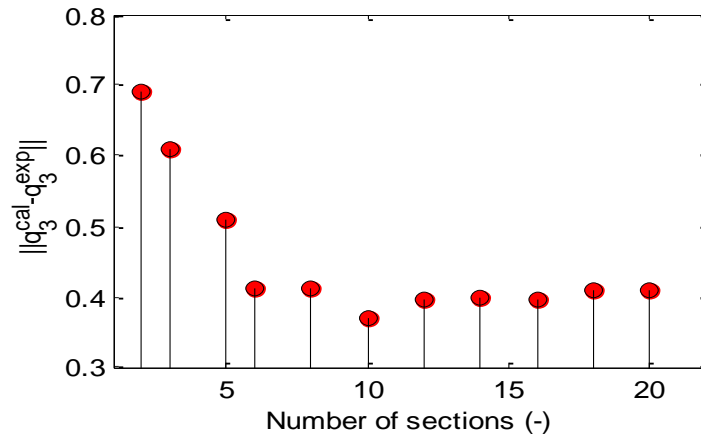


Fig. 3: Convergence of droplet size distribution at the middle of the column by varying the number of sections.

Actually, the mesh size depends on the column height and the number of sections. Two columns were used with heights (2.55 and 4.4 m as reported in Table 3.9) where the number of sections (along particle diameter) were chosen based on Fig. 3 as discussed in section above. For the RDC DN150 column of Modes (1999), the MATLAB ode45 solver was used to solve the column model at steady state with relative error 10^{-6} and the absolute error was 10^{-8} . For the Garthe (2006) DN80 column (4.4 m height) we divided the column height into 50 numerical cells, to simulate the mass transfer profiles, using the first-order flux vector splitting. This number of spatial numerical cells was chosen based on the convergence of the numerical solution as shown in Table 2. The system of ordinary differential equations (w.r.t. space) was then solved using MATLAB ode45 with the same aforementioned error tolerances for the RDC DN150 column. Fig. 4.1 and 4.2 show a comparison between the predicted droplet size distribution and the experimental data (using 15 sections) at three different points along the column height, where a very good agreement is obtained. It can be observed that the DSD is shifted toward smaller droplet sizes, which indicates that the breakage phenomenon is dominant.

Table 2: Convergence test with respect to spatial numerical cells using 15 sections as a reference solution for RDC DN80 extraction column

Number of numerical cells	Holdup relative error %	Mean diameter relative error %
20	0.8508	1.8480
35	0.5987	1.2626
50	0.6300	1.0327
75	0.6467	0.8439

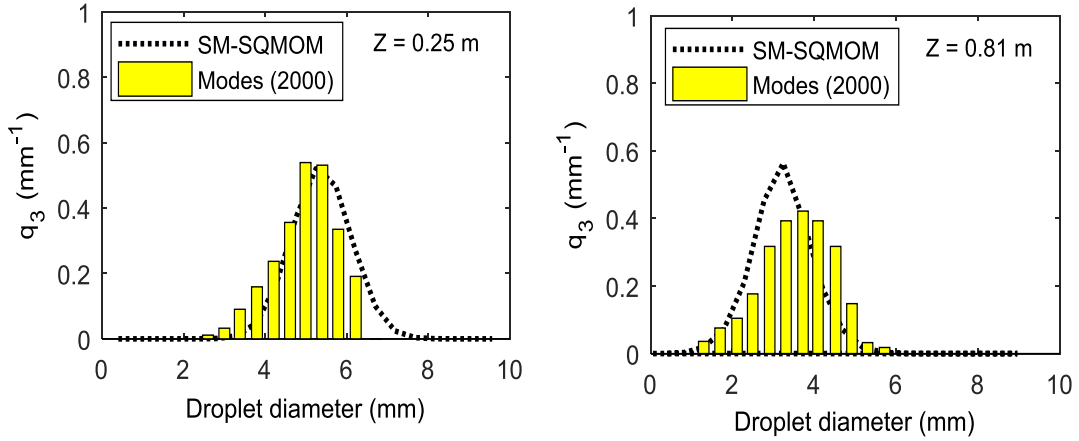


Fig. 4.1: Convergence of droplet size distribution at the middle of the column by varying the number of sections: bottom and middle of the column.

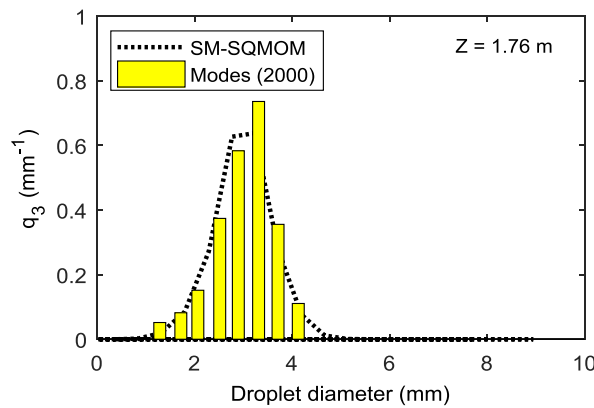


Fig. 4.2: Convergence of droplet size distribution at the middle of the column by varying the number of sections: top of the column.

B) RDC DN80 liquid-liquid extraction column

The SM-SQMOM is tested using PPBLab software RDC module (Attarakih et al., 2012; 2017) and the steady state experimental data published by Garthe (2006). The chemical system used here is water-acetone-toluene chemical test system. The dispersed phase (toluene) flow rate is 48 liter/h, while the continuous phase flow rate is 40 liter/h. The rotational speed is fixed at 200 rpm. The initial conditions are zero for the droplets number and dispersed phase holdup respectively, while the initial concentration is the same as the solute concentration in the continuous phase inlet. The inlet feed is taken as a normal distribution with mean and variance of 2.0 and 0.55 respectively for both chemical systems. The minimum and maximum droplet diameters are 0.025 and 8 mm respectively. Fig. 5 shows a comparison between the simulated dispersed phase holdup profiles using the SM-SQMOM and PPBLab software, and the published experimental data of Garthe (2006). It can be clearly observed that the SM-SQMOM and PPBLab show a very good agreement with the experimental data using the same operating and numerical parameters. Fig. 6 depicts the simulated mean droplet diameter profiles along the column height using PPBLab and the SM-SQMOM as compared to the experimental data. Unlike the holdup measurement, the mean droplet diameter measurement is less accurate

and this explains the slight deviation between the simulation results and the experimental data. As described earlier the column hydrodynamic equations are initially solved then the mass transfer profiles along the column height are estimated. Fig. 7 depicts a comparison between the simulated mass transfer profiles along the column height using the SM-SQMOM and the experimental data, where a very good agreement was obtained using the recommended mass transfer correlations of Kronig and Brink (1951) for circulating droplets.

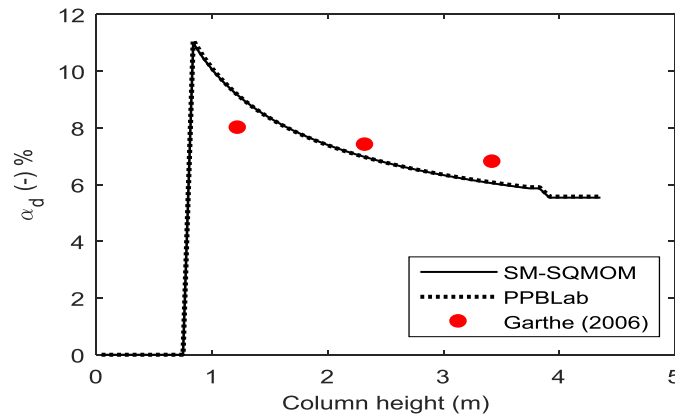


Fig. 5: Comparison between the simulated holdup profiles using the SM-SQMOM and PPBLab (Attarakih et al., 2012; 2017), and the experimental data (Garthe, 2006).

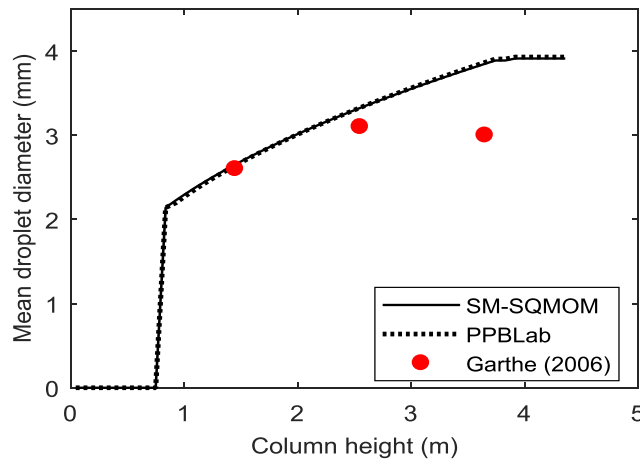


Fig. 6: Comparison between the simulated mean droplet diameter profiles using the SM-SQMOM and PPBLab (Attarakih et al., 2012; 2017), and the experimental data (Garthe, 2006).

To quantify the convergence characteristics of the present numerical model, we calculated the mean percentage relative error between a reference solution and the calculated ones at different discretization levels. Table 3.10 shows the reduction of the mean relative error as function of the number of spatial numerical cells. This error was calculated based on the reference solution using 300 spatial numerical cells where the number of sections was fixed at a value of 15 based on the results of Fig. 3. Similar convergence analyses were carried out by fixing the number of spatial numerical cells at 50 and varying the number of sections along droplet diameter. The reference solution was calculated using 50 sections while the number of sections was varied as 5, 15, 25, and 35. The mean relative error was calculated using global moments as reflected by the mean

dispersed phase holdup ($\sim \mu_{3,0}$) and the mean droplet diameter ($\mu_{3,0}/\mu_{2,0}$). The mean relative error based on these global quantities was found insensitive to the variation of the number of sections with values (0.002 %) and (0.0006 %) for the mean droplet diameter and dispersed phase holdup respectively. This means that the TEqWQ is accurate enough to estimate the population sectional moments without any further need to decrease the domain of integration (Attarakih et al., 2009).

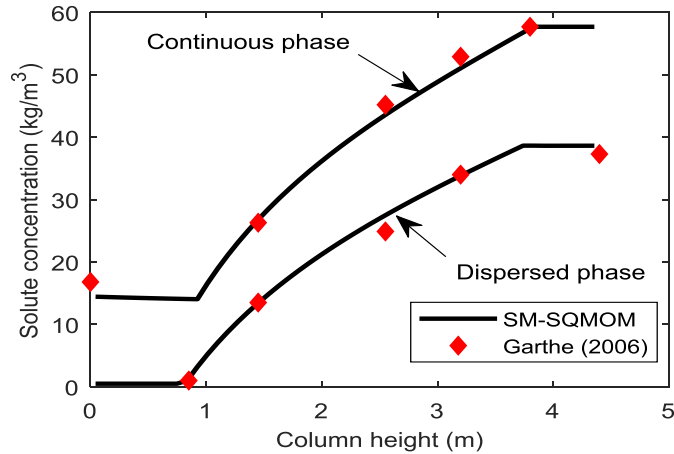


Fig. 7: Comparison between simulated the mass transfer profiles using the SM-SQMOM and the experimental data of Garthe (2006).

2.3.2 Kühni liquid-liquid extraction column

This section is devoted to test the performance of the present spatially mixed model, where the model prediction is validated using the steady state experimental data published by Garthe (2006). The column used in simulation is a pilot plant Kühni DN80 liquid-liquid extraction column, where its detailed dimensions are shown in Table 3. The chemical test system used here is butyl acetate-acetone-water. The operating conditions are shown in Table 4. The simulations were carried out using different inlet flow rates at constant rotational speed. In this case study, the single droplet velocity model is given by Klee and Treybal (1956), which is recommended for low interfacial chemical system (Gourdon et al., 1994). The slowing effects due to the column internals and droplet's swarm is given by Steinmetz (2007).

Table 3: Kühni column geometry (all dimensions are in m)

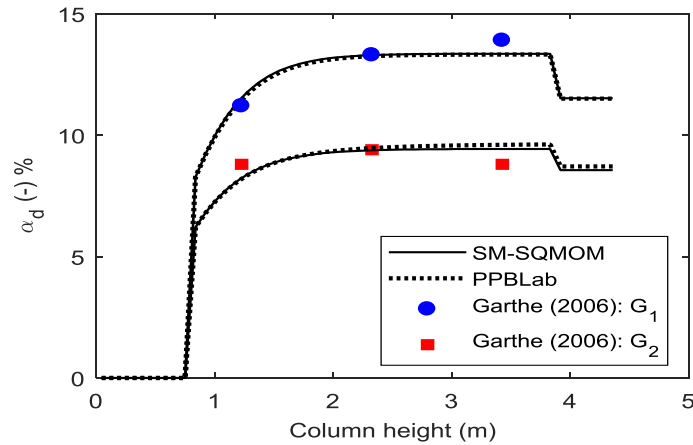
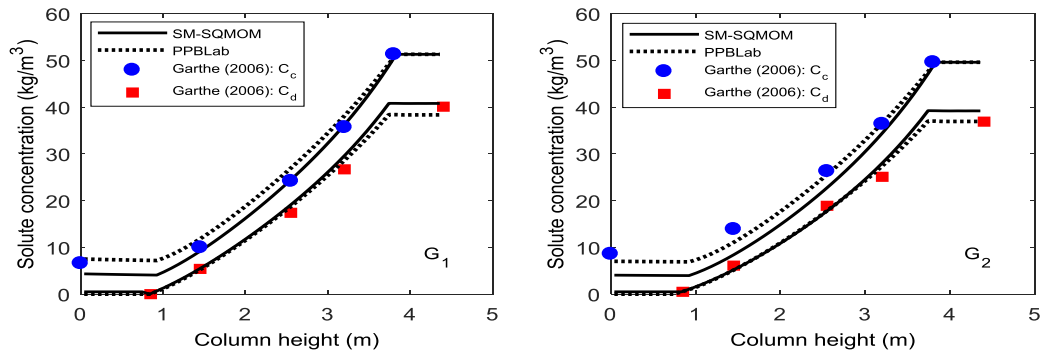
Column height	Column diameter	Compartment height	Stator diameter	Rotor diameter
4.4	0.08	0.05	0.05	0.045

Concerning the droplets interactions, the coalescence between two liquid droplets is given by Coualoglou and Tavlarides model (Coualoglou and Tavlarides, 1977). Indeed, this model contains two fitting parameters which must be identified in order to predict the coalescence kernel. In this regard, the model hydrodynamics (holdup and mean droplet diameter) predictions are matched and adjusted with the available experimental data, then the mass transfer profiles along the column height are predicted independently by solving the solute conservation equations. The same procedure was followed by many researches (Attarakih et al., 2015; Jaradat et al., 2010, 2012; Alzyod, 2013). In this work, the required coalescence model parameters are taken from Alzyod (2013), where the author implemented the OPOSPM to model the hydrodynamics and mass transfer behavior of Kühni liquid extraction column using MATLAB-SIMULINK environment. These parameters are given by $C_1 = 0.01$ and $1.33 \times 10^{10} \text{ (m}^{-2}\text{)}$ respectively.

Table 4: Operating conditions for the steady state validation (Garthe, 2006)

Exp.set	Q_c^{in} (L/h)	Q_d^{in} (L/h)	C_c^{in}	C_d^{in}	Ns
G ₁	30	36	5.0	0.0	100
G ₂	40	48	0.0	0.0	

The droplet breakage probability function is given by Garthe (2006). This function was developed based on the experimental observations using the same column geometry under the same operating conditions. Fig. 8 shows the variation of the simulated dispersed phase holdup profiles along the column height compared to the experimental data G₁ and G₂ experimental data sets. It can be clearly observed that the higher inlet flow rate (G₂ experimental data set) results in a higher holdup values compared to the low flow rate experimental data set (G₁). Indeed, by increasing the continuous phase inlet flow rate, the drag force between the continuous phase and dispersed phase droplets increases (Gomes et al., 2009), this reduces the dispersed phase velocity and increases the residence time inside the column. As a result, the holdup value is increased.


Fig. 8: Comparison between the simulated holdup profiles using the SM-SQMOM and PPBLab (Attarakih et al., 2012; 2017), and the experimental data of Garthe (2006).

Fig. 9: Comparison between the simulated solute mass fraction profiles using the SM-SQMOM and PPBLab (Attarakih et al., 2012; 2017), and the experimental data of Garthe (2006).

During the past years, several correlations had been proposed to evaluate the individual mass transfer coefficient of both contacting phases. However, these correlations are limited for certain droplet states and

therefore more work is needed in this area (Attarakih et al., 2013). Based on the converged hydrodynamics integral properties, the calculated solute mass transfer profiles are shown in Fig. 6. Here, the correlation of Garner and Suckling (1958), which is recommended for rigid droplets (Green and Perry, 2008) is used to predict the continuous phase mass transfer coefficient, while the correlation of Kronig and Brink (1951) which is recommended for long contact time (Green and Perry, 2008) is used to predict the dispersed phase mass transfer coefficient. It can be clearly observed that the predicted profiles show very good agreement with the experimental data.

2.4 Conclusions

A novel reduced steady state algorithm for modelling the hydrodynamics and mass transfer behavior of liquid-liquid equipment columns based on the SQMOM, as a reduced PBM, is developed. The SQMOM is extended and mixed with the MPSPM to model the column hydrodynamics; while the mass transfer behavior is modeled using the OPOSPM. To facilitate the source terms implementation, an analytical solution based on the algebraic velocity model is derived to calculate the required dispersed phase mean droplet velocity. The proposed SM-SQMOM is able to reconstruct the droplets distribution shape and to model the hydrodynamics and mass transfer behavior of liquid-liquid extraction equipment. In this regard, 15 sections, at the droplet discretization level, are found enough to predict the droplet size distribution as compared with the experimental data.

Nomenclature

d	Droplet diameter (m)
F	Flux vector as given by Eq. (7)
N_{pp}	Number of sections (-)
N_q	Number of quadrature points (-)
Q	Flow rate (L/h)
S	Source term
t	Time (s)
u	Velocity (m/s)
w	Quadrature weight
z	Space coordinate

Greek Symbols

$\mu_{r,k}$	Two dimensional moment
α	Volume fraction (-)
δ	Dirac delta function (m^{-1})

References

- Alzyod, S., Attarakih, M., Hasseine, A., Bart H.-J. (2017a), Steady state modelling of a Kühni liquid extraction column using the Spatially-Mixed Sectional Quadrature Method Of Moments (SM-SQMOM). Chem. Eng. Res. Des. 117, 549–556.
- Alzyod, S., Korb, C., Attarakih, M., Bart, H.-J. (2017b). Steady State Population Balance Modelling of Zinc Extraction in a Kühni Liquid-liquid Extraction Column, Proceedings of the International Solvent Extraction Conference (ISEC2017), 63-70. Miyazaki, Japan.
- Alzyod, S. (2013). A one primary one secondary particle method simulink module for the steady state and dynamic modelling of Kühni extraction column, master thesis. The University of Jordan.
- Attarakih M., Alzyod S., Fricke A. (2017). Population balance modelling of pulsed packed bed extraction columns using PPBLab software. Comput. Aided Chem. Eng. 40, 67-72.
- Attarakih, M., Abu-Khader, M., Bart, H.-J. (2013). Modelling and dynamic analysis of an RDC extraction column using OPOSPM. Chem. Eng. Sci. 91, 180-196.
- Attarakih, M. M., Drumm, C., Bart, H.-J. (2009). Solution of the population balance equation using the Sectional Quadrature Method of Moments (SQMOM). Chem. Eng. Sci. 64, 742-752.
- Attarakih, M., Alzyod, S., Hlawitschke, M., Bart, H.-J.(2015). OPOSSIM: a population balance-SIMULINK module for modelling coupled hydrodynamics and mass transfer in liquid extraction equipment. Comput. Aids Chem. Eng. 37, 257–262.
- Attarakih, M., Al-Zyod, S., Abu-Khader, M., Bart, H.-J. (2012a). PPBLAB: A new multivariate population balance environment for particulate system modelling and simulation. Procedia Eng. 42, 144-562.
- Coulaloglou, C. A., Tavlarides, L.L. (1977). Description of interaction processes in agitated liquid-liquid dispersions. Chem. Eng. Sci. 32, 1289–1297.
- Garner, F.H., Suckling, R.D. (1958). Mass transfer from a soluble solid sphere. AIChE4, 114-124.

- Garthe, D. (2006). Fluid dynamics and mass transfer of single particles and swarms of particles in extraction columns. Dissertation. Technische Universität München, Germany.
- Gomes, L.N., Guimaraes, M.L., Stichlmair, J., Cruz-Pinto, J.J., 2009. Effects of mass transfer on the steady state and dynamic performance of a Kuhni column experimental observations. *Ind. Eng.Chem.Res.*48, 3580-3588.
- Gourdon, C., Casamatta, G., Muratet, G. (1994). Population Balance Based Modelling. In: Godfrey & Slater (Ed). *Liquid-liquid extraction equipment*. (pp.140-226), New York, John Wiley and Sons.
- Jaradat, M., Attarakih, M., Bart, H.-J. (2012). RDC extraction column simulation using the multi-primary one secondary particle method: coupled hydrodynamics and mass transfer. *Comput. Chem. Eng.J.*, 37, 22-32.
- Jaradat, M., Attarakih, M., Bart, H.-J. (2010). Effect of phase dispersion and mass transfer direction on steady state RDC performance using population balance modelling. *Chem. Eng. J.* 165, 379-387.
- Klee, A.J., Treybal, R.E. (1956). Rate of rise or fall of liquid drops. *AIChE* 2, 444-447.
- Kronig, R., Brink, J.C. (1951). On the theory of extraction from falling droplets. *Appl. Sci. Res.* 2, 142-154.
- Modes, G. (2000). Grundsätzliche Studie zur Populationsdynamik einer Extraktionskolonne auf Basis von Einzeltropfenuntersuchungen. Shaker Verlag, Aachen
- Perry, R. H., Green, D. W. (2008). *Perry's Chemical Engineers' Handbook*. 8th Edition, McGraw-Hill.
- Steinmetz, T., (2007), Tropfenpopulationsbilanzgestütztes Auslegungsverfahren zur Skalierung einer gerührten Miniplant Extraktionskolonne, Dissertation, Düsseldorf: VDI Verlag GmbH.

Chapter 3

Steady State Modeling of Reactive Liquid-liquid Extraction of Zinc with D2EHPA using the SM-SQMOM

3.1 Introduction

Due to the growing demand for rare earth elements, the extraction of heavy metals has gained more attention during last years. As a result of this, more research efforts to improve the available metals separation processes were spent. The available separation processes include: liquid-liquid extraction, ion exchange, and chemical precipitation (Bart, 2001). Among these processes, liquid-liquid extraction is a common separation process, which can be carried out under mild operating conditions (Attarakih et al., 2015). In such a process, the overall extraction equipment efficiency can be enhanced by adding a chemical reaction to the physical extraction process (Bart et al., 1994), where the extraction efficiency can be enhanced using ion exchangers (Bart et al., 1994). Beside the reactive extraction kinetics, the droplet size distribution plays a major role in the determination of the overall extraction equipment efficiency. As a result of this, mathematical modeling of the reactive extraction equipment is a challenging task and more attention is needed to model the coupled hydrodynamics and mass transfer behavior. In this regard, Veglio and Slater (1996) presented a simple simulation approach to design liquid-liquid equipment using ZnSO₄/ D2EHPA/ n-dodecane chemical test system. The authors reported that the most important design parameter, which affects the column height, is the zinc ions mass transfer coefficient in the continuous phase. Ji et al. (2006) studied the role of kinetics of zinc extraction in a packed bed liquid-liquid extraction column. The authors used a simplified mathematical model based on the backmixing approach to model the reactive extraction of zinc with D2EHPA, where they assumed constant holdup and mean droplet diameter values along the column height. In the same direction, Neto and Mansur (2013) modeled the reactive extraction of zinc with D2EHPA in a short Kühni liquid-liquid extraction column using the back and forward mixing models. The required dispersed phase integral properties (holdup and mean diameter) to conduct the simulation were calculated using published correlations. In addition to this, the mass transfer coefficients of the zinc ions and the zinc complex were assumed constant along the column height. The authors reported a good agreement between the calculated and the experimental data. However, assuming constant dispersed phase integral properties is not realistic because the dispersed phase identity changes along the column height due to the breakage and coalescence phenomena. As a result of this, a detailed description of the dispersed phase behavior is required. The main aim of this work is to develop a general mathematical framework, which is able to take the dispersed phase behavior into account to model the reactive mass transfer behavior of liquid-liquid extraction columns in general and Kühni column in particular. In this regard, a reduced steady state population balance algorithm is developed to model the reactive extraction process of zinc with D2EHPA in a lab scale Kühni DN32 liquid-liquid extraction column. Here, the SM-SQMOM (Alzyod et al., 2017a, b), which is based on the SQMOM as a discrete framework for modeling particulate systems (Attarakih et al., 2009), is utilized and implemented. To facilitate the source terms implementation, an analytical solution (Alzyod et al., 2017a), which is based on the algebraic velocity model, is used to calculate the required dispersed phase mean droplet velocity inside the column.

The resulting integral spatial numerical flux vector is closed using the mean mass droplet diameter (d_{30}), while the hydrodynamics source terms are closed using the TEqWQ formula (Attarakih et al., 2009). A multi-sectional grid (w.r.t droplet diameter) is used to approximate the integral hydrodynamics source terms, where 20 sections were found enough to reconstruct the shape of the droplet size distribution. In addition to this, one section is used to model the steady state reactive mass transfer behavior inside the column. The present model consists of a highly nonlinear system of partial differential equations due to the presence of chemical reactions. These chemical reactions include: an interfacial reaction between the zinc ions and D2EHPA to produce the zinc complex, and a partial dissociation reaction of the zinc complex in the bulk of the dispersed phase (Neto and Mansur, 2013). To facilitate the mathematical model implementation, a finite volume method with a first order upwind scheme is developed to treat the reactive mass transfer transport equations, while the MATLAB ode45 solver is used to solve the hydrodynamic moments transport equations. At the experimental validation level, the model prediction is compared with the experimental data using the reactive ZnSO₄/D2EHPA/isododecane EFCE chemical test system (Korb et al., 2017; Alzyod et al., 2017b). The SM-SQMOM was found able to predict the column hydrodynamics as well as the reactive mass transfer profiles as compared with the experimental data.

This chapter is arranged as follows: in section 3.2 the experimental investigations and the chemical reaction kinetics of zinc with D2EHPA are presented. In section 3.3, the mass transfer transport equations are presented and discussed. In this regard, the hydrodynamic transport equations are the same as given in chapter 2 and in the overview. Therefore only the solute mass transfer transport equations are presented. Finally, section 3.4 is devoted for the proposed model experimental validation.

3.2 Experimental investigations

This section is devoted to present the experimental procedure and the chemical reaction kinetics. The experimental investigations were carried out at TU Kaiserslautern using a mini plant using a countercurrent Kühni liquid-liquid extraction column (Korb et al., 2017; Alzyod et al., 2017b). More details concerning the experimental procedure are given in the next subsections.

3.2.1 Experimental procedure

The experimental investigations were carried out using a countercurrent Kühni DN32 liquid-liquid extraction column, where the column dimensions are shown in Table 1. The chemical test system used in the investigations is ZnSO₄ / D2EHPA/ isododecane chemical test system as recommended by Bart et al. (1999). The column is initially filled with the aqueous phase, and then the rotor is started and after that the dispersed phase has been fed to the bottom of the column. In all cases, the dispersed organic phase (here isododecane) was fed at the bottom of the column using a finger distributor with 8 holes, while the continuous aqueous phase was fed at the top of the column. The dispersed phase holdup was measured in the active height of the column using the corresponding pressures method, while a high-speed camera was used to detect the droplet size distribution at the upper settling zone of the column. In this regard, the effect of changing the rotational speed, phase ratio and the total throughput on the column performance is investigated. The zinc ion concentrations and the pH values were measured at five different positions along the column height, where the column was operated at 80 percent away from the flooding point.

Table 1: Kühni column geometry (all dimensions are in m) (Korb et al., 2017; Alzyod et al., 2017b)

Column height	Column diameter	Blade diameter	Compartment height	Stator diameter
1.4	0.032	0.0195	0.028	0.026

The investigated flow rate ratio ($\lambda_d = Q_d / Q_c$) are 0.2 and 1 respectively, while the rotational speed was varied from 100-300 rpm. In all cases, the zinc ions (Zn^{2+}) concentration was fixed at a constant value of 0.01mol/litter, while the D2EHPA concentration is fixed at 0.25 mol/liter as recommended by many authors (Bart and Rousselle, 1999; Ji et al., 2006; Neto and Mansur, 2013). In addition to this, the sulfuric acid (H_2SO_4) was added to adjust the pH value inside the column. The physical properties of the chemical test system are show in in Table 2.

Table 2: Physical properties of the extraction reaction chemical test system

Chemical compound	Density (kg/m ³)	Viscosity (Pa.s)	Surface tension (N/m)
Aqueous solution (Zn^{2+} , SO_4^{4-})	999.6	0.000913	-
D2EHPA/ isododecane	764.8	0.001543	0.02087

3.2.2 Chemical reaction kinetics

In principle, the chemical reaction of the zinc ions and D2EHPA occurs at the liquid-liquid interface to form the zinc complex as follows (Bart et al., 1994):



where $\overline{(RH)}$ and \overline{ZnR}_2 denote the D2EHPA and the zinc complex respectively. During the last years, several models to describe the equilibrium and kinetics of the $ZnSO_4$ / D2EHPA reactive chemical system were proposed. A review of the available models was presented by Bart et al., (1994). In this regard, Bart and Rousselle (1999) proposed an equilibrium model based on the chemical potential theory of Lewis at a fixed stoichiometric coefficient. Mansur et al. (2002) carried out a statistical analysis to study the equilibrium and kinetics of $ZnSO_4$ / D2EHPA/ n-heptane chemical test system. The authors showed that, the extraction process can be described by means of an interfacial reaction between the zinc ions and the D2EHPA to form the zinc complex followed by a partial dissociation of the zinc complex in the bulk of the dispersed phase as follows (Mansur et al., 2002; 2013):



where the stoichiometric coefficient (n) depends on the solvent type. For isododecane, the value of n is 1.5 (Sainz-Diaz et al., 1996; Bart and Rousselle, 1999). Based on their statistical study, Mansur et al. (2002) proposed a reaction mechanism for the first heterogeneous interfacial chemical reaction (Eq. (2)). The authors assumed that the reaction occurs with excess D2EHPA concentration. Moreover, the mass transfer rate of the protons and D2EHPA are small compared with the other species and can be neglected. Based on this, the reaction rates in the liquid-liquid interface (R) and in the bulk of the organic phase (S) are given by (2002; 2013):

$$R = K_{OE} \left(\frac{C_{Zn} C_{RH}}{C_H} - \frac{C_{ZnR_2RH} C_H}{K_D C_{RH}^{0.5}} \right) \quad (4)$$

$$S = k'_F \left(C_{ZnR_2RH} - \frac{C_{ZnR_2} C_{RH}^{0.5}}{K_C} \right) \quad (5)$$

where K_{OE} is the overall reactive mass transfer coefficient, k_f is the forward reaction rate constant in the bulk of the organic phase, and K_D and K_C are the reactions equilibrium constants. The values of the reaction rates constant are shown in Table 3. The overall mass transfer coefficient (K_{OE}) is given by:

$$K_{OE} = \left(\frac{C_{RH}}{K_{Zn} C_H} + \frac{1}{k_F} + \frac{C_H}{K_D K_{ZnRH_2} C_{RH}^{0.5}} \right) \quad (6)$$

In Eq. (6), K_{Zn} and K_{ZnRH_2} are the local mass transfer coefficients of the zinc ions and the zinc complex in the continuous and in the dispersed phases respectively. More information about these coefficients is given in the following section.

Table 3: Chemical reaction and equilibrium parameters of Eqs. (5 & 6) (Neto & Mansur, 2013)

k_F (m/s)	k'_F (m/s)	K_C (mol/m ³) ^{0.5}	K_D (mol/m ³) ^{0.5}
2.70×10^{-6}	1	0.2118	9.42

3.3 Mathematical model: solute transport equations

In this section, the SM-SQMOM is used to model the hydrodynamics and reactive mass transfer behavior of a Kühni DN32 liquid-liquid extraction column. In this regard, only the mass transfer transport equations are presented in this section. The column hydrodynamics transport equations are the same as presented in chapter 2. For more information, the see chapter 2 and section 4 in the overview. In this section, the mass transfer transport equations are derived by applying a steady state mass balance for each component in each phase. In addition to this, only one section is used to close the SQMOM as given by the SM-SQMOM. Beside the assumptions concerning the reaction rates presented in section 3.2.2, it is assumed that both phases are immiscible and the water solubility in the dispersed phase is neglected. In addition to this, the reaction occurs with excess D2EHPA concentration and the zinc ions diffuse toward the liquid-liquid interface, while the zinc complex diffuses toward the bulk of the dispersed phase. This results in the following set of solute concentration conservation equations for the dispersed phase:

$$\partial_z \left(\alpha_d u_d c_d^{(i)} - D_d \partial_z \left(\alpha_d c_d^{(i)} \right) \right) = u_d^{in} c_d^{in(i)} \delta(z - z_d) + \frac{\alpha_d}{d_{30}} \left(6 \kappa_{R,d}^{(i)} R + d_{30} \kappa_{S,d}^{(i)} S \right) \quad (7)$$

where the reaction rates R and S are given by Eqs.(4 & 5) respectively. Here, the i^{th} index indicates the chemical components, which include: D2EHPA (RH), and the zinc complexes ZnR_2 and ZnR_2Rh respectively. In Eq.(7), $c_d^{(i)}$ is the molar solute concentration in the dispersed phase, $\kappa_{R,d}$ and $\kappa_{S,d}$ are the stoichiometric coefficients vectors. The stoichiometric coefficients vectors for D2EHPA and the zinc complexes are given by:

$$\kappa_{R,d} = [-1.5 \quad 1 \quad 0] \quad (8)$$

$$\kappa_{S,d} = [1 \quad -1 \quad 1] \quad (9)$$

The boundary conditions of Eq. (7) are given by (Attarakih et al., 2013; Alzyod et al., 2017b):

$$u_d \alpha_d c_d^{(i)} - D_d \frac{\partial \alpha_d c_d^{(i)}}{\partial z} = 0 \quad \text{at } z = 0 \quad (10)$$

$$D_d \frac{\partial \alpha_d c_d^{(i)}}{\partial z} = 0 \quad \text{at } z = H \quad (11)$$

where H is the column height. Following the same derivation procedure, the solute conservation equations in the continuous phase could be written as follows:

$$-\partial_z \left(\alpha_c u_c c_c^{(j)} + D_c \partial_z \left(\alpha_c c_c^{(j)} \right) \right) = u_c^{in} c_c^{in(j)} \delta(z - z_c) + \frac{6\alpha_d}{d_{30}} \kappa_{R,c}^{(j)} R \quad (12)$$

where α_c is the continuous phase volume fraction ($\alpha_c = 1 - \alpha_d$), u_c is the continuous phase velocity, D_c is the axial dispersion coefficient, and $c_c^{(j)}$ is the solute concentration in the continuous phase. Here, the j^{th} vector is used to indicate the chemical components which include: the zinc and the proton ions. The elements of the stoichiometric coefficients vector ($\kappa_{R,c}$) are given as follows:

$$\kappa_{R,c} = [-1 \quad 2] \quad (13)$$

The boundary conditions of Eq.(12) are given by (Attarakih et al., 2013; Alzyod et al., 2017b):

$$-D_c \frac{\partial \alpha_c c_c^{(j)}}{\partial z} = 0 \quad \text{at } z = 0 \quad (14)$$

$$-\alpha_c u_c c_c^{(j)} + D_c \frac{\partial \alpha_c c_c^{(j)}}{\partial z} = 0 \quad \text{at } z = H \quad (15)$$

In this work, it is assumed that the dispersed phase axial dispersion coefficient has a minor effect on the mass transfer process inside the column and it can be neglected. The same procedure was proposed by Attarakih et al. (2015) and Schmidt et al. (2006). The required mass transfer correlations to local calculate the zinc ions in the continuous phase and the zinc complex in the dispersed phases are given by Heertjes et al. (1954) and Handlos and Baron (1957) respectively.

3.4 Experimental validation

In this section, the performance of the presented spatially mixed framework is tested, where the model prediction is validated using the steady state experimental data. The column dimensions and the chemical test system physical properties are discussed in detail in section 3.2. The simulations were carried out using two different inlet flow ratios ($\lambda_d = Q_d/Q_c = 0.2$ and 1.0 respectively), while the rotational speed was varied from 100-300 rpm. In this case study, the single droplet velocity model is given by Vigness velocity model (1965). The slowing effects due to the column internals and droplet's swarm is given by Steinmetz (2007). Concerning the droplet-droplet interactions, the coalescence mechanism between two liquid droplets is modeled using Coulaloglou and Tavlarides (1977), while the droplet breakage probability function is given by Fang et al. (1995). Fig. 1 shows a comparison between the calculated dispersed phase holdup and the experimental data using different rotational speed values. It can be clearly observed that a higher phase ratio results in a higher holdup values. In addition to this, the holdup values increase with increasing the rotational speed. A good agreement between the simulated dispersed phase holdup and the experimental data is obtained. Fig. 2 shows a comparison between the simulated droplet size distribution and the experimental data at the top of the column. The simulation was carried out at 350 rpm and a flow ratio of $\lambda_d = 1$. It can be clearly observed that the SM-SQMOM retains the required information concerning the shape of the droplet size distribution, where 20 sections are found enough to reconstruct the shape of the size distribution. In addition to this, the column hydrodynamics is found dominated by the breakage phenomena at high rotor speeds. Based on the

converged steady state droplet size distribution, the reactive solute mass transfer profiles can be predicted along the column height. This can be done by adjusting the coalescence model parameters to fit the predicated droplet size distribution at the top of the column with the experimental data. In this case study, the coalescence model parameters are given by $c_1 = 0.02$ and $c_2 = 1.33 \times 10^{11} \text{ m}^{-2}$ respectively.

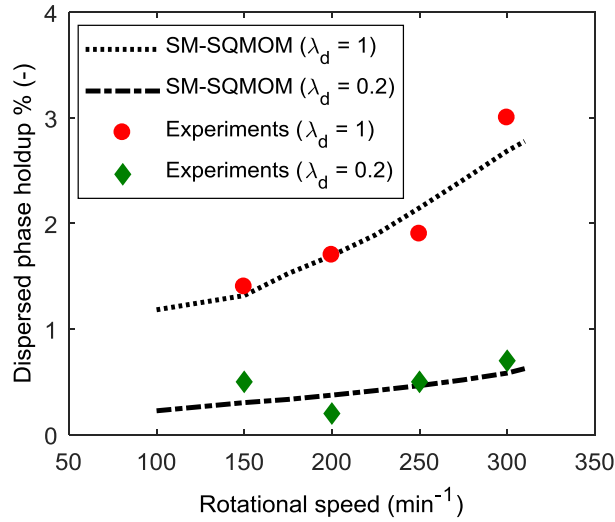


Fig. 1: Comparison between the simulated holdup profiles using the SM-SQMOM and the experimental data.

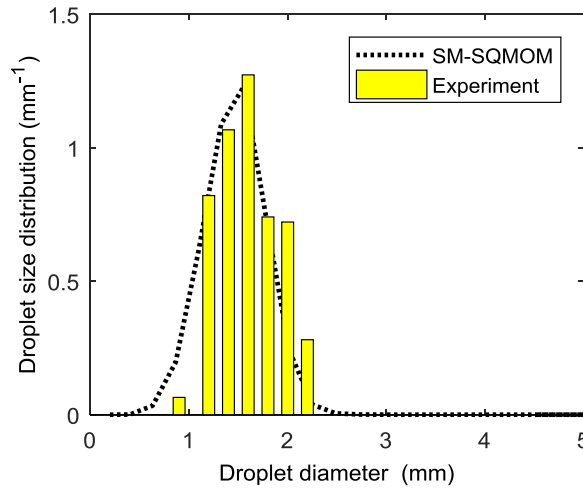


Fig. 2: Comparison between the simulated using the SM-SQMOM and experimental droplet size distribution.

Fig. 3 shows a comparison between the simulated zinc ions concentration in the aqueous phase and the experimental data. In this case study, the correlation of Heertjes (1954) is used to calculate the zinc ions local mass transfer coefficient in the continuous phase, while the correlation of Handlos and Baron (1957) is used to calculate the D2EHPA local dispersed phase mass transfer coefficient. As expected the zinc ions concentration decreases along the column height (from the inlet point at the top to the bottom) due to the

chemical reaction and the mass transfer process inside the extraction column. In addition to this, one section based on the solute concentration as an internal coordinate is found enough to predict the solute mass transfer profiles as compared with the experimental data.

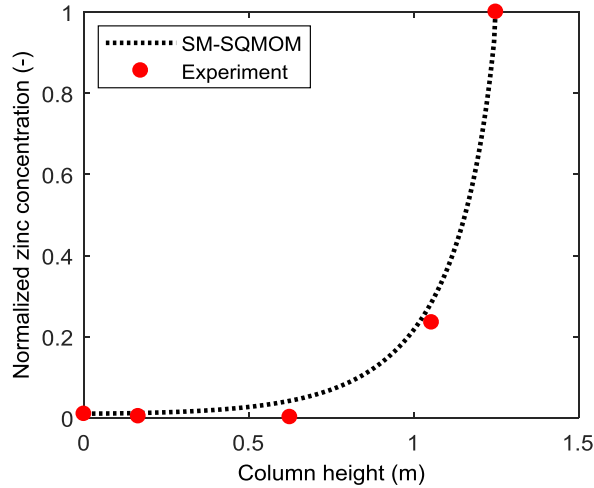


Fig. 3: Comparison between the simulated zinc ions concentration profiles using the SM-SQMOM and experimental data.

Fig. 4 shows the ratio between the mass transfer resistance and the total resistance (E_m) along the column height. It can be clearly observed that the extraction process is controlled by the mass transfer mechanism the top of the column, while the extraction process is controlled by the chemical reaction and mass transfer mechanisms at the bottom and the middle of the extraction column.

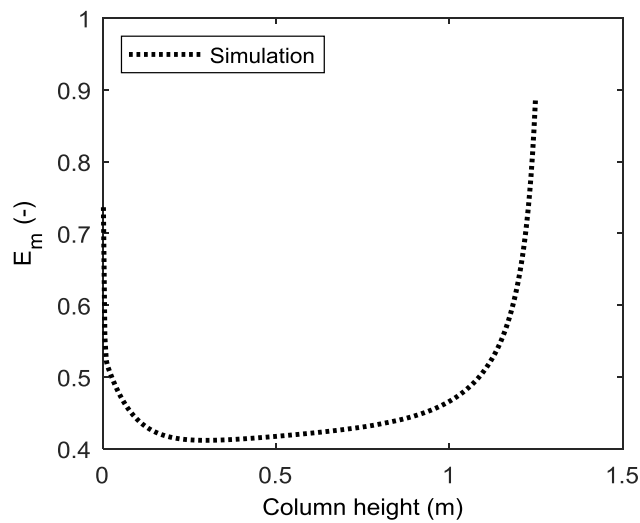


Fig. 4: The ratio of the mass transfer resistance to the total resistance.

Fig. 5 depicts a comparison between the simulated pH values and the experimental data at five different points along the column height using the same simulation conditions. The pH values decrease along the column height (from top to bottom of the column) until it reach a constant values (around 1.4). A very good agreement between the simulation results and the experimental data is obtained.

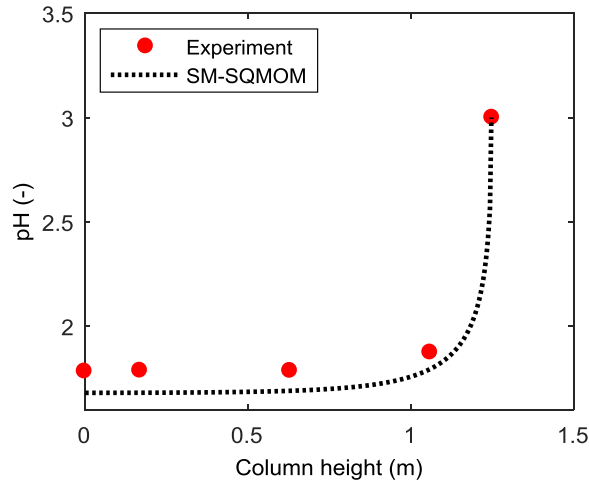


Fig. 5: Comparison between the simulated pH profiles using the SM-SQMOM and the experimental data.

3.5 Conclusions

A steady state framework to model the reactive extraction process of zinc with D2EHPA in liquid-liquid extraction columns is developed, where the SM-SQMOM is utilized as a reduced population balance mathematical framework. To facilitate the mathematical implementation, a finite volume method using the first order upwind scheme is developed to treat the mass transfer transport equations. The proposed framework is found able to describe the column hydrodynamics as well as the reactive mass transfer behavior. In this regard, 20 sections (w.r.t droplet diameter) are found enough to predict the column hydrodynamics, while one section (w.r.t solute concentration) is found enough to predict the reactive solute mass transfer profiles as compared with the experimental data.

Nomenclature

C	Solute concentration (mol/m ³)
D	Axial dispersion coefficient (m/s)
d	Droplet diameter (m)
D _c	Column diameter (m)
D _R	Rotor diameter (m)
D _S	Stator diameter (m)
EFCE	European Federation of Chemical Engineering
H	Column height (m)
H _c	Compartment height (m)
K _C	Reactions equilibrium constants (mol/m ³) ^{0.5}
K _D	Reactions equilibrium constants (mol/m ³) ^{0.5}
k _f	Forward reaction rate constant (m/s)
k _f [*]	Backward reaction rate constant (m/s)
K _{OE}	Overall mass transfer coefficient (m/s)
pH	Potential Hydrogen
Q	Flow rate (L/h)
R	Chemical reaction rate as given by Eq.(4)
S	Chemical reaction rate as given by Eq.(5)
t	Time (s)
u	Velocity (m/s)
z	Space coordinate

Greek Symbols

μ _{r,k}	Two dimensional moment
α	Volume fraction (-)
α	Volume fraction (-)
δ	Dirac delta function (m ⁻¹)
κ	The stoichiometric coefficients vector
λ	Flow rate ratio (-)

Subscripts

c,d	Continuous and dispersed phases respectively
-----	--

References

- Alzyod, S., Attarakih, M., Hasseine, A., Bart H.-J. (2017a), Steady state modeling of a Kühni liquid extraction column using the Spatially-Mixed Sectional Quadrature Method Of Moments (SM-SQMOM). Chem. Eng. Res. Des. 117, 549–556.
- Alzyod, S., Korb, C., Attarakih, M., Bart, H.-J. (2017b). Steady State Population Balance Modeling of Zinc Extraction in a Kühni Liquid-liquid Extraction Column, Proceedings of the International Solvent Extraction Conference (ISEC2017), 63-70. Miyazaki, Japan.

- Attarakih, M. M., Drumm, C., Bart, H.-J. (2009). Solution of the population balance equation using the Sectional Quadrature Method of Moments (SQMOM). *Chem. Eng. Sci.* 64, 742-752.
- Attarakih, M., Alzyod, S., Hlawitschka, M., Bart, H.-J.(2015). OPOSSIM: a population balance-SIMULINK module for modelling coupled hydrodynamics and mass transfer in liquid extraction equipment. *Comput. Aid. Chem. Eng.* 37, 257–262.
- Attarakih, M., Alzyod, S., Hlawitschka, M., Bart, H.-J.(2015). OPOSSIM: a population balance-SIMULINK module for modelling coupled hydrodynamics and mass transfer in liquid extraction equipment. *Comput. Aid. Chem. Eng.* 37, 257–262.
- Attarakih, M., Abu-Khader, M., Bart, H.-J. (2013). Modeling and dynamic analysis of an RDC extraction column using OPOSPM. *Chem. Eng. Sci.* 91, 180-196.
- Bart, H.-J. (2001). *Reactive extraction (heat and mass transfer)*. Berlin: Springer.
- Bart, H.-J., Berger, R., Misek, T., Slater, M.J., Schroter, J., Wachter, B., (1994). Recommended systems for liquid extraction systems. In: J.C. Godfrey and M.J. Slater, (Eds.), *Liquid-Liquid Extraction Equipment*. John Wiley, New York, 15-47.
- Bart, H.-J., Rousselle, H.P. (1999). Microkinetics and reaction equilibria in the system ZnSO₄/D2EHPA/isododecane. *Hydrometallurgy*. 51, 285-298.
- Coulaloglou, C. A., Tavlarides, L.L. (1977). Description of interaction processes in agitated liquid-liquid dispersions. *Chem. Eng. Sci.* 32, 1289–1297.
- Fang, J., Godfrey, J.C., Mao, Z.Q., Slater, M.J., Gourdon, C. (1995). Single liquid drop breakage probabilities and characteristic velocities in Kühni columns. *Chem. Eng. Technol.*, 18, 41-48.
- Handlos, A.E., Baron, T. (1957). Mass transfer from drops in liquid extraction. *AIChE J.*, 3, 127-136.
- Heertjes, P.M., Holve, W.A., Talsma, H. (1954). Mass transfer between isobutanol and water in a spray column. *Chem. Eng. Sci.*, 3, 122-142.
- Ji, J., Mensforth, K. H., Perera, J. M., Stevens, G.W. (2006). The role of kinetics in the extraction of zinc with D2EHPA in a packed column. *Hydrometallurgy*. 84, 139-148.
- Korb, C., Alzyod, S., Attarakih, M., Bart, H.-J. (2017). SQMOM-Modellierung der Hydrodynamik in Kühni-Kolonnen bei der Reaktivextraktion. *Chem. Ing. Tech.*, 12, 1625-1634.
- Mansur, M., Slater, M., Biscaia, E.C. (2002). Kinetic analysis of the reactive liquid-liquid test system ZnSO₄/D2EHPA/n-heptane. *Hydrometallurgy*. 63, 107-116.
- Neto, P., Mansur M.B. (2013). Transient modeling of zinc extraction with D2EHPA in a Kühni column. *Chem. Eng. Res. Des.* 91, 2323-2332.
- Sainz-Diaz, C., Klocker, H., Marr, R., Bart, H.-J. (1996). New approach in the modelling of the extraction equilibrium of zinc with bis-(2-ethylhexyl) phosphoric acid. *Hydrometallurgy*. 42, 1-11.
- Schmidt, S., Simon, M., Attarakih, M., Lagar, L., Bart, H.-J. (2006). Droplet population balance modeling-hydrodynamics and mass transfer. *Chem. Eng. Sci.* 61, 246-256.
- Steinmetz, T., (2007), Tropfenpopulationsbilanzgestütztes Auslegungsverfahren zur Skalierung einer gerührten Miniplant Extraktionskolonne, Dissertation, Düsseldorf: VDI Verlag GmbH.
- Veglio F., Slater, M. J. (1996). Design of liquid-liquid extraction columns for the possible test system Zn/D2EHPA in n-dodecane. *Hydrometallurgy*, 42, 177-195.
- Vigness, A. (1965). Hydrodynamique Des Dispersions - Mouvement D'un Globule Dans un Fluide Immobile et infini. *Genie Chim.* 93, 129-42.

Chapter 4

CFD Modelling of Pulsed Sieve Liquid-liquid Extraction Columns the OPOSPM as Reduced DPBM

4.1 Introduction

Pulsed liquid-liquid extraction columns have the advantage over the other extraction equipment, where they find many applications in chemical, biochemical and pharmaceutical industries. In contrast to the high efficient agitated liquid extraction equipment, pulsed columns provide a wide operating range, especially with low interfacial tension system, and allow easier maintenance in nuclear applications (Garthe, 2006; Perry and Green, 2008). These columns can be classified according to the internal geometry type into: pulsed packed bed, pulsed disc and doughnut, and pulsed sieve plate liquid-liquid extraction columns. Among these column types, pulsed sieve plate columns have the advantage when dealing with high throughput and corrosive or radioactive materials (Perry and Green, 2008; Yadav and Patwardhan, 2008). Using these columns, the counter current flow can't be directly achieved because the hole diameter of the sieve plates is very small compared to the column diameter. To overcome this problem, pneumatic pulsation is applied at the bottom of the column using external energy source. The applied pulsation intensity characterizes the flow patterns inside the column and increases the available interfacial area, which enhances the column efficiency. In spite of the industrial importance of pulsed sieve plate columns, there is still a lack of a detailed CFD modelling based on the DPBM of these columns (Din et al., 2010; Jaradat et al., 2011; Sen et al., 2016; Attarakih et al., 2017; Alzyod et al., 2017, 2018). The available published lumped correlations and mixture models are still insufficient to describe the actual behavior of the dispersed phase, where they ignore the droplet-droplet and the interphase interactions (Schmidt et al., 2006; Drumm, 2010; Sharma, 2011; Jaradat et al., 2011; Hlawitschka, 2013; Jildeh et al., 2014; Attarakih et al., 2012, 2015, 2017; Alzyod et al., 2017; 2018). Indeed, several papers were published during last years to provide more fundamental CFD basis to model the two phase flow behavior inside pulsed sieve plate columns. However, the reported studies ignore the breakage and coalescence phenomena and assume a constant droplet diameter value along the column height. For example, Din et al., (2010) presented a CFD hybrid approach based on the radiotracer RTD analysis to model a DN50 pulsed sieve plate extraction column using water (d)/ kerosene as a chemical test system. The simulation was performed using Euler-Euler approach and the standard κ - ϵ turbulence model assuming a constant mean droplet diameter of 5 mm. In addition to this, the sieve plates were modeled as a porous media. The authors reported an overall deviation of 72.17 % between the simulated and the reported experimental data of the dispersed phase volume fraction. Indeed, modelling of the sieve plates as a porous media is physically not realistic (Sen et al., 2016). Moreover, the reported experimental range of the mean droplet diameter inside pulsed columns is usually around 1.9 mm (Mohanty and Vogelpohl, 1997; Garthe, 2006; Perry and Green, 2008; Yadav and Patwardhan, 2009). Therefore, assuming a constant mean droplet diameter of 5 mm is not practical from experimental point of view as well. Yadav and Patwardhan (2009) presented a CFD model to predict the hydrodynamics behavior of pulsed and non-pulsed sieve plate liquid-liquid extraction columns with downcomers. The Euler-Euler approach and the standard κ - ϵ turbulence model were used to perform the 2D-CFD simulation. The required mean droplet diameter value to close the drag force in the momentum balance equation was calculated using the empirical correlation given by Vedaiyan, (1969). At the validation level, several case studies were presented to study the effect of the pulsation intensity and the dispersed phase inlet velocity on the column hydrodynamics. In this regard, the predicted dispersed phase holdup and the thickness of the accumulated layer blow the plates by the 2D-CFD model were compared with the calculated values by the empirical correlation of Laddha and Degaleesan (1976) without experimental validation.

The authors reported an average deviation of $\pm 10\%$ between the simulation results and the calculated data. However, the correlation of Vedaiyan, (1969) doesn't take the pulsation intensity and the operating conditions into account. In addition to this, the correlation of Vedaiyan, (1969), as a lumped correlation, doesn't provide the local mean droplet diameter inside the column and therefore coupling a lumped correlation with CFD solvers is not practical. In the same direction, Sen et al. (2016) performed a 2D-CFD simulation using a DN50 pulsed sieve plate extraction column. In their work, they used the Euler-Euler approach and the mixture κ - ϵ turbulence model to perform the 2D-CFD simulation. They also studied different drag models and proposed a set of modified parameters for Kumar and Hartland (1985) drag coefficient model. The authors reported a reduction on the average error from 15 % to 10 % using the modified drag model parameters. However, the dispersed phase was assumed to behave as a monodisperse phase and therefore the effects of the breakage and coalescence phenomena were lumped within the proposed modified drag model parameters. At the 1D-CFD level, Jaradat et al. (2011) presented an advanced framework to release the monodisperse phase assumption based the DPBM. In this regard, the authors extended the LLECMOD software (Attarakih et al., 2006) to model and simulate pulsed sieve plate and packed bed extraction columns in a one dimensional domain. The LLECMOD software is able to predict the column hydrodynamics as well as the mass transfer behaviour, as a bivariate DPBM framework, of pulsed liquid extraction columns. Recently Attarakih et al. (2017) presented a new 1D-CFD DPBM based module for modelling pulsed liquid extraction columns using PPBLab software. The new module contains different pulsed column types namely: pulsed sieve plate, pulsed packed bed, and pulsed disc and doughnut extraction columns. The proposed new module utilizes the recent population balance model solution algorithms, which include the PPBLab detailed and reduced Extended Fixed Pivot Technique (EFPT) solvers. These solvers are used to discretize the internal coordinates (droplet diameter and solute concentration), while the PPBLab built-in space time finite volume method solvers are used to discretize the physical spatial domain.

Based on this review, a comprehensive detailed CFD framework based on the PBM to shed more light on the hydrodynamics behavior of pulsed liquid extraction columns is required. This framework should be able to take all of the possible droplet-droplet interactions into account to release the monodisperse phase assumption. In addition to this, extending this CFD framework to model the mass transfer behavior will be helpful to improve the layout strategies of pulsed columns in general and pulsed sieve plate extraction columns in particular. In this regard, a specific coupled DPBM-CFD framework for modelling the mass transfer process in pulsed sieve liquid-liquid extraction columns, to the best of authors' knowledge, is not published yet. Therefore, building such a coupled PBM-CFD framework will help more to understand the effect of turbulence and the local circulations on the overall extraction efficiency. In this regard, the OPOSPM is considered as an attractive reduced PBM in terms of the simplicity, stability, and the computational cost. As a special case of the general SQMOM, OPOSPM conserves directly the zero and the third moments of the droplet size distribution and therefore the DPBM is reduced into two coupled transport equations namely: the total number and the total volume conservation equations. The total volume concentration equation is already solved by the CFD solver and hence only the total number conservation equation is required. In contrast to the other moments based methods, the OPOSPM avoids the divergence problems arise when applying the classical inversion algorithms to close the source terms, which makes it a stable framework. In this chapter, a coupled reduced PBM-CFD for modelling and the simulation of the coupled hydrodynamic and mass transfer behavior is developed. In this regard, the OPOSPM is utilized as a reduced PBM and implemented using ANSYS/FLUENT commercial software. Within this framework, the droplet-droplet interactions (breakage and coalescence) are taken into account using the OPOSPM, while the required information about the velocity field and energy dissipation is estimated by the CFD models and solvers. It is worthwhile to mention here that, the developed coupled reduced OPOSPM-CFD framework is not only restricted to pulse sieve plate extraction columns but it can be also used for other pulsed column types.

This chapter is organized as follows: in section 4.1, the reduced coupled OPOSPM-CFD framework is presented. Section 4.2 is devoted to present the computational domain and the boundary conditions, while section 4.3 is devoted to validated the proposed coupled OPOSPM-CFD framework. At the validation level, two different sieve plate liquid-liquid extraction column geometries are utilized using different EFCE chemical test systems and operating conditions. These geometries include: pulsed sieve plate DN72 (Lade et al., 2013) and DN80 liquid-liquid extraction columns (Garthe, 2006). The first column geometry (DN72) is used to validated the hydrodynamic predictions of the OPOSPM-CFD framework, while the second one (DN80) is used to validate the mass transfer model predictions. In addition to this, the 2D-CFD model

prediction is prediction validated at the numerical level using the PPBLab extended fixed pivot technique PBE solver. This required breakage and coalescence model parameters to perform the 2D-CFD simulation are estimated using the 1D-CFD PPBLab software. A positive validation of the coupled column hydrodynamics and mass transfer behavior with experimental data using different operating conditions is obtained.

4.2 The OPOSPM-CFD framework

The two phase flow inside the extraction equipment is modeled using the Euler-Euler approach, which assumes that both phases can coexist in each cell in the computational domain. The conservation equations are solved for each phase and the continuity equation for the i^{th} phase is given by:

$$\partial_t (\alpha_i \rho_i) + \nabla \cdot (\alpha_i \rho_i \vec{u}_i) = S_m \quad (1)$$

where ρ_i and u_i are the density and the velocity of the i^{th} phase respectively. The source term S_m takes into account the effect of other possible phenomena (e.g. vaporization). The momentum balance equation for the i^{th} phase is given by (Fluent, 2005):

$$\partial_t (\alpha_i \rho_i \vec{u}_i) + \nabla \cdot (\alpha_i \rho_i u_i u_i) - \nabla \cdot (\vec{\tau}_i) = -\alpha_i \nabla p + \alpha_i \rho_i \vec{g} + \vec{F}_i \quad (2)$$

In this equation, τ is the stress strain tensor, p is the pressure shared by all the phases, g is the gravitational acceleration vector. The stress strain tensor is given by (Fluent, 2005):

$$\vec{\tau}_i = \alpha_i \mu_i (\nabla \vec{u}_i + \nabla \vec{u}_i^T) + \alpha_i \left[\lambda_i - \frac{2}{3} \mu_i \right] \nabla u_i \vec{I} \quad (3)$$

where μ_i is the shear viscosity, λ_i and is the bulk viscosity of the i^{th} phase, and I is the unit tensor. In Eq. (3), \vec{F}_i represents the interphase forces. The interphase forces term is given by (Fluent, 2005):

$$\vec{F}_i = \vec{F}_{body,i} + \vec{F}_{lift,i} + F_{vm,i} \quad (4)$$

where $\vec{F}_{body,i}$ is the external body force, $\vec{F}_{lift,i}$ is the lift force, and $\vec{F}_{vm,i}$ is the virtual mass force. In liquid-liquid extraction equipment, the lift force resulting from the continuous phase velocity gradient can be neglected (Drumm, 2010; Sen et al., 2016). In addition to this, the virtual mass force can be also neglected because the density difference between the contacted phases is usually large (Drumm et al., 2010; Hlawitschka, 2013; Attarakih et al., 2015; Sen et al., 2016). Therefore, only the drag force is taken into account in this work. As a result of this, a two-way coupling approach is obtained, where both phases are allowed to interact to correct the flow field variables. Based on this, the drag force is given by (Drumm et al., 2010):

$$\vec{F}_{c,i} = -\vec{F}_{d,i} = \frac{3 \alpha_c \alpha_d \rho_c C_D |\vec{u}_d - \vec{u}_c| (\vec{u}_{d,i} - u_{c,j})}{4 d_{30}} \quad (5)$$

where the subscripts c and d stands for the continuous and the dispersed phases respectively, and d_{30} is the mean droplet diameter. The drag coefficient (C_D) is given by one of the available drag correlations. In this regard, different drag models were developed based on different assumptions to close the drag force term of the momentum balance equation. For modelling of liquid-liquid extraction equipment, models of Schiller and Naumann (1935) and Kumar and Hartland (1985) were intensively used and recommended (Bujalski et al., 2006; Retieb et al., 2007; Yadav and Patwardhan, 2008; Tiwari et al., 2008; Drumm, 2010; Hlawitschka, 2013;

Attarakih et al., 2015; Amokrane et al., 2016; Sen et al., 2016; Hlawitschka et al., 2016; Alzyod et al., 2017, 2018). These drag models are shown in Table 1.

Table 1: Drag coefficient models

Author	Correlation
Schiller and Naumann (1935)	$C_D = \max\left(\frac{24}{\text{Re}}(1 + 0.15 \text{Re}^{0.687}), 0.44\right)$
Kumar and Hartland (1985)	$C_D = \left(0.53 + \frac{24}{\text{Re}}\right)(1 + 4.56\alpha_d^{0.73})$

Indeed, the model of Schiller and Naumann (1935) is recommended for lean dispersions, where it assumes that the droplet is immersed in an infinite pool of the continuous phase. Therefore, this model doesn't take into account the interaction occurring among the other droplets within the continuous phase. In contrast to Schiller and Naumann (1935) model, the empirical model proposed by Kumar and Hartland (1985) takes into account the presence of other droplets. In addition to this, this model is recommended for high dispersions, where a wide range of experimental data was used to fit the model. More information about these models is given in section 4.4. Concerning the turbulence closure, the mixture κ - ε turbulence model is used in this work. In this model, two additional transport equations for the turbulent kinetic energy and the turbulent energy dissipation should be solved. This is needed to take into account the contribution of turbulence part to the average velocity. Based on this, the turbulent kinetic energy and the turbulent energy dissipation transport equations are given by (Fluent, 2005):

$$\partial_t(\rho_m k) + \nabla \cdot (\rho_m \vec{u}_m k) = \nabla \cdot \left(\frac{\mu_{t,m}}{\sigma_k} \nabla k \right) + G_{k,m} - \rho_m \varepsilon \quad (6)$$

$$\partial_t(\rho_m \varepsilon) + \nabla \cdot (\rho_m \vec{u}_m \varepsilon) = \nabla \cdot \left(\frac{\mu_{t,m}}{\sigma_\varepsilon} \nabla \varepsilon \right) + \frac{\varepsilon}{k} (C_{1,\varepsilon} G_{k,m} - C_{2,\varepsilon} \rho_m \varepsilon) \quad (7)$$

where k is the turbulent kinetic energy, ε is the turbulent energy dissipation, and ρ_m and \vec{u}_m are the mixture average values of the density and the velocity respectively. The mixture average values of the density and the velocity are given by:

$$\rho_m = \sum_{i=1}^n \alpha_i \rho_i \quad (8)$$

$$\vec{u}_m = \sum_{i=1}^n \alpha_i \rho_i \vec{u}_i / \sum_{i=1}^n \alpha_i \rho_i \quad (9)$$

In Eqs. (6 and 7), $\mu_{t,m}$ is the turbulent viscosity, and $G_{k,m}$ is the production of turbulent kinetic energy. These terms are given by (Fluent, 2005):

$$\mu_{t,m} = \rho_m C_\mu \frac{k^2}{\varepsilon} \quad (10)$$

$$G_{k,m} = \mu_{t,m} (\nabla \vec{u}_m + \nabla \vec{u}_m^T) : \nabla \vec{u}_m \quad (11)$$

where the parameters C_μ , C_1 , ε , C_2 , σ_k and σ_ε are constant parameters. These parameters are shown in Table 2.

Table 2: Parameters of the κ - ε mixture turbulence model (Fluent, 2005)

C_μ	$C_{1,\varepsilon}$	$C_{2,\varepsilon}$	σ_k	σ_ε
0.09	1.44	1.92	1.0	1.3

As pointed out the previous section, the drag force term of the momentum balance transport equation should be closed using a proper droplet diameter value. This is a crucial issue to predict the correct flow field variables and to reflect the actual prevailing physical behavior of the dispersed phase. In addition to this, the mean droplet diameter value has a substantial effect on the mass transfer phenomena. Therefore, a robust mathematical model should be utilized to predict the droplet diameter value. This model should compromise between the accuracy and the CPU time. In this work, the OPOSPM is implemented as a UDF in fluent 18.2 to model the coupled hydrodynamics and mass transfer behavior of pulsed sieve plate extraction column. The total number transport equation as formulated by the OPOSPM is given by (Attarakih et al., 2009; 2013; 2015; Alzyod et al., 2017; 2018):

$$\partial_t (\alpha_d \rho_d N) + \nabla \cdot (\alpha_d \rho_d \mathbf{u}_d (d_{30}) N) = \alpha_d \rho_d \left[(\mathcal{G} - 1) \Gamma (d_{30}) N - 0.5 \omega (d_{30}, d_{30}) N^2 \right] \quad (12)$$

In Eq. (12), the required breakage and coalescence models parameters are optimized using the 1D-CFD PPBLab software, where the 1D and 2D CFD simulation efforts are combined in order to minimize the computational efforts. In this regard, different breakage and coalescence kernels were used in this work. These kernels are shown in Table 3. In this work, the required energy dissipation correlation to perform the 1D-CFD simulation using PPBLab software is given by Milot et al. (1990).

Table 3: Droplet breakage and coalescence kernels

Kernel	Author	Correlation
Breakage	Gourdon et al. (1994)	$p(d_{30}) = \frac{\exp(-c_1 / We_p(d_{30}))}{\tau_m}$
	Coulaloglou and Tavlarides (1977)	$\Gamma = c_2 \frac{\varepsilon^{1/3}}{d^{2/3} (1 + \alpha_d)} \exp\left(-\frac{c_3 \sigma_d (1 + \alpha_d)^2}{\rho_c \varepsilon^{2/3} d^{5/3}}\right)$
Coalescence	Delichatsios and Probst (1976)	$\omega(v, v') = c_4 \cdot (v^{1/3} + v'^{1/3})^{7/3} \varepsilon^{-1/3}$
	Coulaloglou and Tavlarides (1977)	$\omega = c_5 \frac{\varepsilon^{1/3}}{1 + \alpha_d} (d + d')^2 (d^{2/3} + d'^{2/3})^{1/2} \times \exp\left(\left(-\frac{c_6 \eta_c \rho_c \varepsilon}{\sigma_d^2 (1 + \alpha_d)^3}\right) \left(\frac{dd'}{d + d'}\right)\right)^4$

Concerning the mass transfer behavior, the solute mass transfer conservation equation for the dispersed and continuous phases are given by (Attarakih et al., 2013; 2015; Alzyod et al., 2017c, 2018):

$$\partial_t (\alpha_d \rho_d c_d) + \nabla \cdot (\alpha_d \rho_d \mathbf{u}_d c_d - D \nabla (\alpha_d \rho_d c_d)) = \dot{S}_m \quad (13)$$

$$\partial_t (\alpha_c \rho_c c_c) + \nabla \cdot (-\alpha_c \rho_c \mathbf{u}_c c_c + D \nabla (\alpha_d \rho_d c_d)) = -\dot{S}_m \quad (14)$$

The diffusion coefficient depends on the laminar diffusion coefficient and the turbulent diffusion coefficient and is given by:

$$D = D_{diff} + \frac{\mu_t}{Sc_t} \quad (15)$$

Here, D_{diff} is the laminar diffusion coefficient, and Sc_t is the turbulent Schmidt number, which has a value of 0.7. The source term (\dot{s}_m) appears in Eqs. (13 & 14) is a general source term, which takes the mass transfer phenomena into account and is given by:

$$\dot{S}_m = \rho_d a_p k_{od} (mc_c - c_d) \quad (16)$$

where, a_p is the available interfacial area for mass transfer $a_p = 6\alpha_d/d_{30}$.

4.3 Computational domain and boundary conditions

In this work, FLUENT 18.2 is utilized, where the OPOSPM is implemented as a user defined function. The column used in simulation is a pilot plant sieve plate liquid-liquid extraction column. In this regard, two column geometries are used and studied. These column geometries include: pulsed sieve plate DN80 (Garthe, 2006) and DN72 (Lade et al., 2013) liquid-liquid extraction columns. The detailed dimensions are shown in Table 4. In the present work, only the active height of the column is considered, where an axisymmetric grid is used to model the active height as shown in Fig. 1. To reflect the actual column geometry, the sieve plate hole diameter is kept constant, while the pitch diameter is varied to achieve the experimental free area value as recommended by Sen et al. (2016). As boundary conditions, a velocity inlet boundary condition is used at the bottom of the column, while a pressure outlet boundary condition is used at the top as shown in Fig. 1.

Table 4: Sieve plate column geometry (all dimensions are in m)

Column geometry	Author	Active height	Column diameter	Hole diameter	Free area
DN72	Lade et al. (2013)	1.00	0.076	0.003	20%
DN80	Garthe (2006)	2.95	0.080	0.002	20%

A sinusoidal pulsed velocity is used at the bottom of the column to take the pulsation effect into account:

$$u(t) = (d_p^2/d_c^2)Af \sin(2\pi ft) \quad (17)$$

Here d_p and d_c are the piston and the column diameters respectively, A is the pulsation amplitude, and f is the pulsation frequency. The ratio between the piston and column diameter is introduced to take the geometrical effects on the velocity value into account.

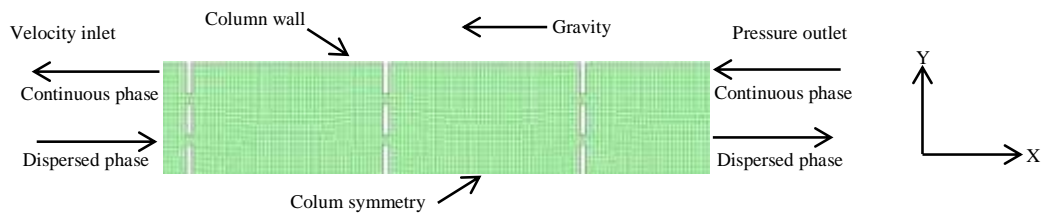


Fig. 1: Part of the computational domain and the implemented boundary conditions (Alzyod et al., 2017; 2018).

4.4 Analytical, numerical and experimental validation

In this section, the proposed OPOSPM-CFD is validated at three different levels: analytical, numerical and experimental levels. At the analytical level, the proposed 2D-CFD framework is validated using a simplified analytical solution, as derived by Attarakih et al. (2009), for the population balance equation in for particle breakage and aggregation. At the second level, the extended fixed pivot solver is used as implemented in PPBLab software is used for the numerical validation. Finally at the experimental level, the proposed 2D-CFD framework is validated using the published experimental data of Lade et al. (2016) and Garthe (2006). In the second part of this section, the OPOSPM-CFD framework is used to model and study the pure hydrodynamic behavior of a pulsed sieve plate DN72 liquid-liquid extraction column as reported by Lade et al., (2013). In the third part of this section, the coupled hydrodynamic and mass transfer behavior of a pulsed sieve plate DN liquid-liquid extraction column as reported by Garthe (2006) is investigated. In both case studies, the breakage and coalescence model parameters are estimated using PPBLab software as discussed in details in the overview.

4.4.1 Analytical validation

In this section, the coupled 2D-CFD OPOSPM framework hydrodynamic predictions are compared with the published simplified analytical solution by Attarakih et al. (2009) using constant breakage and coalescence kernels. In this validation, only one compartment of the sieve plate column is considered and inlet and outlet flow rates are switched to zero. Fig. 2 shows a comparison between the calculated mean integral properties and the analytical solution. It can be clearly observed that the 2D-CFD model predictions agree well with the analytical validation.

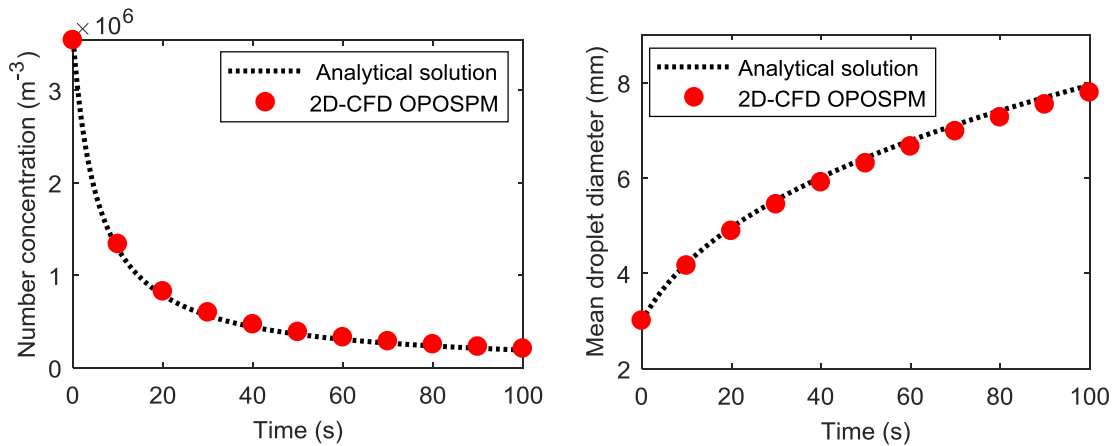


Fig. 2: Comparison between the 2D-CFD OPOSPM framework predictions and the analytical solution (Attarakih et al., 2009) in a single column compartment ($\Gamma=1 \times 10^{-4}$, $\beta = 2$, and $\omega = 1 \times 10^{-7}$).

4.4.2 Pulsed sieve plate DN72 column: numerical and experimental validation

The chemical test system used is 0.3M nitric acid (HNO_3) as a continuous phase and tri-butyl phosphate (TBP) in NPH (Normal Paraffin Hydrocarbon) as the dispersed phase (Lade et al. (2013)). The physical properties are given in Table 4. The dispersed phase inlet velocity, v_d , is varied from 0.2-0.5 cm/s, while the continuous phase inlet velocity, v_c , is fixed at a constant value of 0.207 cm/s. The pulsation intensity, Af , is fixed at a

value of 2 cm/s for all studied cases. The initial conditions are zero for both droplets number and the dispersed phase holdup along the column height. Concerning the column hydrodynamics, the coalescence and breakage kernels are given by Gourdon et al. (1994) and Delichatsios and Probst (1976) (see Table 3), where the models fitting parameters are given by $c_1 = 0.0057$ and $c_4 = 0.0001$ respectively. These values are obtained using PPBLab software. Fig. 3 shows a comparison between the calculated dispersed phase volume fraction and the experimental data using different dispersed phase superficial inlet velocities.

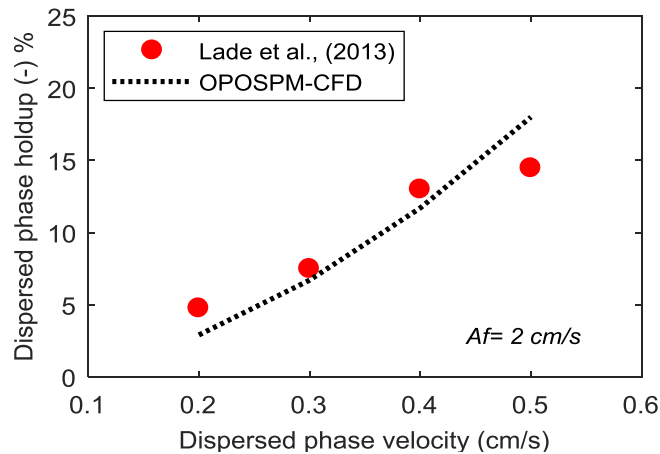


Fig. 3: Comparison between the predicted dispersed phase volume fraction and the experimental data (Lade et al., 2013) using different dispersed phase inlet velocity.

It can be clearly observed that the dispersed phase volume fraction increases when increasing the dispersed phase inlet flow rate. In addition to this, the variation in the inlet flow rate has a minor effect on the breakage and coalescence kernels. Fig. 4 shows the effect of the applied pulsation intensity on the dispersed phase volume fraction during the upstroke and the down stroke instants in the middle of the column, while Fig. 4 shows the effect of the pulsation on the velocity fields of the continuous phase at the same instants of the cycle time and location. It can be clearly observed that the dispersed phase volume fraction varies with the pulsation intensity cycle time, where the maximum value of the dispersed phase volume fraction is achieved during the upstroke instant.

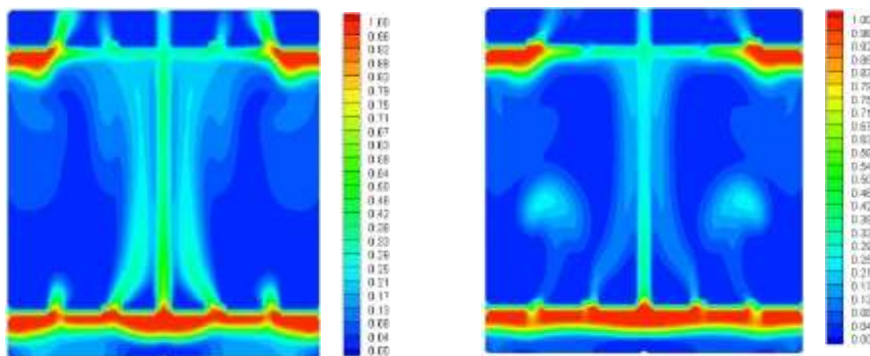


Fig. 4: The effect of the applied pulsation intensity on the dispersed phase volume fraction ($v_c = 0.207$ cm/s, $v_d = 0.4$ cm/s, $A_f = 2$ cm/s) during the upstroke (left) and the down-stroke (right).

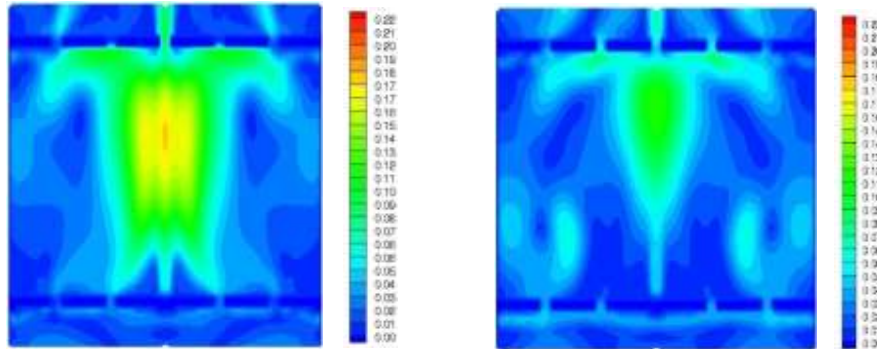


Fig. 5: The effect of the applied pulsation intensity on the dispersed phase volume fraction ($v_c = 0.207$ cm/s, $v_d = 0.4$ cm/s, $A_f = 2$ cm/s) during the upstroke (left) and the down-stroke (right).

This results in a higher axial mixing along the column height and reduces the mass transfer efficiency of the extraction column. The same observations were reported by Sen et al. (2016), where the authors simulated the same column geometry under the same operating conditions using two phase Euler-Euler approach. However, they assumed a constant droplet diameter value inside the column. The authors reported an average error of 0.405 in the predicted dispersed phase volume fraction. This error can be reduced by taking the instantaneous droplet-droplet interactions (breakage and coalescence phenomena) into account. In this work, the average error between the predicted dispersed phase volume fraction and the experimental data is 0.198.

4.4.3 Pulsed sieve plate DN80 column: numerical and experimental validation

The 2D-CFD framework prediction is validated using the published experimental data by Garthe (2006) using toluene (d)/acetone/water chemical system. The dispersed and continuous phases inlet velocities are 40 and 48 liter/h respectively. The pulsation intensity is fixed at a value of 2 cm/s. The inlet dispersed phase solute concentration is 0.4 kg/m³, while the inlet continuous phase solute concentration is 53.5 kg/m³. The initial conditions are zero for both droplets number and the dispersed phase volume fraction, while the initial concentration is the same as in the continuous phase inlet feed. Fig. 6 shows a comparison between the predicted average energy dissipation by the 2D-CFD model and the predicted values using the correlation of Milot et al. (1990).

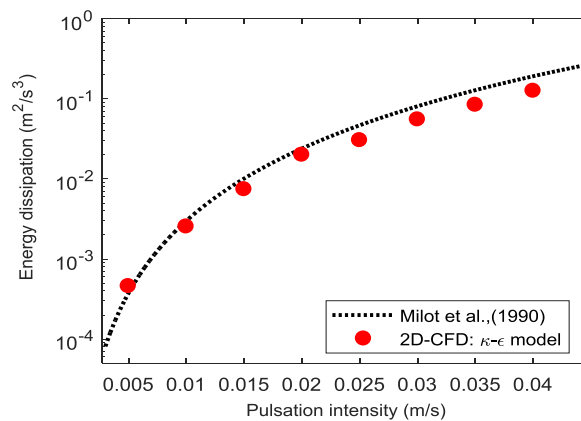


Fig. 6: Comparison between the simulated average energy dissipation using 2D-CFD model and the predicted values using the correlation of Milot et al. (1990).

It is clear that the correlation of Milot et al. (1990) shows a good agreement with the 2D-CFD result. Indeed, this is a substantial validation step because the estimated breakage and coalescence models parameters using PPB Lab software, as a 1D-CFD simulation environment, depend on the energy dissipation. In this case study, the breakage and coalescence kernels are given by Coulaloglou and Tavlarides (1977). The coalescence and breakage kernels parameters are estimated using PPB Lab software, where the parameters values are estimated by matching the 1D-CFD simulation hydrodynamics predictions with the experimental data. The obtained breakage and coalescence kernels are given by: $c_2 = 0.001$, $c_3 = 100 \text{ m}^{-2}$, $c_5 = 0.05$, and $c_6 = 1.33 \times 10^{10} \text{ m}^{-2}$ respectively (see Table 3). Fig. 7 shows a comparison between the simulated mean droplet diameter and the experimental data, where a very good agreement is obtained using both simulation tools. Here, a multi-sectional grid (w.r.t. droplet diameter and solute concentration) is used to perform the 1D-CFD simulation to numerically validate the 2D-CFD simulation results.

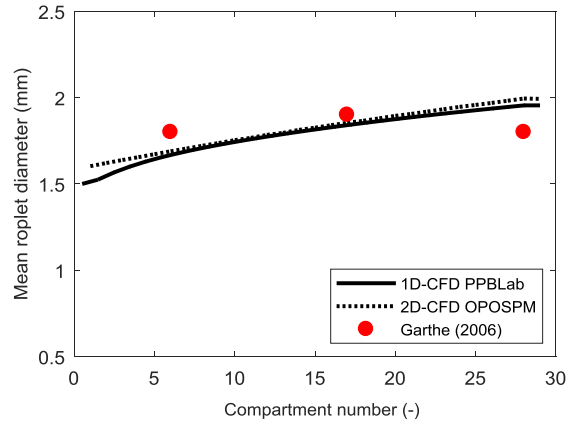


Fig. 7: Comparison between the simulated mean droplet diameter and the experimental data of Garthe (2006).

Fig. 8 depicts a comparison between the simulated light phase solute concentration profiles and the experimental data. In this work, the continuous phase mass transfer coefficient is given by Heertjes (1954), while the dispersed phase mass transfer coefficient is given by Kronig and Brink (1950) respectively. Both CFD simulation tools show a very good agreement with the experimental data. However, a better prediction using PPB Lab software is observed at the bottom of the column. This is because PPB Lab's software PBM solver has the advantage as a detailed multi-sectional numerical solver.

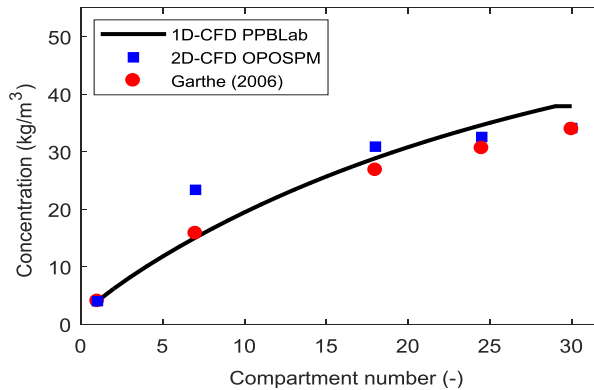


Fig. 8: Comparison between the simulated dispersed phase solute concentration profile and the experimental data of Garthe (2006).

Fig. 9 depicts the effect of the solute mass transfer process on the dispersed phase interfacial tension, where the interfacial tension is decreasing along the column height. Therefore, the droplet breakage is enhanced and the droplet size is shifted toward smaller values.

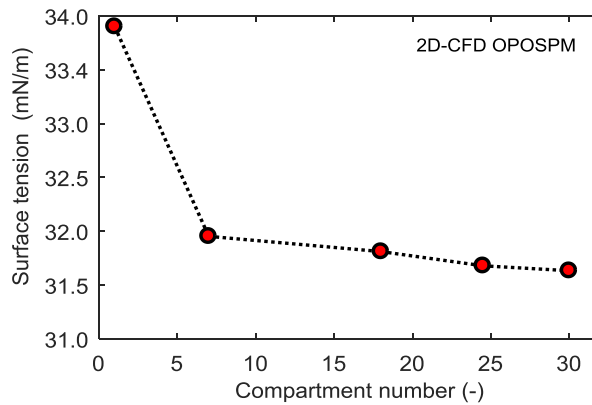


Fig. 9: Effect of the solute mass transfer process on the light phase interfacial tension along the column height.

4.5 Conclusions

A coupled CFD and population balance framework, based on the OPOSPM as a reduced population balance model, is developed to model the coupled hydrodynamic and mass transfer of pulsed sieve plate liquid-liquid extraction columns. The OPOSPM is found efficient in terms of implementation and suitable to describe the two phase flow behaviour inside the liquid-liquid extraction column. The coupled reduced model predictions are compared with published hydrodynamics experimental data, where an axisymmetric grid is used to model the active height of the column. To perform the 2D-CFD simulation, the PPBLab software, as a 1D-CFD model, is used to estimate the required breakage and coalescence kernels parameters. Both simulation frameworks are able to predict the hydrodynamics and the mass transfer behaviour as compared with the published experimental data. In this regard, PPBLab software has the advantage in terms of CPU time and the grid generation. In addition to this, the obtained breakage and coalescence models parameters using PPBLab software are found to be insensitive to the variation in the total throughput. A positive validation at and the experimental levels is obtained.

Nomenclature

A	Pulsation amplitude (m)
C	Concentration (kg/m^3)
C_{1-6}	Fitting parameters as given in Table 3.
C_D	Drag coefficient (-)
D	Dispersion coefficient (m/s)
d_{30}	Mean mass droplet diameter (m)
d_c	Column diameter (m)
d_p	Piston diameter (m)
f	Pulsation frequency (s^{-1})
F	Interphase forces as given by Eq.(4)
k_{od}	Overall mass transfer coefficient (m/s)
m	Distribution coefficient (-)
N	Total number of droplet per unit volume (m^{-3})
S	Source term
t	Time (s)
u	Velocity (m/s)
v	Volume (m^3)

Greek Symbols

ϑ	Number of daughter droplets (-)
μ	Viscosity ($\text{kg}/(\text{m}\cdot\text{s})$)
α	Dispersed phase volume fraction
α	Volume fraction (-)
Γ	Breakage frequency (s^{-1})
ε	Energy dissipation (m^2/s^3)
ρ	Density (kg/m^3)
τ	Stress tensor ($\text{kg}/(\text{m}\cdot\text{s}^2)$)
ω	Coalescence rate (m^3/s)

References

- Alzyod, S., Attarakih, M., Bart, H.-J. (2017). CFD Modelling of pulsed sieve plate liquid extraction columns using OPOSPM as a reduced population balance model, *Comput. Aided Chem. Eng.* 40, 61-66.
- Alzyod, S., Attarakih, M., Bart, H.-J. (2018). CFD modelling of pulsed sieve plate liquid extraction columns using OPOSPM as a reduced population balance model: hydrodynamics and mass transfer. *Comput. Aided Chem. Eng.* 43, 451-456.
- Amokrane, A., Maaß, S., Lamadie, F., Puel, F., Charton, S. (2016). On droplets size distribution in a pulsed column. Part I: In-situ measurements and corresponding CFD-PBE simulations. *Chem. Eng. J.*, 296, 366-376.
- Attarakih M., Alzyod S., Fricke A. (2017). Population balance modelling of pulsed packed bed extraction columns using PPBLab software. *Comput. Aided Chem. Eng.* 40, 67-72.

- Attarakih, M., Abu-Khader, M., Bart, H.-J. (2013). Modelling and dynamic analysis of an RDC extraction column using OPOSPM. *Chem. Eng. Sci.* 91, 180-196.
- Attarakih, M., Al-Zyod, S., Abu-Khader, M., Bart, H.-J. (2012). PPBLAB: A new multivariate population balance environment for particulate system modelling and simulation. *Procedia Eng.* 42, pp. 144-562.
- Attarakih, M., Alzyod, S., Hlawitschka, M., Bart, H.-J. (2015a). OPOSSIM: a population balance-SIMULINK module for modelling coupled hydrodynamics and mass transfer in liquid extraction equipment. *Comput. Aided Chem. Eng.* 37,257-262.
- Attarakih, M., Bart, H.-J., Faqir, N. (2006b), LLECMOD: A windows-based program for hydrodynamics simulation of liquid-liquid extraction columns. *Chem. Eng. Process*, 45(2), 113-123.
- Attarakih, M., Jaradat, M., Drumm, C., Bart, H.-J., Tiwari, S., Sharma, V. Kuhnert, J., Klar, A. (2009). Solution of the population balance equation using the One Primary and One Secondary particle Method (OPOSPM), *Comput. Aided Chem. Eng.*, 26, 1333-1338.
- Bujalski, J. M. , Yang, W., Nikolov, J., Solnordal, C.B., Schwarz, M.P. (2006). Measurement and CFD simulation of single-phase flow in solvent extraction pulsed column. *Chem. Eng. Sci.*, 61, 2930-2938.
- Coulaloglou, C. A., Tavlarides, L.L. (1977). Description of interaction processes in agitated liquid-liquid dispersions. *Chem. Eng. Sci.* 32, 1289–1297.
- Delichatsios, M., Probst, R. (1976). The effect of coalescence on the average drop size in liquid-liquid dispersion. *Ind. Eng. Chem., Fundam.*, 15, 134-138.
- Din, G., Chughtai, I., Inayat, M., Khan, I., Qazi N. (2010). Modelling of a two-phase countercurrent pulsed sieve plate extraction column-A hybrid CFD and radiotracer RTD analysis approach. *Sep. Purif. Technol.*, 73, 302-309.
- Drumm, C. (2010). Coupling of computational fluid dynamics and population balance modelling for liquid-liquid extraction, Dissertation. Technische Universität Kaiserslautern, Kaiserslautern, Germany.
- Fluent, (2005). FLUENT 6.2 User's Guide. Lebanon, NH 03766: Fluent Inc.
- Garthe, D. (2006). Fluid dynamics and mass transfer of single particles and swarms of particles in extraction columns. Dissertation. Technische Universität München, Germany.
- Gourdon, C., Casamatta, G., Muratet, G. (1994). Population Balance Based Modelling. In: Godfrey & Slater (Ed). *Liquid-liquid extraction equipment.* (pp.140-226), New York: Eds. John Wiley and Sons.
- Heertjes, P.M., Holve, W.A., Talsma, H. (1954). Mass transfer between isobutanol and water in a spray column. *Chem. Eng. Sci.*, 3, 122-142.
- Hlawitschka, M. (2013). Computational fluid dynamics aided design of stirred liquid-liquid extraction columns, Dissertation, TU Kaiserslautern, Germany.
- Hlawitschka, M., Attarakih, M., Alzyod, S., Bart, H.-J. (2016). CFD based extraction column design - Chances and challenges. *Chin. J. Chem. Eng.*, 24, 259-263.
- Jaradat, M., Attarakih, M., Bart, H.-J. (2011) Population balance modelling of pulsed (packed and sieve-plate) extraction columns: Coupled hydrodynamic and mass transfer. *Ind. Eng. Chem. Res.*, 50, 14121-14135.
- Jildeh, H.B., Attarakih, M.M., Mickler, M. & Bart, H.-J. (2014). Parameter optimization and validation for droplet population balances. *Can. J. Chem. Eng.* 92, 210-219.
- Kronig, R., Brink, J.C. (1951). On the theory of extraction from falling droplets. *Appl. Sci. Res.* 2, 142-154.
- Kumar A., Hartland, S. (1985). Gravity Settling in Liquid/Liquid Dispersions, *Can. J. Chem. Eng.*, 63, 368-376.

- Laddha, G.S. and Degaleesan, T.E. (1976). *Transport Phenomena in Liquid Extraction*. (McGraw-Hill Publishing Co. Ltd), pp. 305–330.
- Lade, V., Rathod, V., Bhattacharyya, S. Manohar, S., Wattal, P. (2013). Comparison of normal phaseoperation and phase reversal studies in a pulsed sieve plate extraction column. *Chem. Eng. Res. Des.*, 91, 1133-1144.
- Milot, J., Duhamet, J., Gourdon, C., Casamatta, G. (1990). Simulation of a pneumatically pulsed liquid-liquid extraction column. *Chem. Eng. J.*, 45, 111-122.
- Mohanty, S., Vogelpohl, (1997). A simplified hydrodynamic model for a pulsed sieve-plate extraction column, *Chem. Chem. Eng. Process.*, 36, 385-395.
- Perry, R. H., Green, D. W. (2008). *Perry's Chemical Engineers' Handbook*. 8th Edition, McGraw-Hill.
- R. Yadav, Patwardhan A. (2009). CFD modelling of sieve and pulsed-sieve plate extraction columns. *Chem. Eng. Res. Des.*, 87, 25-35.
- Retieb, S., Guiraud, P., Angelov, G., Gourdon C. (2007). Hold-up within two-phase countercurrent pulsed columns via Eulerian simulations, *Chem. Eng. Sci.*, 62, 4558-4572.
- Schiller, L., Naumann, A., (1935). A drag coefficient correlation, *Zeitschrift des Vereins Deutscher Ingenieure* 77, 318–320.
- Schmidt, S., Simon, M., Attarakih, M., Lagar, L., Bart, H.-J. (2006). Droplet population balance modelling-hydrodynamics and mass transfer. *Chem. Eng. Sci.* 61, 246-256.
- Sen, N., Singh, K., Patwardhan, A., Mukhopadhyay S., Shenoy, K. (2016). CFD simulation of two-phase flow in pulsed sieve-plate column – Identification of a suitable drag model to predict dispersed phase hold up. *Sep. Sci. & Tech.* 51, 2790-2803.
- Sharma, V. (2011). *Multi-Phase Flow Model Incorporated with Population Balance Equation in a Meshfree Framework*. Dissertation. Technische Universität Kaiserslautern, Kaiserslautern, Germany.
- Tiwari, S., Christian Drumm, Attarakih, M., Kuhnert, J., Bart, H.-J. (2008). Coupling of the CFD and the droplet population balance equation with the finite pointset method, *Notes in Computational Science and Engineering*, Vol. 65, Griebel, Michael; Schweitzer, Marc Alexander (Eds.).
- Vedaiyan, S. (1969). *Hydrodynamics of two phase flow in spray columns*. Ph.D. Thesis. University of Madras, India.
- Yadav, R., Patwardhan, A. (2009). CFD modelling of sieve and pulsed-sieve plate extraction columns. *Chem. Eng. Res. Des.*, 87, 25-35.

Curriculum Vitae

Name: M. Sc. Chem. Eng. Samer Alzyod



Education

2015-2018 Research Assistant, PhD Student
University of Kaiserslautern/Germany
Chair of Separation Science and Technology

2012-2015 Teaching assistant, Master Student
The University of Jordan/Jordan
Chemical Engineering Department

2006-2011 Bachelor Student
Al-Balqa' Applied University/Jordan
Chemical Engineering Department

Scholar education

2005-2006 General Secondary Education Certificate
Qutaiba School/ Jordan